Austrian Journal of Technical and Natural Sciences

2025, No 9 – 10

PREMIER Publishing

Vienna
2025

Austrian Journal of Technical and Natural Sciences

Scientific journal

№ 9–10 2025

ISSN 2310-5607

Proofreading Kristin Theissen

Cover design Andreas Vogel

Additional design Stephan Friedman

Editorial office Premier Publishing s.r.o.

Praha 8 – Karlín, Lyčkovo nám. 508/7, PSČ 18600

E-mail: pub@ppublishing.org

Homepage: ppublishing.org

Austrian Journal of Technical and Natural Sciences is an international, English language, peer-reviewed journal. The journal is published in electronic form.

The decisive criterion for accepting a manuscript for publication is scientific quality. All research articles published in this journal have undergone a rigorous peer review. Based on initial screening by the editors, each paper is anonymized and reviewed by at least two anonymous referees. Recommending the articles for publishing, the reviewers confirm that in their opinion the submitted article contains important or new scientific results.

Premier Publishing is not responsible for the stylistic content of the article. The responsibility for the stylistic content lies on an author of an article.

Instructions for authors

Full instructions for manuscript preparation and submission can be found through the Premier Publishing home page at: http://ppublishing.org.

Material disclaimer

The opinions expressed in the conference proceedings do not necessarily reflect those of the Premier Publishing, the editor, the editorial board, or the organization to which the authors are affiliated.

Premier Publishing is not responsible for the stylistic content of the article. The responsibility for the stylistic content lies on an author of an article.

Included to the open access repositories:

TOGETHER WE REACH THE GOAL SJIF 2024 = 6.62 (Scientific Journal Impact Factor Value for 2024).

Included to the Uzbekistan OAK journals bulletin.

The Austrian Journal of Technical and Natural Sciences, No 9–10
ISSN 2310-5607

PREMIER Publishing
ppublishing.org

Section 1. Chemistry

DOI:10.29013/AJT-25-9.10-3-7

OXIDATION OF OIL SULFIDES OF THE EAST TASHLA FIELDS WITH HYDROGEN PEROXIDE IN THE PRESENCE OF SULFURIC ACID

Davranova Guzal Turdievna [1], ***Safarova Matluba Alimkulovna*** [1], ***Mamatova Shakhnoza Berdikobilovna*** [1], ***Kurbanov Mingnikul Jumagulovich*** [1], ***Salayev Mirkhojiddin*** [1]

[1] Karshi State University

Cite: *Davranova G. T., Safarova M. A., Mamatova Sh. B., Kurbanov M. J., Salayev M. (2025). Oxidation of Oil Sulfides of the East Tashla Fields With Hydrogen Peroxide in The Presence of Sulfuric Acid. Austrian Journal of Technical and Natural Sciences 2025, No. 9–10.* https://doi.org/10.29013/AJT-25-9.10-3-7

Abstract

In this article, sulfuric acid extraction of sulfide organic compounds from the fuel oil fraction of the Tashlinsky field was carried out. The reaction and conditions of hydrogen peroxide on sulfide compounds from the fuel oil fraction of oil were studied. Organic sulfur compounds in the resulting sulfide concentrate were converted into the corresponding sulfoxides by a 30% peroxide solution.

Keywords: *sulfur, sulfoxide, organosulfur compounds, bitumen, high-sulfur oil, hydrogen peroxide, extract, distillate, refined*

Introduction

Domestic and foreign oil industry suppressed the amount of oil produced – sulfurous and high-sulfur, which are one of the main natural raw materials sources of organosulfur compounds. In this regard, synthetically similar compounds are very important not only as reference preparations for the purposes of identification, but also for a comprehensive study of their physicochemical, chemical, physiological, anti-corrosion and other specific properties, which will greatly facilitate the search for new areas of application of organosulfur compounds of oil.

Cyclic organic sulfur compounds attract more and more attention every year for their theoretical and practical significance. It should be noted that on the basis of organic sulfur compounds, new organic reactions and new effective reagents are discovered, which are successfully used in modern organic synthesis (Rakhmatova G. B., Kurbanov M.Zh., Atakulova D., 2020; Rakhmatova G. B., Kurbanov M.Zh., Ruziboev M. T., 2019; Rakhmatova G. B., Kurbanov M.Zh., Ruziboev M. T., 2020; Vyacheslav Y. Sosnovskikh. 2016). Successes in this direction to a certain extent complement the methods of fine organic synthesis

and theoretical organic chemistry. The development of synthetic work in this direction is also dictated by the need of the national economy for substances with clearly expressed highly effective anti-corrosion and biological activity, which is inherent in many classes of sulfur compounds (Sharaf Demirayak, Leyla Yurttas, Nalan Gundogdu-Karaburun, Ahmet Cagri Karaburun, Ismail Kayagil. 2017; Ya-Li Song, Fan Vu, Chao-Chao Chjan, Guo-Chao Liang, Guan Chjou, Jiao-Jiao Yu., 2015; Henok H. Kurfe, Paseka T. Moshapo, Felix L. Makolo, David W. Gammon, Martin Ehlers, Carsten Schmuck. 2014).

Experimental part

Oxidation to the bituminous broad fraction of high-sulfur oil is carried out as follows: to the bitumen wide fraction of high-sulfur oil in the amount of 200 g, loaded into a three-necked flask with a capacity of 0.5 liters, equipped with a mechanical mixer, a thermometer and a drip funnel. 0.4 g of the emulsifier OS-20 (0.3% to the reaction mixture) was added to this amount of fraction. containing concentrated sulfuric acid in the amount of 0.85 g. Oxidizing mixture is prepared by adding portions of concentrated sulfuric acid to a 30% hydrogen peroxide solution cooled to 0 °C. The addition of the oxidizer was introduced at such a rate that the temperature of the mixture did not exceed 25 °C. After adding hydrogen peroxide, the mixture was stirred for another 2 hours, and then poured into three times the volume of water. They were shaken vigorously and left overnight. The organic layer was separated and dried with calcined calcium chloride.

The oxidized petroleum distillate (organic layer) was loaded into a dividing funnel equipped with an agitator. To this fraction was added 34 g of 60% sulfuric acid, taken at the rate of three equivalents per equivalent of sulphoxide sulfur in solution. The contents of the unit were vigorously stirred for 15 minutes and then left for two hours to stratify. After stratification, the bottom layer (a solution of sulphoxide sulfates in dilute sulfuric acid) was separated from the refined sugar. The acid extract was washed with petroleum ether from the impurity of non-oxidized sulfur and hydrocarbon compounds, and sulfoxides were isolated from the washed sulfuric acid layer when the complex was destroyed by dilution with water up to 15% of the acid concentration. At the same time, the sulfoxides floated and were extracted with ethyl ether. The resulting ether extracts of sulfoxides were washed with water to a neutral reaction (pH = 7), dried with freshly calcined calcium chloride, filtered from the dryer and distilled the solvent. As a result of two treatments of the oxidized broad fraction of oil with 60% sulfuric acid, we obtained 14 g of sulfoxide.

The isolated sulfoxides are dark brown oil, insoluble in water. It is poorly distilled in vacuum, when heated above 110 °C, it darkens. In terms of chemical composition – CnH2nSO, CnH2n-2SO, which correspond to saturated thiocyclanes. Refined, obtained according to both schemes, after purification with 92–93% sulfuric acid, can be used as a component of kerosene – diesel fuel.

Discussion of the results

Sulphide concentrates up to a bituminous wide fraction of high-sulfur oil, released by sulfuric acid, are of considerable interest for the production of petroleum sulfoxides. However, there are various publications in the literature devoted to the study of the oxidation of sulfide oil concentrates. In this regard, we conducted a study of the oxidation of sulphide concentrate isolated from the pre-bitumen wide fraction of the East Tashly deposit with sulfuric acid. High-sulfur oil produced in the south of Uzbekistan does not receive enough qualified use for processing into valuable products. Therefore, the purpose of this work is to develop a technology for desulfurization to a bituminous broad fraction of high-sulfur oil (BCH) by selective oxidation of sulfides, directly in oil distillates, and to isolate the resulting sulfoxides from oxidized distillates by a cheap and safe sulfuric acid method. The sulfuric acid method includes two stages:

1) Oxidation of sulfides contained in the straight-run kerosene-solar fraction of high-sulfur oil by heterogeneous-emulsion method to sulfoxides with 30% hydrogen peroxide with catalytic additives of sulfuric acid.

2) Release of sulfoxides by a dilute solution of sulfuric acid.

In all the experiments carried out, the oxidation temperature was about 80 °C. The amount of hydrogen peroxide consumption was 1.2 g/mol per 1 g/atom of sulfide sulfur oil. It has been established that the oxidation of VSN sulfides in a foam-emulsion reactor has a higher reaction rate than in a reactor with a mechanical agitator due to the greater dispersion of the heterogeneous system. Sulfides separated from spent 60% sulfuric acid oxidize at a higher rate. The separation of sulfoxides from the oxidized fraction of oil is based on the peculiarities of the electronic structure of organosulfur compounds. Sulfoxides, when dissolved in a dilute 60% solution of sulfuric acid, are protonized, giving sulphoxide sulfoxides according to the scheme:

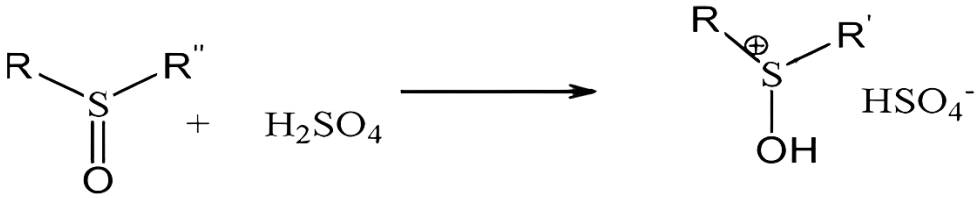

Sulfoxides, forming a complex, pass into a solution of sulfuric acid and, during the stratification of phases, are separated from hydrocarbons and the non-oxidized part of organosulfur compounds. When the sulfuric acid layer is diluted to a 15% concentration of H_2SO_4, the complex is destroyed and the sulfoxides float to the top, and the dilute solution of sulfuric acid remains at the bottom.

$$R-SO-R-H_2SO_4+H_2O\rightarrow$$
$$R-SO-R+H_2O\cdot H_2SO_4$$

To find out the reasons for the different reactivity of sulfide concentrates in the oxidation reaction, their structural and group composition, as well as the nature of the main impurities were studied by mass spectrometry using UV and IR spectroscopy data. It was found that the structural-group composition of both concentrates is quite close and is represented mainly by thiamonocycloalkanes. The characteristics of the resulting sulfoxides are given in Table 1.

Table 1. *Characteristics of oxidized concentrates of organosulfur compounds isolated from the oxidized to bituminous broad fraction of high-sulfur oil from the East Tashly fields*

Name Products	Exit		d204	N20D	Mr (cp)	Sob, %		Sulfoxide, %		S=O, %
	in the year	in %				in a tail-coat	to ex.	in a tail-coat	to ex.	in a tail-coat
Oxidized BCH	201.3	100	0.85256	1.4903	194.0	2.42	100	0.82	100	1.12
Extract (sulfoc seeds)	14.1	6.75	0.99187	1.5405	204.0	13.3	44	–	–	13.1
Cube	184.5	92.3	–	–	–	1.36	54	0.75	93.2	0.021
Petroleum ether leachable product from extract	2.34	1.12	–	–	–	1.78	0.8	–	–	1.15

One of the important points for understanding the mechanism of oxidation of sulfides into sulfoxides using hydrogen peroxide is the diagram below, which assumes the presence of hemolytic and heterolytic reactions.

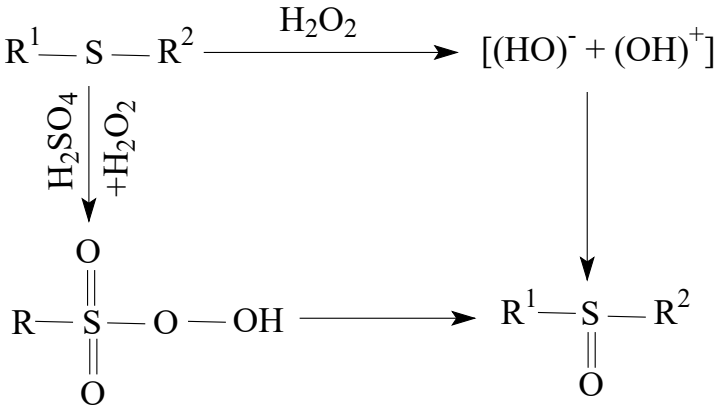

Depending on the nature of the acid and the temperature of the reactions, the proportion of each of these reactions can range from 1 to 100% of the total rate of hydrogen peroxide decay. Closely related to the question of which decomposition predominates under the action of a hemolytic or heterolytic catalyst is the question of the selectivity of sulfide oxidation. In the presence of sulfuric acid, which causes an incomparably faster breakdown of hydrogen peroxide into radicals, the selectivity of oxidation is low. Thus, the question of the catalytic effect of inorganic acids on the mechanism of oxidation of petroleum sulfides is quite complex. In addition, during the oxidation of petroleum sulfides, along with the decomposition of hydrogen peroxide by heterolytic and homolytic mechanisms, the formation of pyroacids takes place. As is known, the products of the reaction of pyroacids with sulfides are the corresponding sulfoxides. Depending on the conditions of oxidation, the concentration of hydrogen peroxide and the nature of the activating additives, the proportion of pyroacids formed under these conditions varies widely.

Based on this, it can be concluded that the specific nature of oxidation of the sulfide concentrate isolated by spent sulfuric acid with hydrogen peroxide forms pyroacids, which are superior to hydrogen peroxide in oxidizing capacity. Even with a lack of oxidant (65% of the stoichiometry), the amount of sulfonic acids in the reaction mixture reaches 0.5% by weight in three minutes. Sulfones appear in oxidation products only when an excessive amount of hydrogen peroxide is used, and they are formed after the conversion of most of the sulfides into sulfoxides. Thus, sulfones are formed from sulfoxides. With an increase in the concentration of hydrogen peroxide, the formation of sulfones occurs more intensively. In the above-described method of obtaining sulfoxides by oxidation of sulfuric acid extracts of sulfides, the yield of the sulfoxide concentrate based on the initial raw material is about 4.7%. In order to increase the rate of conversion of sulfides into sulfoxides, the oxidation process should be carried out in a foam-emulsion apparatus.

References

Rakhmatova G. B., Kurbanov M.Zh., Atakulova D. Bromination of acyl derivatives of the 1-thiaindane series. // Europe, science and we. International scientifuc and practical conference, yuly 2020 Praha, Czech republic. – P. 27–28.

Rakhmatova G. B., Kurbanov M.Zh., Ruziboev M. T. Synthesis and study of the reaction rate of acylation of 1-thiandans and 1-thiochromans. Universum: Chemistry and Biology. 2019. – Issue: 12(66). – P. 82–86.

Rakhmatova G. B., Kurbanov M.Zh., Ruziboev M. T. Synthesis and study of the diacilation reaction of 1-thiaindanes, 1-thiochromans and their derivatives // FarDU ilmiy habarlar. 2020. – No. 4. – P. 11–14.

Vyacheslav Y. Sosnovskikh. Synthesis and chemical properties of thiochroman and its 3-substituted derivatives. Chemistry of heterocyclic compounds. 2016. – 52(7). – P. 427–440.

Sharaf Demirayak, Leyla Yurttas, Nalan Gundogdu-Karaburun, Ahmet Cagri Karaburun, Ismail Kayagil. New chroman-4-one/thiochroman-4-one derivatives as potenyial anticancer agents. Saudi Pharmaceutical Journal. – Vol. 25. – Issue 7. – November 2017. – P. 1063–1072.

Ya-Li Song, Fan Vu, Chao-Chao Chjan, Guo-Chao Liang, Guan Chjou, Jiao-Jiao Yu. Ionic liquid sunthesis of2-(indole-3-yl)-thiochroman-4-ones and their novel antifungal activities. Bio-organic & medicinal Chemistry letters. – Vol. 25. – Issue 2, 15 janvary 2015. – P. 259–261.

Henok H. Kurfe, Paseka T. Moshapo, Felix L. Makolo, David W. Gammon, Martin Ehlers, Carsten Schmuck. Preparation and antimalarial activity of a novel class of carbohydrate-derived, fused thiochromans. European Journal of Medicinal Chemistry. – Vol. 87. – 24 November 2014. – P. 197–202.

submitted 08.10.2025;
accepted for publication 22.10.2025;
published 26.11.2025

Contact: davranovaguzal1988@gmail.com; safarovamatluba86@gmail.com; shahnoza.mamatova.88@mail.com; mengniqulqurbonov@gmail.com; mirhojiddinsalayev54@gmail.com

The Austrian Journal of Technical and Natural Sciences, No 9–10
ISSN 2310-5607

PREMIER Publishing
ppublishing.org

DOI:10.29013/AJT-25-9.10-8-12

QUALITATIVE AND QUANTITATIVE ANALYSIS OF FAT-SOLUBLE VITAMINS IN VITAMIN-MINERAL COMPLEXES

***Jabborkhonova Nodirakhon Abdumalik kizi*[1], *Murzaev Rustam Kamilovich*[2]**

[1] Customs Institute of the Customs Committee of the Republic of Uzbekistan

[2] Central Customs Laboratory of the Customs Committee of the Republic of Uzbekistan

Cite: *Jabborkhonova N.A., Murzaev R.K. (2025). Qualitative and Quantitative Analysis of Fat-Soluble Vitamins in Vitamin-Mineral Complexes. Austrian Journal of Technical and Natural Sciences 2025, No 9–10*. https://doi.org/10.29013/AJT-25-9.10-8-12

Abstract

In this article, the qualitative and quantitative analysis of fat-soluble vitamins in biologically active additives consisting of 6 different vitamin-mineral complexes was investigated by the method of high-performance liquid chromatography. Fat-soluble vitamins in the samples were compared with the quantity indicated on the label of biologically active additives and the standard values for biologically active additives. The results obtained from the study samples showed that the fat-soluble vitamins in all samples corresponded to normal indicators.

Keywords: *biologically active additives, fat-soluble vitamins, high-performance liquid chromatography, vitamin A, vitamin E, vitamin D, antioxidant*

Indtroduction

Among physiologically active natural organic compounds, alkaloids, hormones, antibiotics, and other fat-soluble vitamins (A, D, E, K) occupy a special place. They are irreplaceable therapeutic agents necessary for the body and enhance the body's protective functions. Vitamins are widely used as food additives with antioxidant effects and are important in the diet and healthcare (Denisova L. V., Filimonov V. N., 2014). Therefore, monitoring the composition and levels of vitamins is crucial for the qualitative and quantitative analysis of pharmaceutical preparations, especially food-grade biologically active supplements.

High-performance liquid chromatography was used to determine the content of fat-soluble vitamins (A, E, D) in vitamin and mineral complexes (Baklykov A. V., Artemiev G. A., Glavatskikh S. A., Kopchuk D. S., 2017; Mikheeva E. V., Anisimova L. S., 2005; Mikheev E. V., Anisimov L. S., Pikul N. P., 2004; Methodology M 04–44–2006; GOST R 50928–96; De Lechneer A. P., 1979; Ruperez F. J., 2001; Salo-Väänänena P., Ollilainena V., Mattilab P., 2000). For vitamins A and E, a metal column filled with a 120 × 4 mm nucleosil C18 sorbent was used, and for vitamin D, a MZ-AquaPerfect C18 column of 200 × 4 mm was used.

Materials and Methods

When studying the composition of all samples taken for the study, it was established that all of them contain vitamins A, D, E.

Test solutions and standard samples were prepared in 6 different samples taken for the study, and 20 *μl* of samples and standards were sent to the HPLC for research, and a qualitative and quantitative analysis of fat-soluble vitamins was carried out (Fig. 1–4).

Calculations were performed according to the data of high-performance liquid chromatography, and the qualitative and quantitative analysis of fat-soluble vitamins is presented in (Table 1).

Figure 1. *Chromatogram of standard solutions of vitamin A (13.214) and vitamin E (17.841). Analysis conditions: column Nucleosil C18, 120 × 4 mm (5 μm); mobile phase methyl alcohol; flow rate 1 ml/min, absorption spectrum – 284 nm*

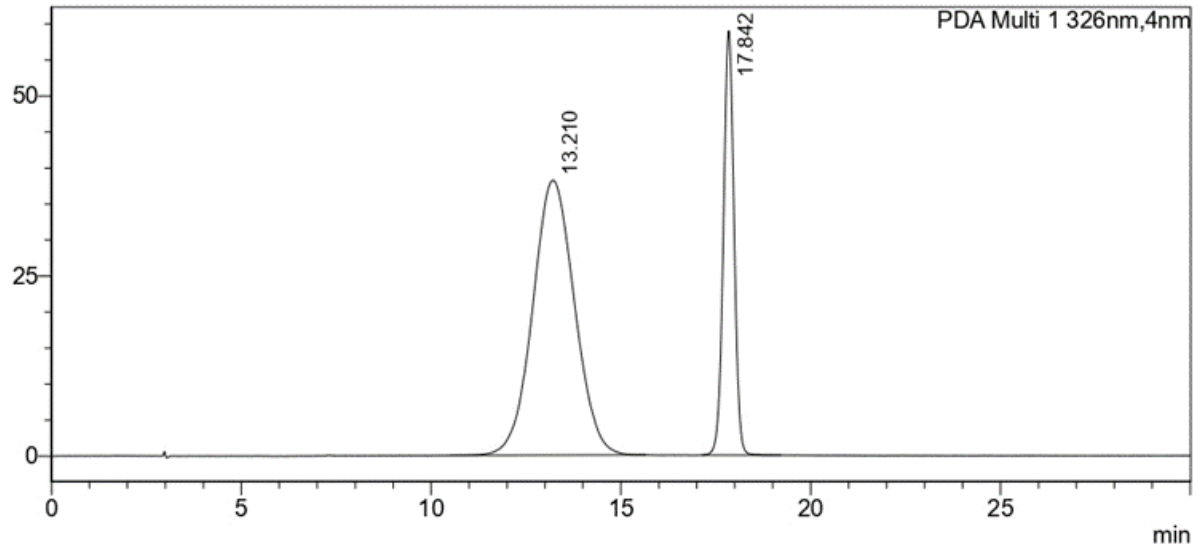

Figure 2. *Chromatogram obtained by high-performance liquid chromatography of vitamins A (13.214) and E (17.841) contained in the biologically active supplement "Supravit multi active"*

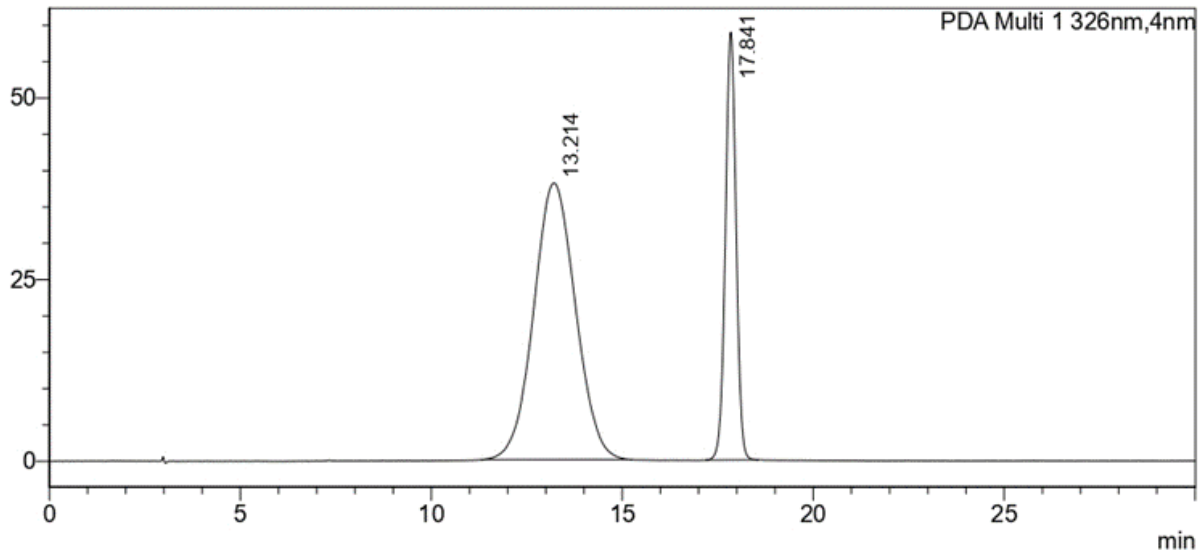

Figure 3. *Chromatogram of standard solutions of vitamin D (14.482). Analysis conditions: MZ-AquaPerfect C18 column 200x4 mm, (3μm); mobile phase methanol (70): acetonitrile (30); flow rate 0.8 ml/min, absorption spectrum-265 nm*

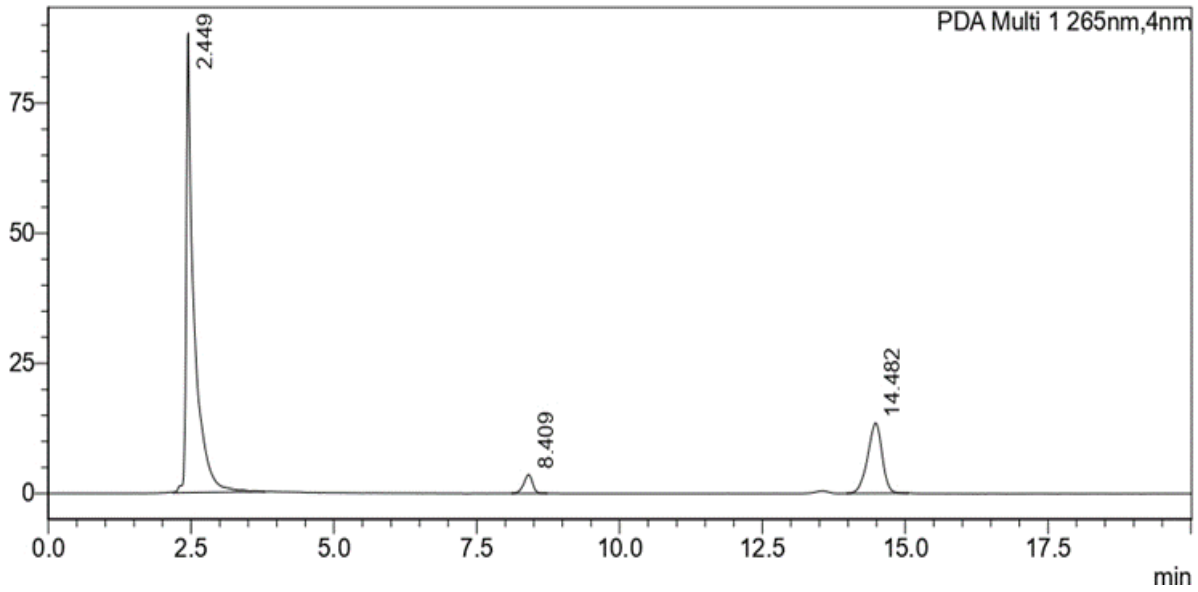

Figure 4. *Chromatogram of vitamins A (13.509) contained in the biologically active supplement "Supravit multi active," obtained by high-performance liquid chromatography*

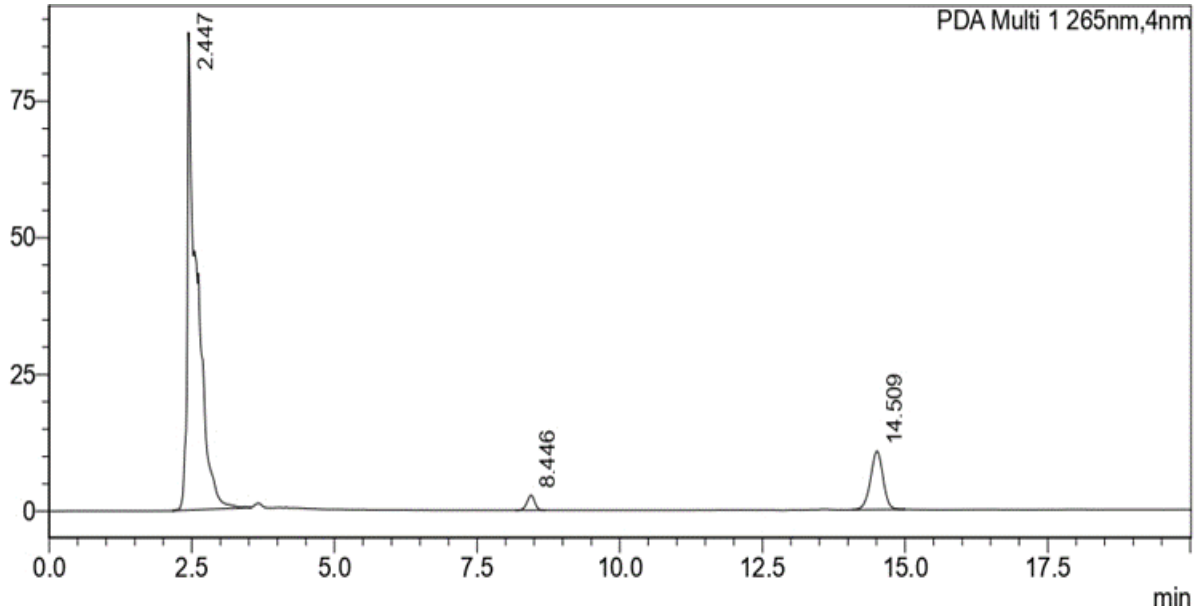

Chromatographic separation of fat-soluble vitamins was carried out in the mobile phase. Methyl alcohol, the mobile phase, was used for vitamins A and E. The UV absorption spectrum was 326 nm for retinol acetate (vitamin A) and 284 nm for α-tocopherol acetate (vitamin E). A 70:30 ratio of the mobile phase methanol and acetonitrile was used for vitamin D. The UV absorption spectrum for cholecalciferol (vitamin D) was 265 nm.

As can be seen from the results obtained from the study samples, the fat-soluble vitamins in all samples corresponded to normal indicators. That is, the requirements of the Eurofarm standard indicate that the standard indicator for vitamins A, E, and D can be 10% less or 65% more than the indicator indicated on the package. In the samples we took as a study, it was found that all fat-soluble vitamins (A, D, E) are at the normal level.

Table 1. *Vitamin content in samples*

No.	Samples	Fat-soluble vitamins					
		Vitamin A		Vitamin E		Vitamin D	
		passport, µg/tab	Found mcg/tab	passport, µg/tab	Found mcg/tab	passport, µg/tab	Found mcg/tab
1.	Duovit	2646–4851	3050	9–16.5	12.5	180–330	265
2.	Komplivit	720–1320	805	1.8–4.9	3.4	–	–
3.	O-252 Life Factor	–	–	6.7–12.3	10.2	11.3–20.6	12
4.	Supravit multi aktiv	450–825	560	22.5–41.2	20	4.5–8	5.2
5.	Vitrum pre-natal	774–1400	880	18–33	20.5	9–16.5	13.8
6.	Multi tabs klassik	720–1320	860	9–16.5	12.8	4.5–8.25	6.5

Based on the results obtained from standard samples of vitamins, it is possible to conduct qualitative and quantitative analysis of water-soluble and fat soluble vitamins in vitamin-mineral complexes using the HPLC method.

Conclusion

In conclusion, it can be said that studies conducted using high-performance liquid chromatography have practically proven that water-soluble and fat-soluble vitamins in vitamin-mineral complexes give repeatable results with rapid, convenient, and high sensitivity, as well as statistical reliability.

References:

Denisova L. V., Filimonov V. N. Chromatographic behavior of fat-soluble vitamins in reversible-phase systems of HPLC / Bulletin of TulS U. Natural Sciences. 2014. – Issue. 1. – Part 2.

Baklykov A. V., Artemiev G. A., Glavatskikh S. A., Kopchuk D. S. Quantitative determination of vitamins A, D3 and E in the composition of “mauervit” and “grandvitam” premixes by the ultra-high-temperature HPLC method // Development and registration of medicinal products – No. 4 (21). 2017 y.

Mikheeva E. V., Anisimova L. S. Physical and chemical methods for determining vitamin E in various objects (review) // Factory Laboratory. Diagnostics of materials. 2005. – Vol. 71. – P. 3–9.

Mikheev E. V., Anisimov L. S., Pikul N. P. The content of vitamin E in multivitamin preparations // Pharmacy. 2004. – No. 5. – P. 16–17.

Methodology M 04-44-2006. Determination of vitamins A, D, and E in premixes and vitamin concentrates.

GOST R 50928-96. Premixes. Methods for determining vitamins A, D, E.

De Lechneer A. P. Simultaneous detection of retinol and α-tocopherol in human serum by high performance liquid chromatography // J. Chromatogr. A. 1979. – No. 162. – P. 408–413.

Ruperez F. J. Chromatographic analysis of α-tocopherol and related compounds in various matrices // J. Chromatogr. A. 2001. – No. 935. – P. 45–69.

Salo-Väänänena P., Ollilainena V., Mattilab P. Simultaneous HPLC analysis of fat-soluble vitamins in selected animal products after small-scale extraction // Food Chemistry. 2000. – Vol. 71. – No. 4. – P. 535–543.

submitted 08.10.2025;
accepted for publication 22.10.2025;
published 26.11.2025

Contact: nodirabarno@gmail.com

The Austrian Journal of Technical and Natural Sciences, No 9–10
ISSN 2310-5607

PREMIER Publishing
ppublishing.org

DOI:10.29013/AJT-25-9.10-13-17

INVESTIGATION OF PHYSICAL-MECHANICAL AND RHEOLOGICAL PROPERTIES OF POLYMER-BITUMEN BINDERS MODIFIED WITH COMPLEX ADDITIVES

Jasurbek E. Babajanov [1], Ruslan R. Hayitov [2], Shohrukh B. Mavlonov [2], Temirbek Kh. Naubeyev[1], Ikramjan Ya. Sapashov[1]

[1] Karakalpak State University named after Berdakh, Nukus, Uzbekistan

[2] Bukhara State Technical University, Bukhara, Uzbekistan

Cite: *Babajanov J. E., Hayitov R. R., Mavlonov Sh. B., Naubeyev T. Kh., Sapashov I. S.(2025). Investigation of Physical-Mechanical and Rheological Properties of Polymer-Bitumen Binders Modified With Complex Additives. Austrian Journal of Technical and Natural Sciences 2025, No 9–10.* https://doi.org/10.29013/AJT-25-9.10-13-17

Abstract

Polymer-modified bitumen (PMB) is an advanced binder designed to improve road pavement durability and eliminate failures such as rutting and cracking. This study examines polymer-bitumen binders modified with destructed polypropylene (DPP), diatomite, and montmorillonite. The synergistic combination of these additives enhances the binder's elasticity, heat and cold resistance, and structural stability, resulting in improved performance and extended service life of asphalt pavements.

Keywords: *polymer-modified bitumen, complex additives, rheology, destructed polypropylene, diatomite, montmorillonite*

Introduction

Polymer-modified bitumens (PMBs) are advanced binder materials developed to enhance the strength and durability of road pavements, as well as to minimize the most common operational problems such as cracking, brittleness, and aging (Sengoz B., Topal A. G., Isikyakar G., 2009). In recent years, research aimed at improving the performance and service life of asphalt pavements through the use of polymer-modified bitumen has been rapidly expanding (Zhu J., Birgisson B., Kringos N., 2014). These materials are characterized by superior physical and mechanical properties and are considered an effective solution, particularly for heavily loaded road structures (Duarte G. M., Faxina A. L., 2021).

Conventional petroleum bitumens tend to lose their plasticity and become brittle under the influence of temperature fluctuations, ultraviolet radiation, and mechanical stresses. Therefore, improving the rheological and physical-mechanical characteristics of bitumen is one of the key scientific and technical directions for extending the service life of road pavements (Ayupov D. A., Murafa A. V., 2009).

Polymer-modified bitumens represent complex dispersed systems, where interfacial

interactions significantly affect elasticity, viscosity, softening temperature, and brittleness limits (Al-Azawee E. T., Qasim Z. I., 2018). Polymer components form a stable structural network within the bitumen matrix, enhancing its thermal stability, deformation resistance, and crack resistance (Gohman L. M., 2008). In addition, polymer-modified binders provide asphalt mixtures with high elasticity, and resistance to moisture and chemical reagents (Kim Y., Lee S. J., Amirkhanian S. N., 2010).

Studies by Kotenko et al. (Kotenko N. P., Shcherba Yu. S., Evforitskiy A. S., 2019) demonstrated that modification of BND 70/100 grade road bitumen with styrene-butadiene-styrene (SBS), ethylene-vinyl acetate (EVA) polymers, and carbon nanotubes (CNTs) increased the heat resistance of the modified bitumen by 1,17 times and the cold resistance by 1,2 times. These effects are attributed to the branching of polymer chains and the formation of strong interfacial bonds within the bitumen matrix (Yildirim Y., 2007).

In the present study, a similar concept was applied using destructed polypropylene (DPP), diatomite, and montmorillonite as complex modifiers to investigate their effect on the physical-mechanical and rheological properties of polymer-bitumen binders. The synergistic interaction of these modifiers enhances the thermal resistance, elasticity, and deformation stability of the binder (Khairutdinov R. F., Shakhov A. V., Ibragimov R. A., 2017). This, in turn, extends the service life of road pavements, reduces maintenance costs, and improves overall economic efficiency.

Materials and methods

The modified bitumen was prepared using the following composition: destructed polypropylene (DPP) – 3–5 wt%, diatomite and montmorillonite – 2 wt % each, and the remaining part consisted of BND 50/70 grade road bitumen. This bitumen grade is intended for use in hot climatic regions and for pavements subjected to heavy traffic loads.

The mixing process was carried out in two stages:

Stage 1: high-speed dispersion at 180 °C and 3000 rpm for 90 minutes;

Stage 2: low-speed homogenization at 600–700 rpm for an additional 90 minutes.

Table 1. *Polymer-bitumen binder samples prepared using thermo-oxidatively destructed polypropylene (JM-380)*

Sample	Bitumen BND 50/70 (%)	DPP (%)	Diatomite (%)	Montmorillonite (%)
PB-DP-1	93	3	2	2
PB-DP-2	92	4	2	2
PB-DP-3	91	5	2	2

Results and discussion

The experimental results revealed that the physical-mechanical and rheological properties of polymer–bitumen binders are significantly influenced by the content of destructed polypropylene (DPP), diatomite, and montmorillonite. During the modification process, these components exhibit a synergistic interaction that leads to the formation of an elastic, thermally stable, and deformation-resistant phase structure within the bitumen matrix.

The analysis of the results was carried out through three main groups of parameters:

- Penetration and ductility – characterizing the mechanical flexibility and hardness of the binder;
- Softening and brittleness temperatures – determining the thermal stability and the brittleness threshold at low temperatures;
- Elasticity (elastic recovery) – assessing the ability of the modified binder to recover its shape after deformation.

As shown in Figure 1, the penetration and ductility values of polymer-bitumen binders vary significantly with DPP content.

The base bitumen (BND 50/70) exhibited a penetration of 75 × 0,1 mm and ductility of 58 cm at 25 °C, and 20 × 0,1 mm and 3,4 cm at 0 °C. With increasing DPP concentration, penetration decreased while ductility sharply increased.

This indicates that the modified binder becomes stiffer and denser, yet more elastic and flexible under deformation.

The synergistic action of DPP, diatomite, and montmorillonite leads to the formation of an interpenetrating viscoelastic network that enhances both the flexibility and crack resistance of the bitumen matrix.

Figure 1. *Effect of DPP content on penetration and ductility of polymer-bitumen binders*

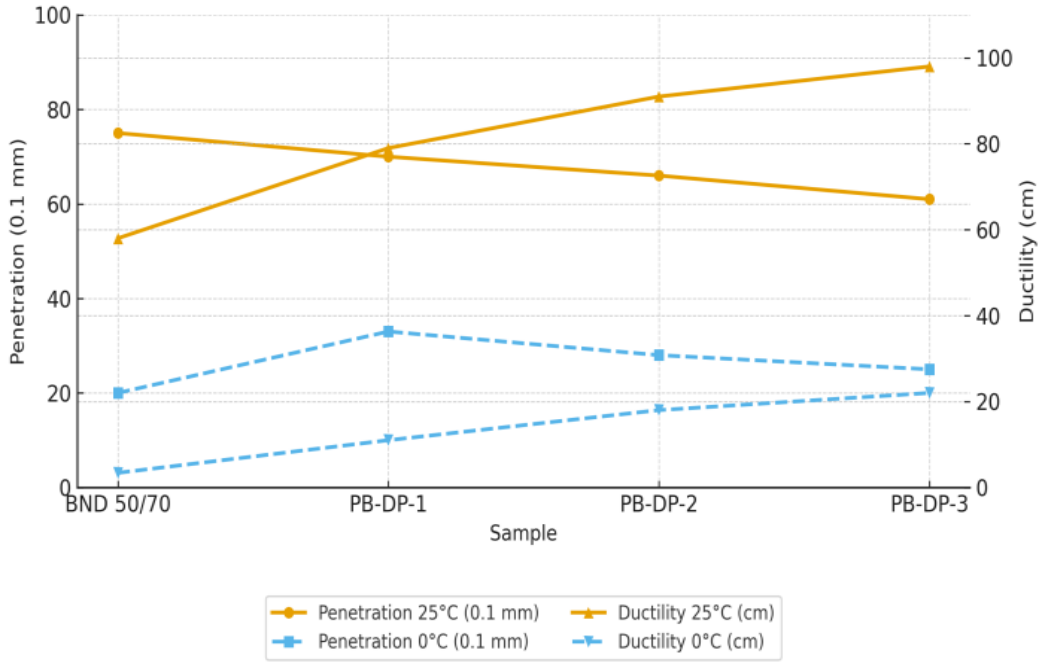

As DPP content increases, the softening temperature rises while the brittleness temperature decreases, indicating a broader operational temperature range and improved thermal stability.

The variation of softening and brittleness temperatures with increasing DPP content clearly demonstrates the improvement of thermal stability and low-temperature flexibility of the modified binders.

As seen in Figure 2, the softening point of the base bitumen (BND 50/70) was 54 °C, while that of the modified binders increased to 69 °C, 76 °C, and 82 °C for PB-DP-1, PB-DP-2, and PB-DP-3, respectively.

Figure 2. *Effect of DPP content on softening and brittleness temperature of polymer-bitumen binders*

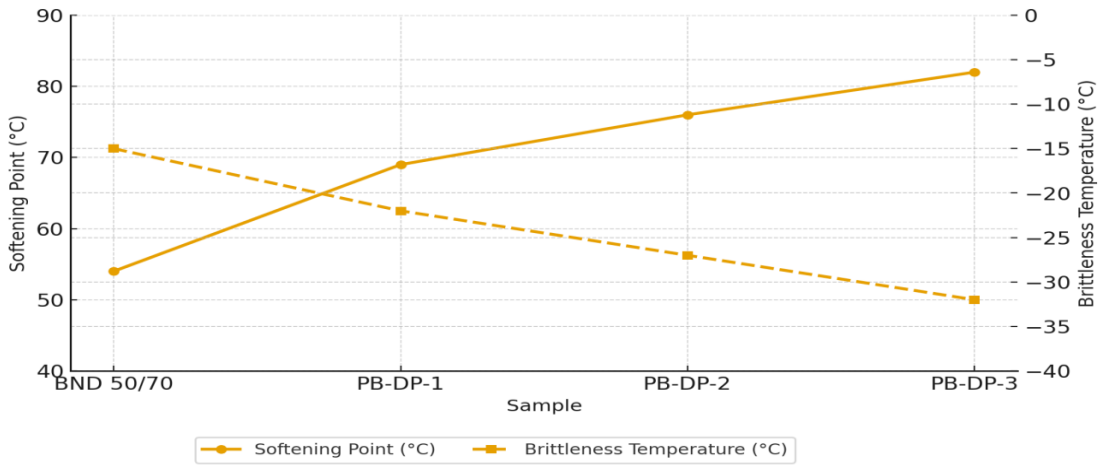

Conversely, the brittleness temperature decreased from –15 °C to –22 °C, –27 °C, and –32 °C. This behavior confirms that the polymer network restricts molecular mobility and prevents crack propagation under thermal stress.

Diatomite and montmorillonite further act as thermal stabilizers, dispersing heat uniformly and delaying crystallization at low temperatures.

As DPP content increases, the softening temperature rises while the brittleness temperature decreases, indicating a broader operational temperature range and improved thermal stability.

The results of elastic recovery tests at 25 °C and 0 °C show a remarkable increase in deformation recovery ability after modification.

As illustrated in Figure 3, the base bitumen exhibited almost no recovery, whereas the modified samples achieved 62, 73, and 81%·cm at 25 °C, and 48, 59, and 70%·cm at 0 °C for PB-DP-1, PB-DP-2, and PB-DP-3, respectively.

This confirms that destructed polypropylene contributes to the formation of a three-dimensional elastic network within the bitumen matrix.

The oxidized polymer chains interact physically with the bitumen components, enabling the binder to recover its shape after deformation.

Moreover, the micro-porous structure of diatomite and the layered configuration of montmorillonite reinforce this network, enhancing overall flexibility and durability.

Figure 3. *Effect of DPP content on elastic recovery of polymer-bitumen binders at 25 °C and 0 °C*

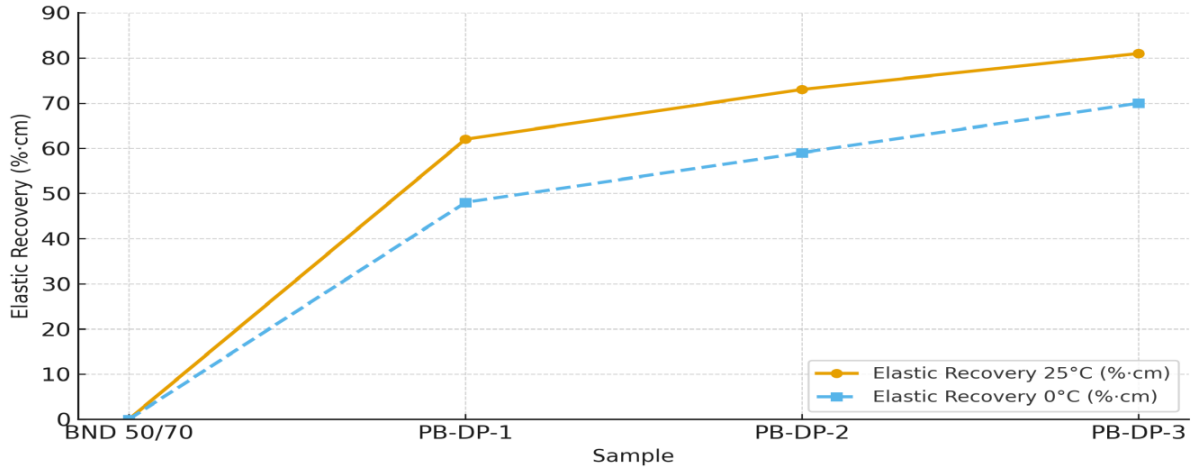

Elastic recovery increases sharply with DPP addition – from 0 to 81% cm at 25 °C and from 0 to 70% cm at 0 °C confirming the formation of a stable elastic structure within the modified binder.

Conclusion

The study demonstrated that complex modification of BND 50/70 bitumen with destructed polypropylene, diatomite, and montmorillonite leads to substantial improvement in its rheological, mechanical, and thermal properties. The modified binders exhibit increased softening temperature (up to 82 °C), decreased brittleness (down to –32 °C), and improved elastic recovery (up to 81%·cm), confirming the formation of a three-dimensional viscoelastic structure. Such materials are promising for road pavements operating in extreme climatic conditions, ensuring higher durability and service life. Future work will focus on optimizing additive ratios and studying long-term aging resistance of the modified systems.

References

Sengoz B., Topal A. G., Isikyakar G. (2009). Morphology and image analysis of polymer modified bitumens. Construction and Building Materials, – 23(5). – P. 86–92.

Zhu J., Birgisson B., Kringos N. (2014). Polymer modification of bitumen: Advances and challenges. European Polymer Journal, – 54. – P 18–38.
Duarte G. M., Faxina A. L. (2021). Asphalt concrete mixtures modified with polymeric waste by the wet and dry processes: A literature review. Construction and Building Materials, – 312. – P. 125–139.
Ayupov D. A., Murafa A. V. (2009). Modifikatsiyalangan bitumli bog‘lovchilar qurilishda qo‘llanilishi. Stroitelnyye materialy, – 8. – P. 50–51.
Al-Azawee E. T., Qasim Z. I. (2018). The influence of crumb rubber modifier (CRM) on the properties of asphalt concrete mixtures. Journal of Engineering and Sustainable Development, – 22(3). – P. 45–54.
Gohman L. M. (2008). Bitumy, polimerno-bitumnye vyazhushchie, asfal’tobeton, polimerasfal’tobeton. – Moscow: Transport.
Kim Y., Lee S. J., Amirkhanian S. N. (2010). Rheological properties of modified asphalt binders with polymer additives. Construction and Building Materials, – 24(4). – P. 511–518.
Kotenko N. P., Shcherba Yu. S., Evforitskiy A. S. (2019). Effect of polymer and functional additives on the properties of bitumen and asphalt concrete. Plasticheskie Massy, 11–12. – P. 47–49. URL: https://doi.org/10.35164/0554-2901-2019-11-12-47-49
Yildirim Y. (2007). Polymer modified asphalt binders. Construction and Building Materials, – 21(1). – P. 66–72.
Khairutdinov R. F., Shakhov A. V., Ibragimov R. A. (2017). The use of polymer additives to improve the performance of bitumen binders. Procedia Engineering, – 189. – P. 397–403.

submitted 08.10.2025;
accepted for publication 22.10.2025;
published 26.11.2025

Contact: sapashov85@mail.ru

The Austrian Journal of Technical and Natural Sciences, No 9–10
ISSN 2310-5607

PREMIER Publishing
ppublishing.org

DOI:10.29013/AJT-25-9.10-18-22

STUDY OF THE PROCESS OF OBTAINING CARBON-HUMIC BENTONITE FERTILIZERS

Jumanova Miyasar Ortikovna [1]

[1] Tashkent Institute of Chemical Technology, Uzbekistan

Cite: *Jumanova M. O. (2025). Study of The Process of Obtaining Carbon-Humic Bentonite Fertilizers. Austrian Journal of Technical and Natural Sciences 2025, No 9–10.* https://doi.org/10.29013/AJT-25-9.10-18-22

Abstract

Mixing brown coal from the Angren deposit, oxidised in an optimal mode with a mixture of nitric and sulphuric acids, with bentonite (from the Azkamar and Navbahor deposits) is a promising method for obtaining highly effective carbon-humic bentonite fertilizer. With a ratio of organic coal to bentonite from the Azkamar deposit of 100:10, a carbon-humic bentonite fertilizer was obtained containing 3.14% nitrogen, 73.20% organic matter, 54.92% humic acids, with a granule strength of 2.28 MPa and a moisture content of 5.2%, which does not cake and retains its friability even at higher moisture levels.

Keywords: *coal, bentonite, humic acids, carbon-humic bentonite fertilizer, granule strength*

Introduction

About 50% of the world's food production relies on synthetic fertilizer application, hence to meet food production, its use has been increased tremendously during the last 4 to 5 decades (FAO, 2021). Inorganic fertilizers are frequently used to increase soil fertility and crop yield. However, they are not a permanent solution to tackle soil infertility. The long-term application of mineral fertilizers into soils with a low percentage of organic compounds accelerates the mineralization of soil organic matter (SOM) and disrupts the natural metabolic processes of soil organisms. This leads to a reduction in the SOM content, nutritional imbalance, and soil acidification. Therefore, natural amendments, such as bentonite and its combination with organics, could be useful tools to maintain or increase the SOM in a sustainable way (Hernández, T. et al., 2016).

Bentonite is classified as an agronomic ore. Abroad, bentonites and preparations made from them are used in agriculture: as fillers in pesticides to combat agricultural pests; as additives to sandy and other low-fertility soils to improve their agronomic properties; as diluents and accumulators of mineral fertilizers to reduce their harmful effects on soil biocenoses, to prevent the leaching of fertilizers from the soil and, as a result, to prevent the contamination of groundwater with mineral salts; in the production of liquid complex fertilizers as suspending and stabilising agents (Mi J. et al., 2020; Umar W. et al., 2022; Eslek Koyuncu D. D. et al., 2024)

Bentonite is recommended for use on light (sandy and sandy loam) soils. It im-

proves their water-physical and thermal properties, increases maximum moisture capacity, and reduces the water permeability of sandy soils. As a result, the living conditions of soil microorganisms and the nutrition of cultivated plants are improved. The high sorption capacity of bentonite prevents the leaching of fertilizers from the soil (Mi J. et al., 2020). Bentonite clay composite has also been evaluated as a tool for the remediation of heavy metal-contaminated soil (Myasnikov, S. K. et al., 2016).

Environmental studies by American scientists have shown that bentonite prevents the spread of phytopathogenic microorganisms in the soil. The use of bentonite provides high economic efficiency in agriculture (Agafonov E. V., Khovansky M. V., 2014). About 200 deposits and occurrences of bentonite clays have been identified in Uzbekistan, with estimated reserves of more than 2 billion tonnes (Avliyakulov A. et al., 2003).

Research method

We decided to combine the high agrochemical properties of carbon-humic compounds (oxidised carbon) with the equally high agrochemical properties of bentonite clays to obtain carbon-humic bentonite fertilizers.

In our work, we used bentonite clays from three deposits in Uzbekistan: Azkamar, Navbahor and Lagon. Their composition is shown in Table 1.

Table 1. *Chemical composition of bentonites*

No.	Bentonite deposit	CO_2	SiO_2	TiO_2	Al_2O_3	Fe_2O_3	MgO	MnO	CaO	Na_2O	K_2O	P_2O_5	SO_3	H_2O
1.	Azkamar	3.41	50.34	0.73	15.21	5.67	2.3	0.03	4.76	2.31	2.36	0.13	1.48	5.42
2.	Navbahor	9.35	46.06	0.39	8.78	3	4.33	0.27	12.2	0.75	1.05	0.77	1.39	6
3.	Lagon	2.97	49.73	0.73	14.74	5.57	4.45	0.02	2.26	2.15	4.75	0.1	0.57	3.8

To obtain oxidised coal, a representative sample of BOMSSH grade coal fine from the Angren deposit, which, after drying to an air-dry state and grinding in a ball mill to a size of 0.25 mm, had the following composition (wt.%): moisture 14.1; ash 13.7; organic matter 72.2; humic acids 4.1% of organic mass. Nitric acid was taken from Maxam-Chirchik JSC with a concentration of 59%. The initial sulphuric acid had a concentration of 93%. The oxidation process was carried out at a nitric acid concentration of 5 to 30%, a temperature of 40 to 80 º C, a duration of 2 hours and a weight ratio of coal: HNO3 equal to 1:2. Sulphuric acid was added to nitric acid in such an amount that its concentration in the nitric acid solution was between 2.5 and 20%. The experiments were carried out in a glass cylindrical reactor equipped with a thermostatic jacket and a screw stirrer. The acid mixture was poured into the reactor, the set temperature was set, the stirrer was turned on, and a sample of brown coal was loaded. At the end of the process, the reaction mass was separated into liquid and solid phases. The solid phase was washed with distilled water from acids to a neutral reaction, dried to an air-dry state, and its ash content, moisture content, organic matter, and yield of humic and fulvic acids were determined. The ash content was determined according to GOST 11022–75, the moisture content according to GOST 11014–70, the organic matter according to the difference between the ash and the sum of the percentage contents of ash and moisture, and the yield of humic acids according to GOST 9517–76 (Zhumanova M. O. et al. 2009).

Nitrogen oxides released during the oxidation of brown coal with a mixture of nitric and sulphuric acids were identified. Using a water jet pump, they were passed through absorbers with a 0.5 N NaOH solution. All solutions were collected together, brought to the 500 ml mark, from where an aliquot was taken to determine nitrogen according to Kjeldahl (Pozin M. E., 1980).

Results and discussion

After oxidising brown coal from the Angren deposit with a mixture of nitric and sulphuric acids, the resulting mass was

separated into solid and liquid phases by filtration. The liquid phase was used to dilute the initial 59% nitric acid. The wet solid phase was ammoniated to a pH of 3.5–4.0.

Initially, we studied the process of producing granular carbon-humic fertilizers by adding finely ground bentonite from various deposits to the wet solid phase of oxidised coal without washing. The mass ratio of the organic part of oxidised coal to bentonite clay (OU : BG) varied in the range of 100: (3–15). The suspension was granulated in a porcelain cup by rolling. The product was then dried in a thermostat at 80 °C. The chemical composition of the obtained carbon-humic fertilizers with the addition of bentonite clays is given in Table 2.

Table 2. *Chemical composition of carbon-humic bentonite fertilizers obtained from oxidised coal without washing*

Ratio of organic carbon to bentonite	N, %	Organic matter, %	Humic acids, %	Moisture, %
When using Lagon bentonite				
100: 3	6.22	75.53	56.81	5.33
100: 7	5.98	66.25	53.07	5.18
100: 10	5.75	63.23	51.59	5.26
100: 15	5.39	60.17	48.61	5.64
When using Navbahor bentonite				
100: 3	6.32	70.57	56.17	5.22
100: 7	5.95	66.94	53.21	5.58
100: 10	5.76	64.77	51.43	5.50
100: 15	5.53	59.06	48.19	5.47
When using Azkamar bentonite				
100: 3	6.23	75.22	55.58	5.74
100: 7	5.87	71.73	53.95	5.48
100: 10	5.63	69.05	51.92	5.56
100: 15	5.39	65.81	48.78	5.44

However, the nitrogen content in the fertilizer is high. Therefore, in order to reduce the nitrogen content in fertilizers, processes for obtaining organic fertilizers were investigated by twice washing oxidised coal with water at a weight ratio of organic coal to H_2O of 1:0.28, then adding bentonite to the wet product and granulating it by rolling.

The wet product was then dried. The composition of the fertilizers is shown in Tables 3.

Table 3. *Chemical composition of carbon-humic bentonite fertilizers obtained on the basis of twice-washed solid phase products of coal oxidation*

Ratio of organic carbon to bentonite	N, %	Organic matter, %	Humic acids, %	Moisture, %
When using Navbahor bentonite				
100: 5	5.35	69.96	52.73	5.71
100: 10	5.00	66.41	50.10	5.26
100: 15	4.74	60.15	47.01	5.60
When using Azkamar bentonite				
100: 5	5.23	75.69	56.30	5.71
100: 10	4.90	72.88	53.03	5.22
100: 15	4.76	68.05	50.74	5.37

In the composition of the carbon-humic bentonite fertilizers obtained by double washing of the solid phase of oxidised coal, the reduction in nitrogen content compared to the unwashed variant is only about 1%. Therefore, to achieve a significant reduction in nitrogen content, the coal oxidation products were subjected to triple washing.

The triple washing of the oxidation products was carried out periodically. The filtration of the nitric acid coal pulp was carried out on a Buchner funnel under vacuum.

For the first washing of the oxidation products, a mixture of HNO3 washing solutions with a concentration of 21.3% obtained during the second and third washing stages was used. The mixture of filtrates obtained after separation of the oxidation product and the first stage of washing with a content of 27.1% HNO3 is sent to the technological cycle for dilution of the initial HNO3. The oxidised part of the coal after threefold washing was mixed with bentonite. The weight ratio of the organic part of coal to bentonite is 100: (3–15). Next, the resulting wet product was granulated, dried, and the chemical composition and strength of the granules were determined. The results are shown in Table 4.

Table 4. *Chemical composition and strength of carbon-humic bentonite fertilizer granules obtained from triple-washed solid phase coal oxidation products*

Ratio of organic carbon to bentonite	N, %	Organic matter, %	Humic acids, %	Moisture, %	Granule strength, MPa
When using Navbahor bentonite					
100:5	3. 65	71.60	54.03	5.06	2.01
100:10	3.16	67.07	50.48	5.15	2.34
100:15	3.08	62.96	47.04	5.19	2.59
When using Azkamar bentonite					
100:5	3.75	76.53	57.61	5.01	2.09
100:10	3.14	73. 20	54.92	5.20	2.28
100:15	3.02	69.45	52.01	5.18	2.65

The data shows that the nitrogen content decreased from 5.63 to 3.14%, while the organic matter content in the fertilizer was 73.20% and the humic acid content was 54.92%. The strength of the granules reached 2.28 MPa.

Conclusion

Based on laboratory studies and a series of experiments conducted on a large-scale laboratory setup, the main technological parameters of the process have been developed.

Main technological parameters of the process.

Particle size of crushed coal, mm –0,25––0,5; coal moisture content –12–15%; nitric acid concentration-30%; sulphuric acid concentration-92,5–93,0%; sulphuric acid concentration in 30% nitric acid –5%; weight ratio of coal (organic part): HNO3 (mg) acid –1: 2; oxidation temperature, °C-35–40; oxidation duration –120 min; concentration of HNO3 formed after the first washing-27,4%; mass ratio of organic part of coal: H_2O at the second and third washing stages –1: 0,2; neutralisation temperature, °C– 60; pH value of ammoniated coal pulp –3,5–4,0; mass ratio of organic coal component: bentonite – 100: 10; mixing time, min –15; temperature of furnace gases at the inlet to the drying drum, °C -.400–500; gas temperature at the outlet of the drying drum, °C – 85–100; product temperature, °C- 80–90. Fertilizer composition, %: Total N-3,14; organic matter –73,20; humic acids- 54,92; total nutrients, (N+organic matter) –76,34.

Thus, by oxidising brown coal from the Angren deposit with nitric acid in the presence of sulphuric acid, followed by triple washing of the solid phase of the oxidised coal and mixing with bentonite clays, drying and granulation, it is possible to obtain granular carbon-humic bentonite fertilizers with a high humic substance content.

References

Avliyakulov A., Tungushova D., Slesareva L. Application of agricultural waste under cotton // Agriculture of Uzbekistan. 2003. – No. 9. – 15 p.

Agafonov, E. V., Khovansky, M. V. The effect of bentonite on increasing the fertility of ordinary chernozem // Soil Science. 2014. – No. 5. – P. 597–601.

Eslek Koyuncu D. D., Okur M., Temuçin B., Şen S. M., Şahbaz E., Eroğlu Ş., Akın Z. S., Topaloğlu G. Evaluation of the Nitrogen Release Properties of ChitosanBentonite Beads 2024. *Journal of the Turkish Chemical Society Section B: Chemical Engineering*, – 7(2): 183–192. DOI: 10.58692/jotcsb.1434727.

Hernández, T., Chocano, C., Moreno, J.-L.; García, C. Use of compost as an alternative to conventional inorganic fertilizers in intensive lettuce (Lactuca sativa L.) crops – Effects on soil and plant. Soil Tillage Res. 2016. – 160. – P. 14–22.

Myasnikov, S. K., Tikhonov, A. Y., Chipryakova, A. P., Kulov, N. N. Removal of heavy metal ions from water by an combined sorption–crystallization process using activated clays. Theor. Found. Chem. Eng. 2016. – 50. – P. 366–382.

Mi J., Gregorich E. G., Xu S., McLaughlin N. B., Liu J. Effect of bentonite as a soil amendment on field waterholding capacity, and millet photosynthesis and grain quality. 2020. *Scientific Reports*, – 10: 18282. DOI: 10.1038/s41598-020-75350-9.

Pozin M. E. Guide to practical exercises in inorganic substances technology. – L.: Chemistry, 1980. – 368 p.

Umar W., Czinkota I., Gulyás M., Aziz T., Hameed M. K. Development and characterization of slow release N and Zn fertilizer by coating urea with Zn fortified nanobentonite and ZnO NPs using various binders. 2022. *Environmental Technology & Innovation*, – 26. DOI: 10.1016/j.eti.2021.102250.

Zhumanova M. O., Usanboev N., Namazov S. S., Beglov B. M. Oxidation of Brown Coal of Angren Deposit with a Mixture of Nitric and Sulfuric Acids печатный Russian Journal of Applied Chemistry. 2009. – Vol. 82. – Number 12. – P. 2223–2229.

submitted 08.10.2025;
accepted for publication 22.10.2025;
published 26.11.2025

Contact: jumanova@mail.ru

The Austrian Journal of Technical and Natural Sciences, No 9–10
ISSN 2310-5607

PREMIER Publishing
ppublishing.org

DOI:10.29013/AJT-25-9.10-23-33

TECHNOLOGY FOR THE SYNTHESIS OF 4′, 4′′-DI-(1-METHYL-1-HYDROXYETHYNYL)-DIBENZO-18-CROWN-6

Kozinskaya Lyubov [1], ***Mirkhamitova Dilorom*** [2], ***Juraev Vais*** [3]

[1] Tashkent State Technical University, the Faculty of Oil and gas hemistry, Academic Lyceum of the Tashkent Pharmaceutical Institute

[2] Almalyk Branch of Tashkent State Technical University

[3] Tashkent State Technical University, the Faculty of Oil and gas hemistry

Cite: *Kozinskaya L., Mirkhamitova D., Juraev V. (2025). Technology for the Synthesis of 4′,4″-di-(1-methyl-1-hydroxyethynyl)-dibenzo-18-crown-6. Austrian Journal of Technical and Natural Sciences 2025, No 9–10.* https://doi.org/10.29013/AJT-25-9.10-23-33

Abstract

The synthesis and technology process of 4′,4″-di-(1-methyl-1-hydroxyethynyl)-dibenzo-18-crown-6 are proposed, the characteristics of the initial reagents and reaction products are given, the chemistry of the process with the most probable by-products and parallel reactions is described. The material balance of production is described, the parameters of the synthesis technology are studied, possible operational malfunctions and methods for their elimination are described, and analytical control of production is proposed.

Keywords: *4′,4″-di-(1-methyl-1-hydroxyethynyl)-dibenzo-18-crown-6, technology, material balance, control*

The best available technology is a product production technology determined on the basis of modern achievements of science and technology and the best combination of criteria for achieving environmental protection, provided that it is technically possible to use it.

One of the most large-scale and widely used industrial products is acetylene. Applications of acetylene include the production of polyvinyl chloride (Ma X., Wei H., Luo Z., 2024, 917–9490, acetylenides (explosives) (Trujillo-Lemon M., 2025, 1176–1187), acetic acid (Shuhrat o‘g‘li. O. B., 2025, 182–186), aromatic hydrocarbons (Bedenko S. P., Dement’ev K. I., Maximov A. L., 2022)., 989–1026), solvents (Fromme T., Reichenberger S., Tibbetts K. M., Barcikowski S., 2024, 638–663), rubbers (Agbaba O., Trotus I. T., Schmidt W., Schüth F., 2023, 1819–1825), acetaldehyde and many others (Zhang Z., Nabera A., Guillén-Gosálbez G., Pérez-Ramírez J., 2025, 1–11).

The production technology of 4′,4″-di-(1-methyl-1-hydroxyethynyl)-dibenzo-18-crown-6 was developed jointly with employees of the Department of Oil and Gas Industry Technology, Faculty of Oil and Gas, Tashkent State Technical University (Kozinskaya L., Mirkhamitova D., 2021, 18–21). A pilot plant was installed to test the process.

The process is periodic. Power is set. The developed process consists of the interaction of acetylene with 4′,4″-diacetyldibenzo-18-crown-6 in the presence of a solvent (diethyl ether, tetrohydrofuran, benzene, toluene, etc.) and a catalyst – powdered potassium hydroxide.

No solid waste is generated during the production of 4′,4″-di-(1-methyl-1-hydroxyethynyl)-dibenzo-18-crown-6. A spent aqueous solution of caustic potassium is formed as a liquid waste, which is sent for disposal, and the gaseous waste is unreacted acetylene, which is sent to a flare.

1. Characteristics of finished products

1.1. 4′,4″-di-(1-methyl-1-hydroxyethynyl)-dibenzo-18-crown-6

Amorphous white powder.

Empirical formula $C_{28}H_{32}O_8$

Structural formula

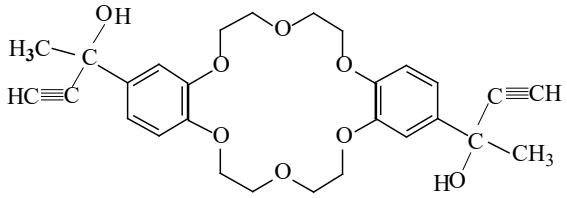

Molecular weight, c.u.	496
Melting point,°C	164–168
Solubility in: water	insoluble
organic solvents	dissolves well
chloroform	dissolves well
benzene	dissolves well
dimethyl sulfoxide	dissolves well

2. Characteristics of feedstock, materials and intermediate products

2.1. Acetylene, ethylene. C_2H_2; HC≡CH

Pure acetylene is a colorless gas with a faint ethereal odor.

Molecular weight, c.u.	26.04
Melting point,˚C	80.8
Boiling point, °C	83.8 (pressure 760 mm. Hg)
Sublimation temperature, °C	84.1

Table 1. *Characteristics of acetylene*

Temperature °C	0	10	20	30	40
pressure 0.5 atm	0.5833	0.5624	0.5430	0.5248	0.5879
pressure 1.0 atm	2.1716	0.1290	1.0805	1.0528	1.0285
pressure ë1.5 atm	1.7850	1.7000	1.6308	1.5898	1.5318

The auto-ignition temperature of acetylene at atmospheric pressure is 635 °C

Table 2. *Self-ignition temperature of acetylene-air mixtures*

Content in the mixture, % vol.	10	20	30	45–55
Temperature, °C	500	400	374	135

Critical temperature, ˚C	35.6
Critical pressure, atm.	61.6
Calorific value (00, 760 mm Hg)	12710–13377 kcal/m^3

Acetylene is highly soluble in many organic and inorganic solvents. The solubility of acetylene in water is measured by the number of its volumes soluble in 1 volume of water at 0 ˚Cand a partial pressure of acetylene of 760 mm Hg. Art., and is characterized by the following data.

Table 3. *The solubility of acetylene in water is measured by the number of its volumes soluble in 1 volume of water at 0 °C*

Temperature, °C	0	5	10	15	20	25	30	35	40	45
Solubility, m^3/m^3	1.75	1.52	1.32	1.16	1.03	0.93	0.85	0.77	0.71	0.65

Table 4. *Solubility of acetylene in organic solvents (pressure 760 mm Hg)*

Solvent	Acetylene solubility, m^3/m^3					
	–20 °C	0 °C	20 °C	40 °C	60 °C	80 °C
Acetone	76	42	24	6.5	–	–
γ-Butyrolactone	–	19.5	11.5	6.1	4.4	–
Dimethylformamide	–	67.0	37.4	21.4	13.0	8.0
Methanol	40	20	11.2	6.0	–	–
N- methyl pyrrolidone	–	65	38.7	23	10	7

2.2. 4′,4″- diacetyldibenzo-18-crown-6

Amorphous white powder.

Empirical formula $C_{24}H_{28}O_8$

Structural formula

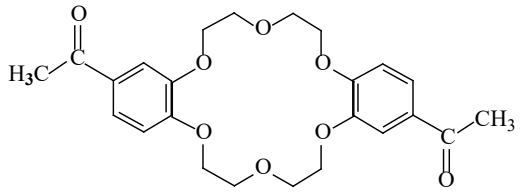

Molecular weight, c.u.	444
Melting point,0C	194–200
Solubility in: water	insoluble
organic solvents	dissolves well
chloroform	dissolves well
benzene	dissolves well
dimethyl sulfoxide	dissolves well

Chemistry of preparation of 4′,4″-di-(1-methyl-1-hydroxyethynyl) -dibenzo-18-crown-6

The reaction of the formation of acetylene alcohols in the presence of potassium hydroxide was discovered by A. Favorsky in 1905 (Favorsky A. E., 1905, 643–645).

The interaction of ketones with a suspension of powdered KOH in a solvent (ether, benzene, toluene, etc.) is carried out at a temperature of 0 °C+40 °C, a pressure of 0.4–0.9 MPa. The interaction of 4′,4″-diacetyldibenzo-18-crown-6 with acetylene was carried out according to the following scheme:

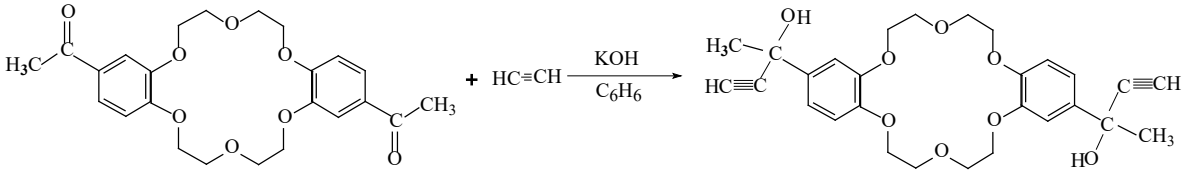

The mechanism of nucleophilic addition to the carbonyl group of the acetylenide ion formed upon deprotonation of the terminal alkyne has been proven (Reutov O. A., Kurts A. L., Butin K. P., 2021, 35–52). By analogy, the following mechanism for the formation of 4′,4″-di-(1-methyl-1-hydroxyethynyl)-dibenzo-18-crown is presented –6:

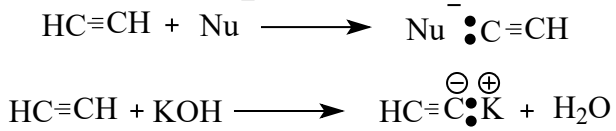

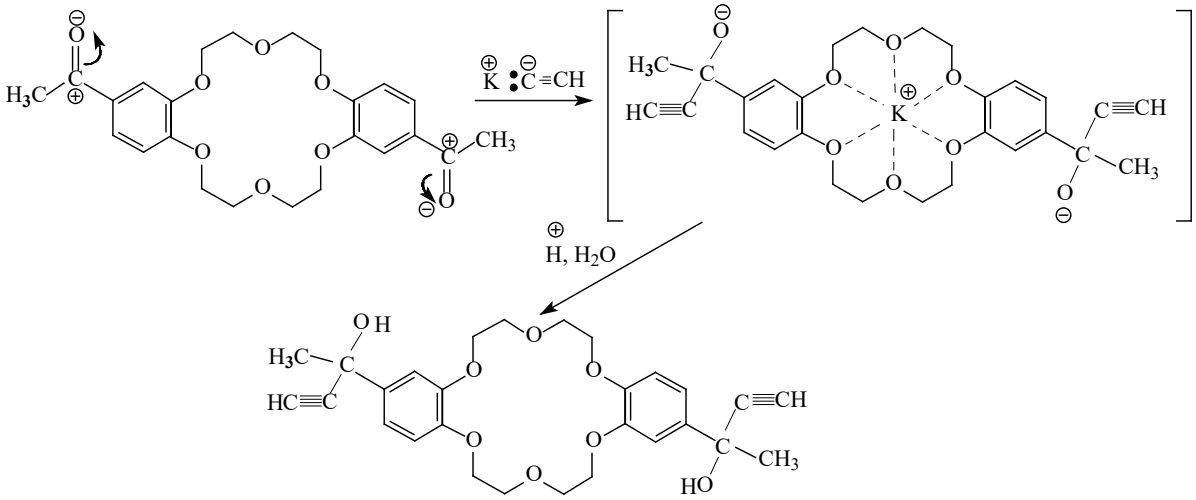

It has been experimentally established that the amount of 4′,4″-di-(1-methyl-1-hydroxyethynyl)-dibenzo-18-crown-6 formed per unit time is directly proportional to the concentration of potassium hydroxide. With an excess of acetylene, the reaction is pseudo-monomolecular with respect to potassium hydroxide. Changing conditions, using a slight excess of acetylene at a temperature of ~20 °C leads to the formation of acetylene 1,4-glycols:

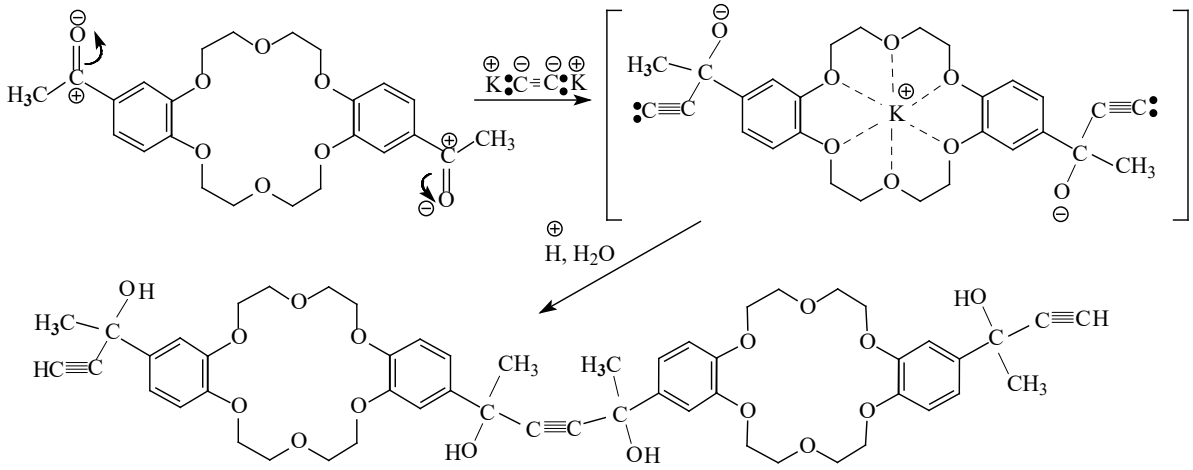

The rate of formation of acetylene 1,4-glycols at a temperature of 20+22 °C significantly exceeds the rate of formation of tertiary acetylene alcohols. The yield reaches 80%. As the temperature increases, the process is completely directed towards the formation of 1,4-glycols.

Experimental part

4′,4″-di-(1-methyl-1-hydroxyethynyl)-dibenzo-18-crown-6. To 5.0 g (11.26 mmol) of 4′,4″-diacetyldibenzo-18-crown-6 in 200 ml of benzene, 63.06 g (112.6 mmol) of potassium hydroxide was added and heated for 20–30 min, then acetylene 630 ml (28.15 mmol), the mixture was boiled for 3 hours. The progress of the reaction was monitored by TLC on silufol in the system acetone: hexane, 2:1. Then hydrolysis was carried out in a weakly acidic medium, the precipitate was washed, purified by fractional crystallization from hexane, and dried in an oven at 40 °C. The compound was obtained in a yield of 2.35 g (42%), m.p. 164–168 °C.^{1}H-NMR ($CDCl_3$, 400 MHz) δ_H, mp: 1.82 (6H, s, α-C**H**$_3$), 2.65 (2H, s, -O**H**), 3.21 (2H, s, ≡C**H**), 3.87–4.26 (16H, m, α- and β-O-C**H**$_2$), 6.71–6.73 (2H, m, Ar-**H** 6′), 6.84 (2H, d, Ar-**H** 3′, *J*= 8,9 Hz), 6.87–6.89 (2H, d, Ar-**H** 5′, *J*= 6,3 Hz).^{13}C-NMR ($CDCl_3$, 100 MHz) δ, mp.: 33.10 (R-**C**H$_3$), 67.41 (–**C**-), 69.64–70.49–71.08 (β-α-O-**C**H$_2$), 73.10 (ArC≡**C**-), 87.20 (Ar**C**≡), 112.13 (Ar-**C**3′), 114.78–137.31 (Ar-**C**4′,5′,6′), 147.60–151.36 (Ar**C**-O-CH$_2$). Elemental analysis: found, %: C 67.93, H 6.44. Calculated, %: C 67.75, H 6.45 Gross formula: $C_{28}H_{32}O_8$.

Description of the technological process for the production of 4′,4″-di-(1-methyl-1-hydroxyethynyl)-dibenzo-18-crown-6

Acetylene from the gas holder is supplied through a fire arrester to the lower part of the reactor. Acetylene consumption is measured by a gas meter. The reactor contains operating quantities of solvent, 4′,4″-diacetyldibenzo-18-crown-6 and potassium hydroxide.

4′,4″-diacetyldibenzo-18-crown-6 is saturated with acetylene at a temperature of 5–100C, which is created by cooled water supplied to the reactor jacket. Unreacted acetylene enters the reactor.

Picture 1. *Production flow diagram 4′,4″-di-(1-methyl-1-hydroxyethynyl)-dibenzo-18-crown-6*

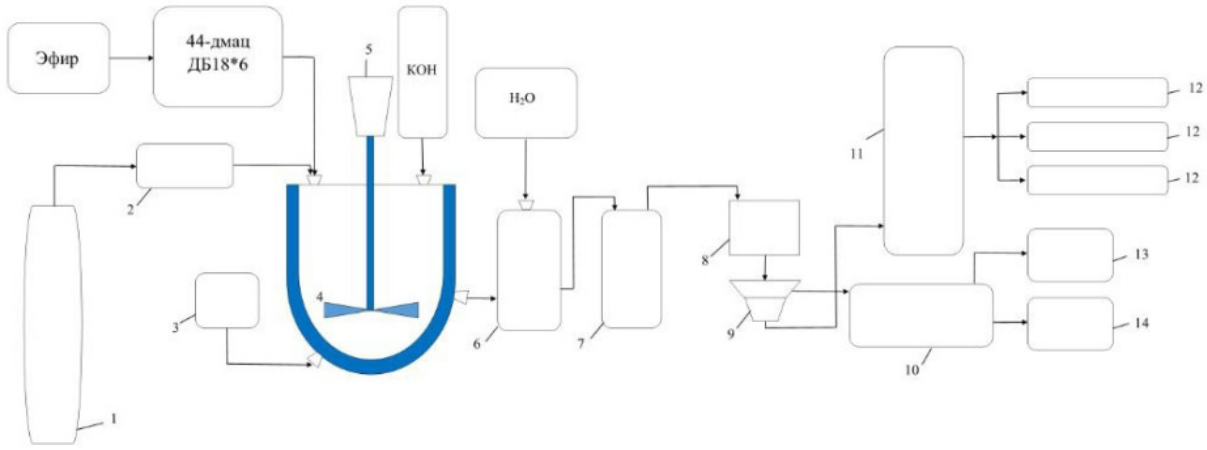

1-cylinder with acetylene, 2-gas meter with pressure gauge, 3-thermocouple, 4-reactor, 5-mixer, 6-hydrolyzer, 7-separator, 8-stripping, 9-filtration, 10-crystallization, 11-distillation column, 12 – containers for fractions, 13 – drying, 14 – container for the finished product

During the interaction of 4′,4″-diacetyldibenzo-18-crown-6 acetylene into reactor 4 with constant mechanical mixing, diethyl ether is supplied from the container, and potassium hydroxide is supplied from the hopper. The contents are heated until the potassium hydroxide dissolves in the reaction mixture. After this, acetylene is continuously supplied from gas tank 1 into the reaction mixture through fire arrester 2 at a rate of 34.94 l/hour. 4 hours after cooling, the resulting catalyzate enters hydrolyzer 6 and passes through the stage of filter 9 and crystallization 10. The organic layer is collected in a rectification column 11 for further separation of the mixture in container 12. In this case, diethyl ether is sequentially determined. And the sediment of the target product is sent for drying 13 and collected in 14, 4′,4″-di-(1-methyl-1-hydroxyethynyl)-dibenzo-18-crown-6 at 155^{0}C, unreacted acetylene after purification was returned to the cycle.

Material balance of production of 4′,4″-di-(1-methyl-1-hydroxyethynyl)-dibenzo-18-crown-6

60% DEE solution in terms of 1 ton of finished product

Table 5.

Consumption	Weight. kg	Coming	Weight. kg
1. Acetylene 100%	52.945	Solution of 4′,4′′-di-(1-methyl-1--hydroxyethynyl)-diben-zo-18-crown-6	1595.15

	Consumption	Weight. kg	Coming	Weight. kg
	Including C_2H_2 99%	52.416	Wt.h 4′,4″-di-(1-methyl-1-hydroxyethynyl)-dibenzo-18-crown-6 62.69%	1000
	N_2 0.3%	0.1588	DEE 40%	638,06
	O_2 0,1%	0.0529	N_2 0.0099%	0.1588
	CO_2 0,2%	0.1059	O_2 0.0033%	0.0529
2.	4′,4″-diacetyldibenzo-18-crown-6	895.104	CO_2 0.00664%	0.1059
	Incl. 4′,4″-diacetyldibenzo-18-crown-6 99.8%	904.145	H_2O 0.1133%	1.808
	H_2O 0.2%	1.808		
3.	DEE 100%	638.06		
	Total	**1595.15**	**Total**	**1595.15**

Calculation of acetylene consumption per 1 ton of 4′,4″-di-(1-methyl-1-hydroxyethynyl)-dibenzo-18-crown-6

HC≡CH

$$\frac{1000}{496} = 2.016 \text{ k mole}$$

2.016 × 26 =52.416 kg 100% C_2H_2

Let's find 99% consumption C_2H_2

$$\frac{52.416}{0.99} = 52.945 \text{ kg } C_2H_2$$

of which 1% impurities by weight:

52.945 × 0.003 = 0.1588 kg N_2

52.945 × 0.001 = 0.0529 kg O_2

52.945 × 0.002 = 0.1059 kg CO_2

Acetylene volumetric flow:

$$\rho = 1.09 \quad V = \frac{52.945}{1.09} = 48.573\ m^3$$

Calculation of consumption of 4′,4″-diacetyldibenzo-18-crown-6 per 1 ton of finished product

2.016 kmol x 444 kg/kmol = 895.104 kg 100% 4′,4″-diacetyldibenzo-18-crown-6

consumption of 4′,4″-diacetyldibenzo-18-crown-6 99%:

$$\frac{895.104}{0.99} = 904.145 \text{ kg } 4',4''\text{- dia-}$$

cetyldibenzo-18-crown-6

0.2% impurity (moisture)

904.145 x 0.002 =1.808 kg moisture

DEE consumption 40% of the resulting solution:

52.945+904.145=957.09 kg of product

$$\frac{957.09}{0.6} = 1595.15 \text{ kg}$$

Consumption of 100% DEE:

19995.15–957.09=638.06 kg

Total: 52.945+904.145+638.06=1595.15 kg

Calculation of the concentration of the main and by-products:

$\frac{1000}{1595.15} \cdot 100 = 62.69\%$ 4′,4″- dia-cetyldibenzo-18-crown-6

$$\frac{638.06}{1595.15} \cdot 100 = 40\% \text{ DEE}$$

$$\frac{0.1588}{1595.15} \cdot 100 = 0.009955\% \ N_2$$

$$\frac{0.0529}{1595.15} \cdot 100 = 0.003316\% \ O_2$$

$$\frac{0.1059}{1595.15} \cdot 100 = 0.006639\% \ CO_2$$

$$\frac{1.808}{1595.15} \cdot 100 = 0.1133\% \ H_2O$$

Study of the technology parameters for the synthesis of 4′,4″-di-(1-methyl-1-hydroxyethynyl)-dibenzo-18-crown-6:

— the technological process is carried out under atmospheric lighting;

— the total duration of the process is 10 hours, of which 2 hours are preparation and suspension; interaction of reagents with each other 4 hours, hydrolysis of intermediate products – 1 hour, separation 1 hour and fractional separation of the resulting products – 2 hours;

— for the initial three stages the temperature of the process is 0 °C, the fourth stage is 100 °C and for the rectification of the process 180 °C;

— the process is carried out periodically and continuously, and the supply of acetylene is 0.365 l/hour, 4′,4″-diacetyldibenzo-18-crown-6 0.294 l/hour, DEE 0.264 l/hour and KOH 0.112 kg/hour;

— the yield of 4′,4″-di-(1-methyl-1-hydroxyethynyl)-dibenzo-18-crown-6 is 3.15 mol/l hour and the reaction rate is 0.28 mol/l. hour. In this case, the activation energy of the reaction is 8.05 kcal/mol;

— during the process, safety and environmental protection requirements are observed;

— it was established that the melting point of 4′,4″-di-(1-methyl-1-hydroxyethynyl)-dibenzo-18-crown-6 is 164–168 °C, the structure was established according to IR, ^{1}H- and ^{13}C-NMR data – spectroscopy, the composition was determined by elemental analysis, and the purity was determined by GLC.

Industrial waste, wastewater and air emissions

The production of 4′,4″-di-(1-methyl-1-hydroxyethynyl)-dibenzo-18-crown-6 produces liquid and solid waste. After rectification, liquid organic waste is returned to the cycle; the potassium hydroxide solution, after neutralization, is sent for disposal.

Table 6. *Technological standards*

No.	Name of stage and reagent flows	Operation time, hour	Temperature, °C	Pressure, MPa	Component ratio, mol	Conversion, %
	Formation of acetylene-KOH complex	1	0	atm	1:1	~100
	Synthesis 4′,4″-di-(1-methyl-1-hydroxyethynyl)-dibenzo-18-crown-6	4	34	atm	1:2.5	64–70

Table 7. *Production control and process control. Technological production control*

No.	Position number on the diagram	Parameter name and sampling location	Frequency and method of control	Standard and technical parameters	Installation location	Name and characteristics	Model type	Who controls
				Formation of acetylene-KOH complex				
	R4	R4 reactor temperature control	Constantly	0 °C	On the R4 reactor on the CPU	Thermocouple GRHA, automatic potentiometer. Recorder showing GRHA measurement limits 0–600 °C intrinsically safe design	THA 0515 Ts2.821.71 102, KSP 44. Modification 41.540 50.540 50.008/41	Operator

No.	Position number on the diagram	Parameter name and sampling location	Frequency and method of control	Standard and technical parameters	Installation location	Name and characteristics	Model type	Who controls
Synthesis of 4′,4″-di-(1-methyl-1-hydroxyethynyl)-dibenzo-18-crown-6								
	R4	R4 reactor temperature control	Constantly	34 °C	On the R4 reactor on the CPU	Thermocouple GRHA, automatic potentiometer. Recorder showing GRHA measurement limits 0–600 °C intrinsically safe design	THA 0515 C2.821.71 102, KSP 44. Modification 41.540 50.540 50.008/41	Operator

Table 8. *Analytical production control*

No	Name of process stages, sampling location or parameter changes	Controlled parameter	Frequency and method of control	Standards and technical indicators	Test method and controls	Who controls
1	Mixing acetylene with KOH	Acetylene content	1 time per shift	Not less than %	According to GOST 236–54	Laboratory assistant
2	Mixing ingredients in R4	Content of 4′,4″-diacetyldibenzo-18-crown-6	1 time per shift	Not less than %	Chromatographically	Laboratory assistant
3	Purity of 4′,4″-di-(1-methyl-1-hydroxyethynyl)-dibenzo-18-crown-6 after recrystallization	Purity 4′,4″-di-(1-methyl-1-hydroxyethynyl)-dibenzo-18-crown-6	1 time per shift	Not less than %	By melting point	Laboratory assistant

Table 9. *Possible malfunctions and ways to eliminate them*

Problems	Possible causes of problems	Personnel actions and troubleshooting method
Formation of acetylene-KOH complex		
Reactor temperature rises	Increased coolant supply to R4	The supply of coolant to the R4 reactor has decreased
Synthesis of 4′,4″-di-(1-methyl-1-hydroxyethynyl)-dibenzo-18-crown-6		
The content of the main substance in the R4 reactor has increased	The residence time of substances in the reactor has increased over 4 hours	Carry out hydrolysis and recrystallization of the main product

Environmental protection and basic rules for safe process management

The technological process for producing 4′,4″-di-(1-methyl-1-hydroxyethynyl)-dibenzo-18-crown-6 occurs using explosive and toxic substances – diethyl ether, acetylene, etc.

In accordance with the established fire safety category (A), classes of premises PUE (B-1g), as well as the category and condi-

tions of explosion hazard of operating mixtures. The installations must be operated in full compliance with the safety and industrial sanitation requirements set out in the "Rules and Standards for Safety and Industrial Sanitation for the Design and Operation of Fire and Explosion Hazardous Plants in the Chemical and Petrochemical Industry", "Sanitary Standards for the Design of Industrial Enterprises", "Rules for Construction" electrical installations."

The main condition for the safe conduct of the production process of 4′,4″-di-(1-methyl-1-hydroxyethynyl)-dibenzo-18-crown-6 is strict adherence to workplace instructions, technological standards, safety regulations and fire safety regulations.

In order to ensure safe working conditions for maintenance personnel and protect equipment from destruction and fire, as well as reduce the consequences of accidents in production, the following measures are provided:

1. Installation for the synthesis of 4′,4″-di-(1-methyl-1-hydroxyethynyl)-dibenzo-18-crown-6 located outside the building.
2. Automatic stroke control from the CPU.
3. Electric motors, electrical equipment, as well as automation and remote control devices installed in an explosive state.
4. To prevent the spread of diethyl ether combustion, fire arresters are installed on the lines.
5. Safety valves are installed on devices and pipelines where overpressure is possible.
6. Pipelines and devices with temperatures above 60^0C are insulated.

In addition to the above, it is necessary:

1. Have emergency supplies of serviceable filter and hose gas masks in the production area.
2. Before putting the equipment into operation, ensure the availability of raw materials, energy, water and materials. Check the installation locations of the plugs on the fittings of the devices and on the pipelines, the positions of the shut-off devices, the presence and serviceability of all necessary devices.
3. Load KOH wearing respirators and gloves.
4. Smoking and the use of open fire in the premises and on the territory of the workshop, except in specially designated areas, is prohibited.
5. Do not allow work in the presence of toxic and explosive products in the atmosphere of the premises in concentrations exceeding the permissible value.
6. Have first aid kits at work places with the necessary first aid supplies.

Table 10. *Specification of main process equipment*

Position number on the diagram	Equipment name	Quantity	Material, methods of protection	Specifications
1,2 R4	Solvent containers Reactor	2 1	Art. carbon. 12 × 18 H10 T	V=1m^3 V=2,5 m^3, P=0.-006, MPa=Pj=0.4 MPa, D_{app}=1400, D_{rub}=1500, H_{sum}=2406, N=5,5 kW, n=970 min^{-1}, $U_{сп}$=VZTU
2	Pump	1	12 × 18 H10 T	Brand 2x1–5·4,5–1. Q=10m^3/r, n=4 m. $N_{(эл.дв.)}$=4,5 kW, $N_{(эл.дв.)}$=970 min^{-1}
8	Parc	1	12 × 18 H10 T	L_{ap}=2140, D ap=273, P=6m^3
12,13,14	Containers for substances	5	Art. carbon	V=0,3m^3

Where: V – apparatus capacity, m^3; Dapp – apparatus diameter, mm; H_{app} – apparatus height, mm; L_{app} – apparatus length, mm; P_{app} – pressure in the apparatus, MPa; P_j – pressure of the coolant, in the jacket, MPa; H – pressure, m.st.zh; N – motor power, kW; n – speed, min^{-1}; Q – pump capacity, m^3/hour

Table 11. *List of mandatory workshop instructions*

	Name of instructions
13.1.	Instructions for safety and fire safety of the workshop.
13.2.	Plan for eliminating emergency situations and accidents in the workshop.
13.3.	Instructions for preparation, delivery of equipment for repair and acceptance
13.4.	from repair
13.5.	Instructions for manual control of the fire extinguishing unit in workshops.
13.6.	Instructions for stopping the workshop for major repairs and starting the workshop after major repairs.
	Instructions for the synthesis operator of the installation for the production of 4′,4″-di-(1-methyl-1-hydroxyethynyl)-dibenzo-18-crown-6
	Filter sheet for changes to the current regulations.

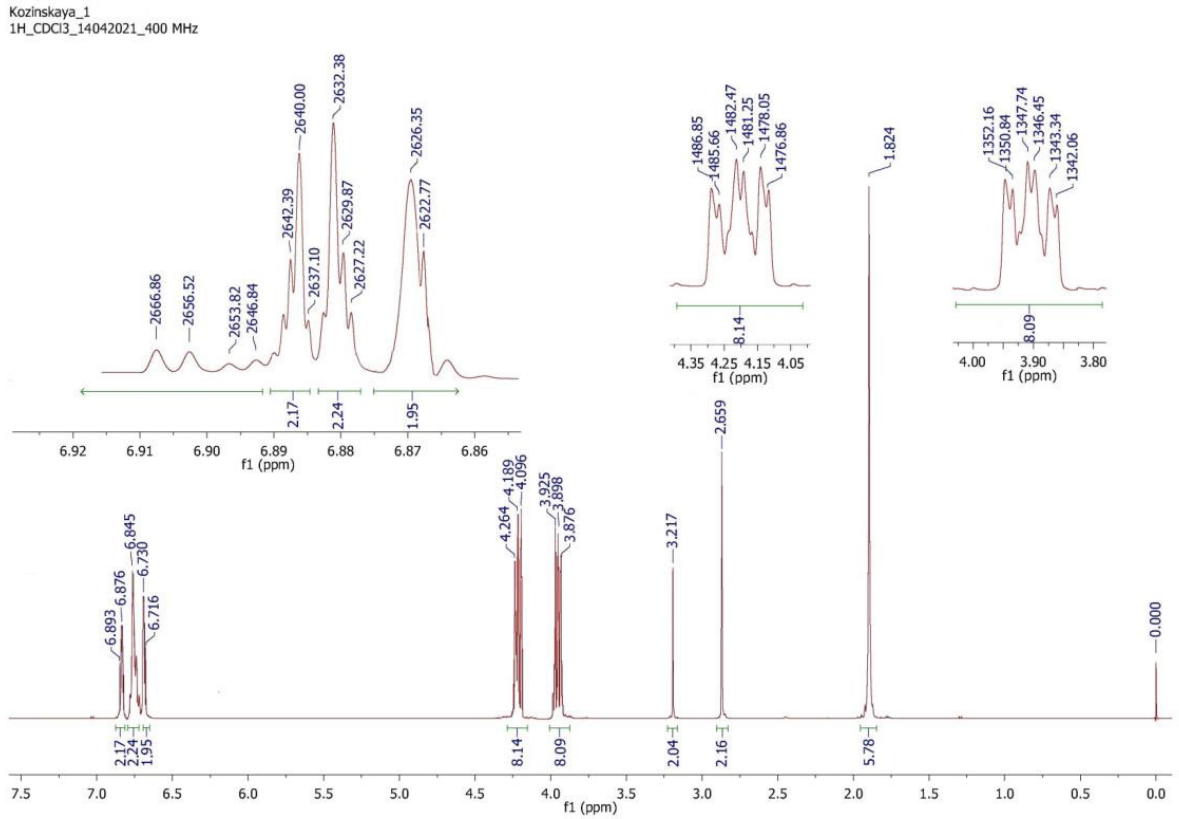

[1]H-NMR spectrum of 4′,4″-di-(1-methyl-1-hydroxyethynyl)-dibenzo-18-crown-6

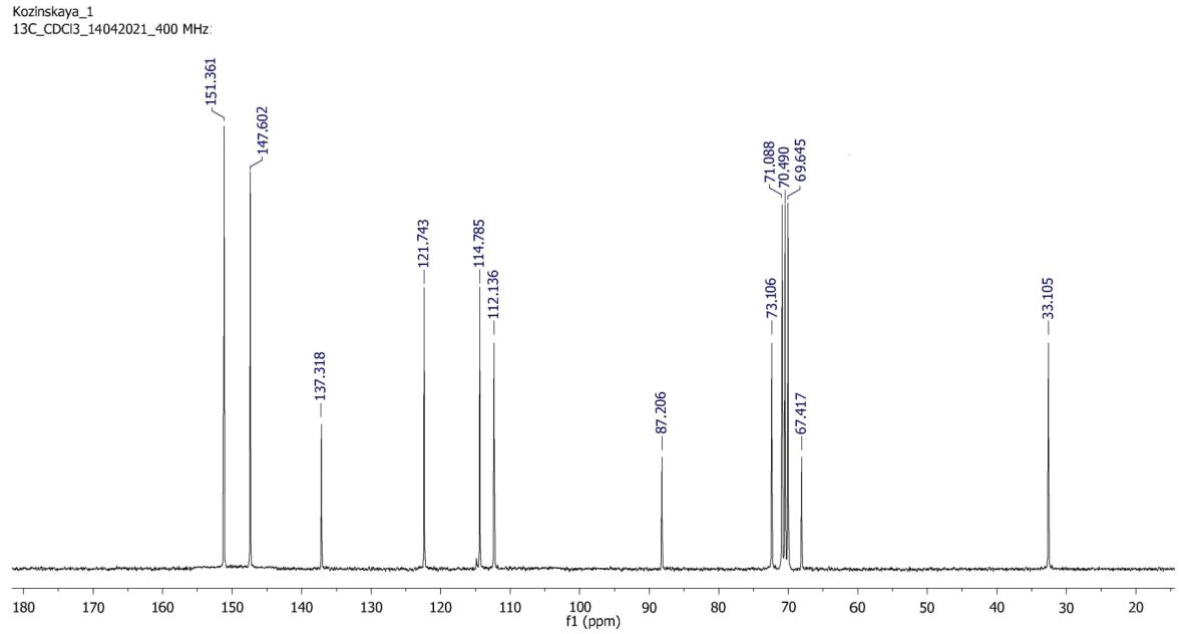

[13]C-NMR spectrum of 4′,4″-di-(1-methyl-1-hydroxyethynyl)-dibenzo-18-crown-6

References

Ma X., Wei H., Luo Z. (2024). *Reviews in Chemical Engineering* 2024. – 40 (8). – P. 917–949. URL: https://doi.org/10.1021/acsapm.5c02860

Trujillo-Lemon M. (2025). *Polymer Chemistry*, 2025. – 16 (10). – P. 1176–1187. DOI: 10.1039/D4PY01337A

Shuhrat o'g'li. O. B. (2025). *Web of Medicine: Journal of Medicine, Practice and Nursing*, 2025. – 3 (4). – P. 182–186.

Bedenko S. P., Dement'ev K. I., Maximov A. L. (2022). *Petroleum Chemistry*, 2022. – 62 (9). – P. 989–1026. DOI: 10.1134/S0965544122090031

Fromme T., Reichenberger S., Tibbetts K. M., Barcikowski S. (2024). *Beilstein Journal of Nanotechnology*, 2024. – 15 (1). – P. 638–663. DOI: 10.3762/bjnano.15.54

Agbaba O., Trotus I. T., Schmidt W., Schüth F. (2023). *Industrial & Engineering Chemistry Research*, 2023. – 62 (4). – 1819–1825. URL: https://doi.org/10.1021/acs.iecr.2c03430

Zhang Z., Nabera A., Guillén-Gosálbez G., Pérez-Ramírez J. (2025). *Nature Chemical Engineering*, 2025. – P. 1–11. DOI:10.1038/s44286-025-00185-y

Kozinskaya L., Mirkhamitova D. (2021). *Science and Peace*, 2021. – (4). – P. 18–21.

Favorsky A. E. (1905). *Journal of the Russian Physical and Chemical Society*, 1905. – 37. – P. 643–645.

Reutov O. A., Kurts A. L., Butin K. P. (2021). *Organic chemistry*. 2021. – 4. – P. 35–52.

submitted 08.10.2025;
accepted for publication 22.10.2025;
published 26.11.2025

Contact: lubasha_1985@mail.ru

DOI:10.29013/AJT-25-9.10-34-39

SYNTHESIS, CRYSTAL STRUCTURE AND PROPERTIES OF A NEW BI-DENTATE DECAVANADATE $[CO(H_3SO_3)+(H_2O)_5]_2[H_2V_{10}O_{28}]\cdot 2H_2O\cdot 2SO_3$

Mehribon Pirimova [1], ***Malika Yakubxodjayeva*** [1], ***Muparrax Xodjayeva*** [1]

[1] Tashkent State Medical University, Tashkent, Uzbekistan

Cite: *Pirimova M., Yakubxodjayeva M., Xodjayeva M. (2025). Synthesis, crystal structure and properties of a new bi-dentate decavanadate* $[Co(H_3SO_3)+(H_2O)_5]_2[H_2V_{10}O_{28}]\cdot 2H_2O\cdot 2SO_3$. *Austrian Journal of Technical and Natural Sciences 2025, No 9–10.* https://doi.org/10.29013/AJT-25-9.10-34-39

Abstract

A new bi-dentate decavanadate compound formulated $[Co(H_3SO_3)^+(H_2O)_5]_2[H_2V_{10}O_{28}]\cdot 2H_2O\cdot 2SO_3$ (1), has been synthesized under hydrothermal condition by using sulfuric acid as the initiator at 110 °C. And 1 crystallizes in the triclinic, space group P-1 with a = 9.8954(7) Å, b = 10.4827(9) Å, c = 12.8466(7) Å, α = 76.395(6), β = 82.024(6), γ = 68.836(7), V = 1205.7 Å^3, R1(I > 2s(I) = 3.61), and Z = 5. X-ray diffraction analysis reveals that 1 is constructed from bi-dentate decavanadate formed by decavanadate clusters coordinated to $[Co(H_3SO_3)^+(H_2O)_5]^{2+}$ complexes and free water molecules.

Keywords: *X-ray diffraction, cobalt complex, polyoxovanadate, sulfate coordination, triclinic crystal structure, supramolecular assembly*

Introduction

Polyoxometalates (POMs) are a unique class of metal-oxygen clusters that display remarkable structural diversity and a wide range of physicochemical properties. Among them, polyoxovanadates (POVs), particularly decavanadate anions $[H_nV_{10}O_{28}]^{6-}$, have attracted significant attention due to their high stability in acidic media, versatile coordination behavior, and potential applications in catalysis, materials science, and biomedicine (Liu, H., Wang, J., Jian, F., & Xiao, H., 2009; Msaadi, I., Rayes, A., Benito, M., Issaoui, N., Molins, E., & Ayed, B., 2022). The decavanadate unit, which consists of ten edge-sharing VO_6 octahedra, exhibits rich structural chemistry and can form hybrid frameworks with transition metal ions and organic ligands.

Transition metal–POM hybrids have become an important area of research due to their multifunctional characteristics, such as redox activity, magnetism, photoluminescence, and catalytic efficiency. In particular, cobalt-based polyoxovanadate complexes have been intensively studied because Co(II) ions can provide redox flexibility and variable coordination geometries, leading to extended hydrogen-bonded supramolecular architectures. Moreover, their synthesis under hydrothermal or aqueous acidic conditions often results in well-defined crystalline frameworks stabilized by

extensive O–H···O interactions (Pope, M. T., & Müller, A., 2001).

Recent investigations have demonstrated that modifying the cationic environment or introducing auxiliary ligands, such as protonated amines or sulfate groups, significantly influences the structural organization and electronic properties of decavanadate-based systems (Hill, C. L., 1998). These hybrid materials have shown potential as model systems for redox catalysis, photoactive materials, and biologically active agents due to their stability and charge-transfer capabilities.

In this study, we report the X-ray crystal structure of a new cobalt(II)–polyoxovanadate complex formulated as $0.4(H_{13}CoO_8S)\cdot 0.2(H_2O_{28}V_{10})\cdot 0.4(O_3S)\cdot 0.4(H_2O)$. The complex was synthesized under mild aqueous conditions using cobalt(II) nitrate, sodium metavanadate, and sodium sulfate, and characterized by single-crystal X-ray diffraction. The structure reveals a triclinic crystal system (space group $P1^-$) composed of Co(II) centers octahedrally coordinated by oxygen atoms from sulfate and polyoxovanadate groups. The study focuses on the crystallographic parameters, coordination geometry, and supramolecular hydrogen-bonding framework of the newly obtained compound, contributing to a deeper understanding of cobalt–decavanadate hybrid assemblies.

Materials and Methods

Synthesis of the Complex

The complex was obtained by slow evaporation of an aqueous solution containing cobalt(II) nitrate, sodium metavanadate, and sodium sulfate in stoichiometric proportions. The reaction mixture was kept at room temperature for several days, during which blue crystals suitable for X-ray diffraction were formed.

X-ray Diffraction Analysis

Single-crystal X-ray diffraction data were collected on a Bruker D8 QUEST diffractometer using Mo Kα radiation (λ = 0.71073 Å) at 298 K. The structure was solved by direct methods and refined by full-matrix least squares on F^2 using SHELX-2018 software.

The compound crystallizes in the triclinic crystal system with space group $P1^-$. Crystallographic parameters:

Picture 1. *The chemical formula was refined as $0.4(H_{13}CoO_8S)\cdot 0.2(H_2O_{28}V_{10})\cdot 0.4(O_3S)\cdot 0.4(H_2O)$, confirming the presence of both cobalt–sulfate and polyoxovanadate fragments*

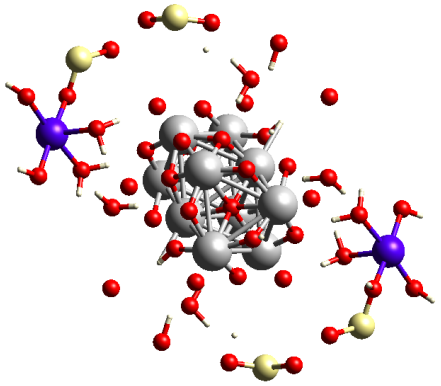

Formula	$0.4(H_{13}Co\,O_8\,S),0.2(H_2\,O_{28}\,V_{10}),0.4(O_3\,S),0.4(H_2\,O)$
Formula weight	321.22 g/mol
Crystal system	triclinic
Space-group	P –1 (2)
Cell parameters	a=9.895(7) Å, b=10.482(9) Å, c=12.846(7) Å α=76.395(6)° β=82.024(6)° γ=68.836(7)°
Cell ratio	a/b=0.9440 b/c=0.8160 c/a=1.2982
Cell volume	1205.70(17) Å^3
Z	5
Calc. density	2.21185 g/cm^3
RAll	0.189
R(I>2σ(I))	3,61
Temperature	Room Temp.(283–303)
Packing coefficient	0.685956

3. Results and Discussion

3.1. Molecular and Crystal Structure

The cobalt(II) ion is octahedrally coordinated by oxygen atoms from sulfate and polyoxovanadate groups. The Co–O bond lengths range between 2.04–2.21 Å, typical for Co(II)–O coordination. The asymmetric

unit also includes crystallization water molecules that participate in hydrogen bonding. The polyoxovanadate cluster ($H_2O_{28}V_{10}$) acts as a polynuclear anion with bridging oxygen atoms connecting vanadium centers. Sulfate groups serve as charge-compensating and hydrogen-bond donors, leading to the formation of an extended 3D network.

Picture 2. *The appearance of the complex compound* $[Co(H_3SO_3)(H_2O)_5]_2[H_2V_{10}O_{28}]\cdot 2H_2O\cdot 2SO_3$ *in the a, b, and c projections*

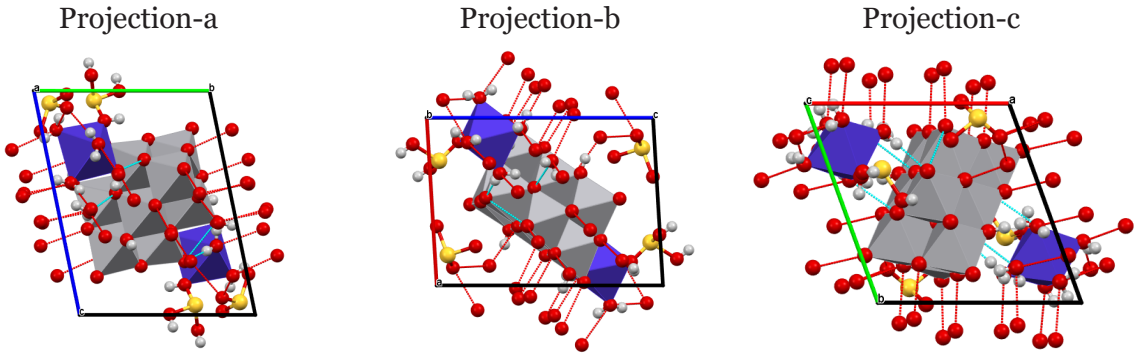

Table 1.

Atomic parameters							
Atom	**Ox.**	**Wyck.**	**Site**	**x/a**	**y/b**	**z/c**	**U [Å²]**
Co01		2i	1	–0.1063(2)	0.7681(2)	0.73379(15)	
V02		2i	1	0.3489(2)	0.4743(2)	0.55360(15)	
V03		2i	1	0.6236(2)	0.2269(2)	0.48889(15)	
V004		2i	1	0.5478(2)	0.5437(2)	0.68995(14)	
V005		2i	1	0.5297(2)	0.2462(2)	0.72770(15)	
V006		2i	1	0.8113(2)	0.2974(2)	0.62959(16)	
S00		2i	1	–0.2565(3)	0.6689(4)	0.9565(3)	
S1		2i	1	0.1806(3)	0.9260(4)	0.9435(3)	
O009		2i	1	0.4177(9)	0.3477(8)	0.4565(6)	
O00A		2i	1	0.3552(9)	0.6149(9)	0.6258(7)	
O00B		2i	1	0.5569(9)	0.1447(9)	0.6171(7)	
O00C		2i	1	0.4216(8)	0.6018(8)	0.4233(6)	
O00D		2i	1	0.8069(9)	0.1881(9)	0.5282(7)	
O00E		2i	1	0.7286(9)	0.1938(9)	0.7356(6)	
O00F		2i	1	0.7459(8)	0.4513(9)	0.6928(6)	
O00G		2i	1	0.3326(9)	0.3552(8)	0.6653(6)	
H00K		2i	1	0.2440(15)	0.377(7)	0.689(4)	0.0050
O00H		2i	1	–0.079(1)	0.6158(9)	0.6422(8)	
H00A		2i	1	–0.05864	0.64640	0.57620	0.0180
H00B		2i	1	–0.15981	0.60352	0.64161	0.0180
O00I		2i	1	0.5000(9)	0.4053(9)	0.7821(7)	
O00J		2i	1	0.1801(9)	0.5571(9)	0.5115(7)	
O00K		2i	1	–0.1478(9)	0.9178(9)	0.8258(8)	
H00C		2i	1	–0.13171	0.99311	0.78791	0.0170

Atomic parameters							
Atom	**Ox.**	**Wyck.**	**Site**	**x/a**	**y/b**	**z/c**	**U [Å²]**
H00D		2i	1	–0.08588	0.88919	0.87639	0.0170
O00L		2i	1	0.5231(9)	0.6601(9)	0.7612(7)	
O00M		2i	1	–0.0677(10)	0.8953(9)	0.5893(7)	
H00E		2i	1	0.01649	0.85425	0.55741	0.0160
H00F		2i	1	–0.05713	0.97084	0.60056	0.0160
O00N		2i	1	–0.3305(10)	0.8586(10)	0.6927(9)	
H00G		2i	1	–0.37362	0.79774	0.71493	0.0250
H00H		2i	1	–0.33602	0.87743	0.62395	0.0250
O00O		2i	1	0.6461(10)	0.1144(9)	0.4154(7)	
O00P		2i	1	0.1168(10)	0.6939(12)	0.7615(8)	
H00I		2i	1	0.13254	0.72733	0.81293	0.0260
H00J		2i	1	0.16564	0.72593	0.70615	0.0260
O00Q		2i	1	0.9802(10)	0.2366(11)	0.6510(8)	
O00R		2i	1	0.4828(10)	0.1427(10)	0.8312(7)	
O00S		2i	1	–0.1409(10)	0.6337(9)	0.8654(8)	
H00S		2i	1	–0.101(14)	0.5456(17)	0.874(7)	0.0260
O00T		2i	1	0.2580(11)	0.1756(11)	0.5412(10)	
H00L		2i	1	0.34396	0.16030	0.55664	0.0310
H00M		2i	1	0.26528	0.10814	0.51232	0.0310
O00		2i	1	0.1058(11)	0.8316(12)	0.9238(10)	
O00V		2i	1	–0.3018(17)	0.5143(16)	0.9979(13)	
H00V		2i	1	–0.35064	0.51675	1.05490	0.0680
O00W		2i	1	–0.1573(18)	0.6547(19)	1.0686(13)	
H00W		2i	1	–0.21077	0.65544	1.12342	0.0780
O1		2i	1	0.352(2)	0.817(3)	0.984(2)	
O2		2i	1	0.233(4)	1.009(4)	0.818(2)	

Table 2. *Torsion bond angle*

Atoms 1,2,3,4	**Tors. an. 1,2,3,4 [°]**	**Atoms 1,2,3,4**	**Tors. an. 1,2,3,4 [°]**
V02-V005-O00E-V006	2.1(6)	O00C–V02-O00J-V006^{i}	1.9(4)
V02-V005-O00I–V004	–52.1(4)	O00C–V02-O00J-V006^{i}	0.9(19)
V02-V006-O00E-V005	–3.2(6)	O00C–V03-O00B-V005	–8.6(4)
V02-V006-O00F-V004	55.1(4)	O00C–V03-O00D-V006	9.7(4)
V03-V004-O00F-V006	–86.2(5)	O00C–V004-O00F-V006	–11.1(4)
V03-V004-O00I–V005	82.0(5)	O00C–V004-O00I–V005	6.8(4)
V03-V005-O00E-V006	48.2(4)	O00C–V005-O00E-V006	2.2(4)
V03-V005-O00I–V004	–6.3(6)	O00C–V005-O00I–V004	–6.7(4)
V004-V03-O00B-V005	–85.8(5)	O00C–V006-O00E-V005	–2.2(4)
V004-V03-O00D-V006	86.2(5)	O00C–V006-O00F-V004	11.0(4)

Atoms 1,2,3,4	Tors. an. 1,2,3,4 [°]	Atoms 1,2,3,4	Tors. an. 1,2,3,4 [°]
V004-V005-O00E-V006	–44.8(4)	O00D-V03-O00B-V005	71.4(5)
V004-V006-O00E-V005	45.0(4)	O00D-V006-O00E-V005	–79.1(5)
V005-V02-O00J-V006^{i}	–178.73(15)	O00D-V006-O00F-V004	29.8(11)
V005-V03-O00D-V006	–38.5(4)	O00E-V005-O00I–V004	73.8(5)
V005-V004-O00F-V006	37.1(4)	O00E-V006-O00F-V004	–70.3(5)
V005-V006-O00F-V004	–37.6(4)	O00F-V004-O00I–V005	–71.7(5)
V006-V02-O00G-V005	178.44(16)	O00F-V006-O00E-V005	76.1(5)
V006-V004-O00I–V005	–41.1(4)	O00G-V02-O00J-V006^{i}	–178.1(4)
V006-V005-O00I–V004	41.5(4)	O00G-V005-O00E-V006	3.3(12)
O009-V02-O00G-V005	80.3(4)	O00G-V005-O00I–V004	–83.2(5)
O009-V02-O00J-V006^{i}	–78.7(4)	O00I–V004-O00F-V006	68.3(5)
O009-V03-O00B-V005	–84.9(5)	O00I–V005-O00E-V006	–75.4(5)
O009-V03-O00D-V006	31.7(11)	O00J-V02-O00G-V005	–179.4(4)
O009-V004-O00F-V006	–86.2(5)	O00J-V006-O00E-V005	–8.4(12)
O009-V004-O00I–V005	25.2(11)	O00J-V006-O00F-V004	86.2(5)
O00A-V02-O00G-V005	–79.8(4)	O00L–V004-O00F-V006	174.1(5)
O00A-V02-O00J-V006^{i}	82.2(4)	O00L–V004-O00I–V005	–175.6(5)
O00A-V03-O00B-V005	–33.5(12)	O00O-V03-O00B-V005	176.3(5)
O00A-V03-O00D-V006	86.1(5)	O00O-V03-O00D-V006	–174.6(5)
O00A-V004-O00F-V006	–34.8(11)	O00Q-V006-O00E-V005	179.8(5)
O00A-V004-O00I–V005	83.6(5)	O00Q-V006-O00F-V004	–176.7(5)
O00B-V03-O00D-V006	–70.9(5)	O00R-V005-O00E-V006	–178.5(5)
O00B-V005-O00E-V006	79.5(5)	O00R-V005-O00I–V004	177.8(5)
O00B-V005-O00I–V004	–20.3(12)	O00V-S00-O00S-Co01	147.0(9)
O00C–V02-O00G-V005	0.4(18)	O00W-S00-O00S-Co01	–108.6(10)
O00C–V02-O00G-V005	0.8(4)		

(i) 1-x, 1-y, 1-z.

Hydrogen Bonding and Packing Analysis

Intermolecular O–H···O hydrogen bonds link neighboring clusters, creating a layered supramolecular arrangement along the b-axis. Weak van der Waals forces stabilize the packing along c. The overall structure displays a typical polyoxometalate–transition metal framework with water-mediated hydrogen bridges.

Crystallographic Features

The triclinic symmetry ($P1^{-}$) results in non-equivalent Co–O coordination environments, indicating slight distortions from ideal octahedral geometry. The moderate cell volume (V = 1205.7 Å^3) suggests dense packing with strong inter-anionic interactions.

Conclusion

The single-crystal X-ray diffraction study revealed that the synthesized cobalt–polyoxovanadate complex crystallizes in a triclinic system (space group $P1^{-}$) with mixed sulfate and vanadate anionic species. The structure consists of Co(II) centers octahedrally coordinated by oxygen donors, forming a robust hydrogen-bonded framework. These findings

contribute to the understanding of cobalt–POM hybrid materials and open perspectives for their potential applications in redox catalysis and materials chemistry.

References

Liu, H., Wang, J., Jian, F., & Xiao, H. (2009). *Synthesis and crystal structure of two decavanadates cluster metal complexes: [Co(H2O)6]2[H2V10O28]·6H2O and (NH4)2[Ca(H2O)7]2[V10O28]. Journal of Cluster Science,* – 20(4). – P. 621–627. URL: https://doi.org/10.1007/s10876-009-0265-2

Msaadi, I., Rayes, A., Benito, M., Issaoui, N., Molins, E., & Ayed, B. (2022). *A combined experimental and theoretical study of two new decavanadates: (C6N2H9)4[H2V10O28]·4H2O and (C7H9NF)4[H2V10O28]·2H2O. Journal of Molecular Structure, – 1262*. – 133085 p. URL: https://doi.org/10.1016/j.molstruc.2022.133085

Pope, M.T., & Müller, A. (2001). *Polyoxometalate Chemistry: From Topology via Self-Assembly to Applications*. Springer.

Hill, C.L. (1998). *Polyoxometalates: Reactivity and catalytic applications. Chemical Reviews, – 98*(1). – P. 1–390. URL: https://doi.org/10.1021/cr9603980

Sheldrick, G.M. (2015). *Crystal structure refinement with SHELXL. Acta Crystallographica Section C: Structural Chemistry,* – 71(1). – URL: 3–8. https://doi.org/10.1107/S2053229614024218

Sheldrick, G.M. “Crystal structure refinement with SHELXL.” Acta Crystallographica Section C 71 (2015): 3–8.

Pope, M.T., Müller, A. Polyoxometalate Chemistry: From Topology via Self-Assembly to Applications. Springer, 2001.

Hill, C.L. “Polyoxometalates: Reactivity and Catalytic Applications.” Chemical Reviews – 98. – No. 1 (1998): 1–390.

pirimova021293@gmail.com

submitted 14.09.2025;
accepted for publication 28.09.2025;
published 26.11.2025

Contact: pirimova021293@gmail.com

The Austrian Journal of Technical and Natural Sciences, No 9–10
ISSN 2310-5607

PREMIER Publishing
ppublishing.org

DOI:10.29013/AJT-25-9.10-40-45

CHROMATOGRAPHIC-MASS SPECTRUM ANALYSIS OF BIOLOGICALLY ACTIVE SUBSTANCES SEPARATED FROM THE HEXANE EXTRACT OF FUNGUS FUSARIUM OXYSPORUM SCHLECHT BELONGING TO THE CATEGORY FUSARIUM

***Ruzieva Zarnigor*[1], *Kamolov Lukmon*[1], *Gulboeva Dilafruz*[1], *Hasanova Madina*[1], *Jovliyev Shakhriyor*[1], *Meyliyeva Muxlisa*[2]**

[1] Faculty of Chemistry and Biology, Karshi State University, Uzbekistan, Karshi

[2] Faculty of Medicine, Turon University, Uzbekistan, Karshi

Cite: *Ruzieva Z., Kamolov L., Gulboeva D., Hasanova M., Jovliyev Sh., Meyliyeva M. (2025). Chromatographic-Mass Spectrum Analysis of Biologically Active Substances Separated From the Hexane Extract of Fungus Fusarium Oxysporum Schlecht Belonging to the Category Fusarium. Austrian Journal of Technical and Natural Sciences 2025, No 9–10*. https://doi.org/10.29013/AJT-25-9.10-40-45

Abstract

In recent years, the type of microfungi that have a pathogenic effect on many micronutrients plants has been on the rise. But these fungi themselves also have the ability to synthesize biologically active metabolites. In our research, we aimed to investigate the fungal metabolites of the constellation Fusarium. Hexane extract of cultivated biomass of *Fusarium oxysporum Schlecht* fungus at 6–7 days were analyzed by the GC–MS method and a wide variety of substances were revealed. In this study, secondary metabolites of hexane extract obtained from the cultured biomass of Fusarium oxysporum Schlecht fungus for 6–7 days were analyzed. Gas chromatography–mass spectrometry (GC–MS) revealed a number of bioactive compounds, including 4-(1,1,3,3-tetramethylbutyl)phenol, methyl sis-3-[p-anisido]acrylate, formic acid, 1-(4,7-didro-2-methyl-7-oxopyrazolo[1,5-a]pyrimidine-5-yl)-, methyl ether, galactose, 4,6-O-nonidene, and 2,6-di-gesaddecanoate ether of L-(+)-ascorbic acid. These substances belong to the class of phenolic derivatives, acrylate ethers, nitrogen-sparing heterocyclic systems, carbohydrate complexes and ascorbate ethers of lipid nature and confirm the metabolic diversity of the fungus. The identified metabolites are distinguished by their antioxidant, antimicrobial, and cytoprotective properties, which indicates their practical value for fields of pharmaceuticals and biotechnology. The results obtained indicate that the species Fusarium oxysporum is structurally diverse and a source of biologically active natural compounds. In the future, it is promising to study these substances through isolation and mechanism studies on deeper bioactivity.

Keywords: *Fusarium oxysporum Schlecht, hexane extract, secondary metabolites, GC–MS, bioactive compounds, phenolic derivatives, ascorbate ethers.*

Log in

In recent years, biologically active metabolites of plant-pathogenic fungi have aroused special interest in science and practice. In particular, fatty acids, phenolic compounds, and various volatile organic compounds synthesized by strains belonging to the order Schlecht Fusarium oxysporum have been found to have broad-spectrum biological interactions (Raffaele et al., 2009; Liu et al., 2008). These microorganisms are studied not only as disease-causative pathogens in plants, but also as a source of secondary metabolites (Druzhinina et al., 2011). Many studies have shown that the substances isolated from the biomass or extract of Fusarium oxysporum Schlecht have antifungal, antibacterial, and cytotoxic properties (Pan et al., 2013; Stracquadanio et al., 2020). For example, fatty acids and sterol derivatives from hexane extracts may regulate plant–pathogen interactions in the soil microbiota (Abdel-Naime et al., 2019; Ding et al., 2019). Among such metabolites, cytotoxic and antimicrobial active substances have also been noted (Davis et al., 1997; Ghavam et al., 2021). Fatty acids, including palmitic, linoleic, and palmitoleic acids, have been recorded in many micromycetes, and they play important roles in natural defense mechanisms against plant diseases (Guo et al., 2010; Perez-Vich et al., 2016; Zhao et al., 2019). Among the many volatile metabolites identified through GC–MS analyses, benzene derivatives, terpenoids, and phenolic isomers are of particular importance (Reghmit et al., 2024; Azami et al., 2024; Nitish and Kumar, 2017). Such metabolites have been extensively studied in many studies on the genera Trichoderma and Fusarium (Ivan et al., 2023; Zeiad et al., 2023). There are prospects for application of the isolated secondary metabolites from extracts of F. oxysporum in pharmaceutical, agricultural, and biotechnology fields. Some of them inhibit the growth of pathogenic microorganisms and stimulate plant growth (Singh et al., 2021; Gajera et al., 2020). Also, substances identified in different extracts are being proposed as novel biomarkers (Khairillah et al., 2021; Jurakulova and Kamolov, 2021). Therefore, the aim of this study is to determine the composition of bioactive substances isolated from the hexane extract of Fusarium oxysporum and to elucidate their biological significance (Nomozova et al., 2025; Kamolov et al., 2021; Van Leeuwen et al., 2008). Substances identified through GC–MS. The application of antitumor, antioxidant, antimicrobial, and growth-stimulating properties of these fungal metabolites by researchers in the fields of pharmaceuticals, biotechnology, and agriculture is a promising direction. Also, studies by (Mishra et al., 2022) and Rahman and Singh (2023) have found that secondary metabolites synthesized by certain strains belonging to the genus Fusarium increase beneficial microorganism activity in plant root zones while inhibiting the growth of plant pathogens. El-Hassan et al., 2024) have highlighted the potential of these metabolites as bioconcentrates in the development of environmentally friendly fertilizers and pesticides. Therefore, the main goal of the present investigation is to determine the composition of bioactive substances isolated from hexane extract of Fusarium oxysporum, to analyze their biological activity and to elucidate the practical value of the obtained results. Research in this direction provides an important scientific basis for the development of environmentally friendly biotechnological solutions for the control of plant pathogens.

Research methodology

1. Fungal cultivation and biomass preparation

The strain of Fusarium oxysporum Schlecht was isolated from the soil and stored under sterile conditions. For experiment, fungus was incubated in a potato dextrose agar (PDA) environment at a temperature of 24.5–28 °C for 6–7 days. Subsequently, 250 ml of Potato Dextrose Broth (PDB) feed medium was poured into 500 ml Erlenmeyer tubes and a suspension of 107–108 spores/ml concentration was inoculated into it. Fungal biomass was isolated from the cultured liquid cultured for 6–7 days in the shaker incubator (180 rpm). The resulting biomass was washed with distilled water, dried at high 38 °C temperature and used in the following extraction process.

2. Extract using hexane

To extract bioactive substances from the dried biomass, an extraction apparatus was used. 50 g of dried litter powder were extracted for 8–10 hours with 500 mL hexane. The resulting crude extract was concentrated under vacuum using a rotary evaporator (Büchi R-210) at a temperature of 40 °C. The result

was a dark yellow extract. The extract, comprising of a total complex of secondary metabolites, was given to chromatographic mass spectrum for determination of biologically active compounds contained in the formed yellow extract.

Results and discussion

Hexane extract from the grown biomass of Fusarium oxysporum Schlecht fungus for 6–7 days was analyzed using gas chromatography–mass spectrometry (GC–MS). According to the results of the analysis, several bioactive components were revealed in the extract, indicating that they contained such substances as 4-(1,1,3,3-tetramethylbutyl) phenol, methyl sis-3-[p-anisido]acrylate, formic acid, 1-(4,7-didro-2-methyl-7-oxopyrazolo[1,5-a]pyrimidine-5-yl)-, methyl ether, galactose, 4,6-O-nonidene, and I-(+)-ascorbin acid, 2,6-dihexadecanoate.

Figure 1. *Spectrum of phenol 4-(1,1,3,3-tetramethylbutyl) substance obtained by GC–MS method*

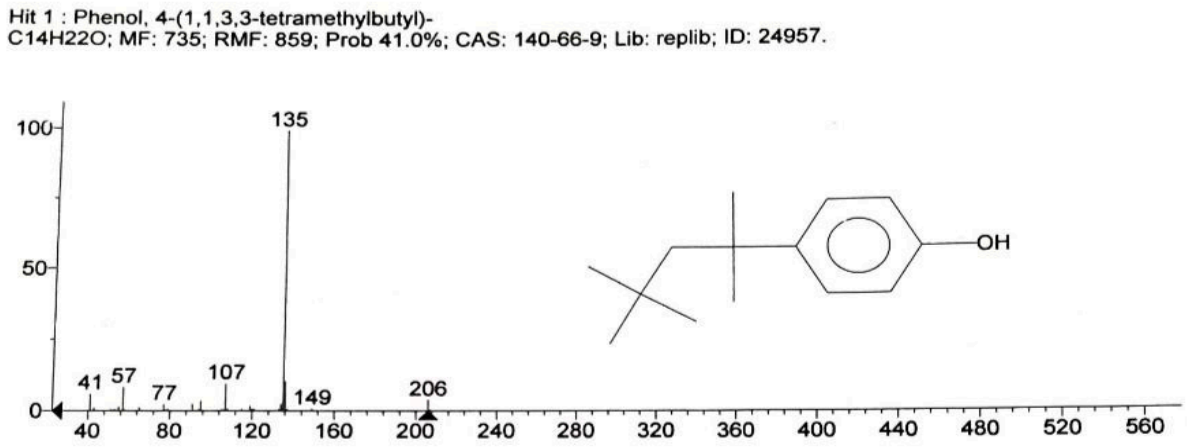

The chemical structure and bioactive properties of the identified compounds indicate their synthesis through various metabolic pathways. 4-(1,1,3,3-tetramethylbutyl)phenol is a substance of phenolic nature, which has a strong antioxidant and antimicrobial effect was previously noted in fungi of the genus Aspergillus and Penicillium. Its presence indicates the presence of protective mechanisms in the fungus of F. oxysporum that inhibit lipid peroxidation processes.

Figure 2. *Spectrum of methylcis-3-[p-anisido]acrylate obtained by GC–MS method*

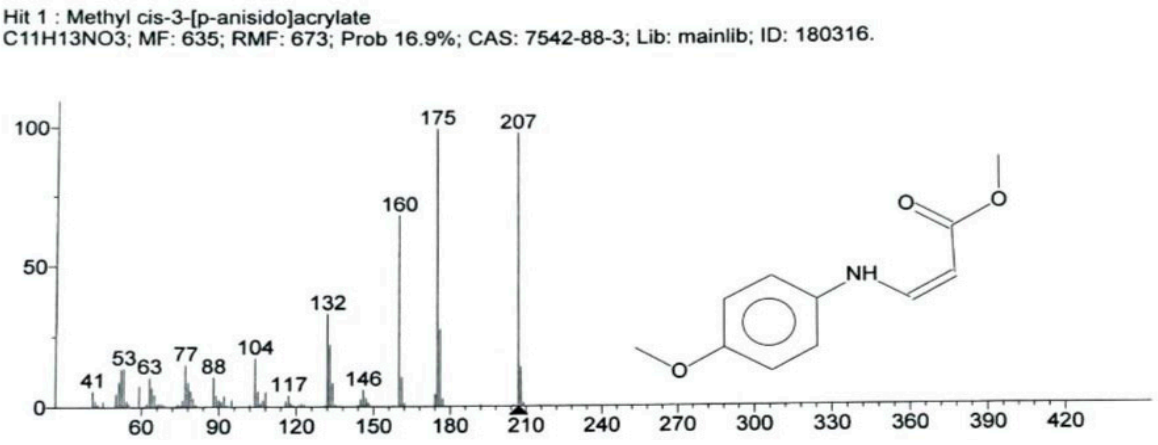

Meanwhile, methyl sis-3-[p-anisido]acrylate belongs to the class of acrylate ethers and is characterized by anti-inflammatory and antibacterial activity. The presence of this compound indicates the presence of a complex biosynthetic pathway of phenolic and etheric components in the genus Fusarium.

Figure 3. *Spectrum of formic acid, 1-(4,7-dihydro-2-methyl-7-oxopyrazolo[1,5-a] pyrimidin-5-yl)-methyl ester obtained by GC–MS method*

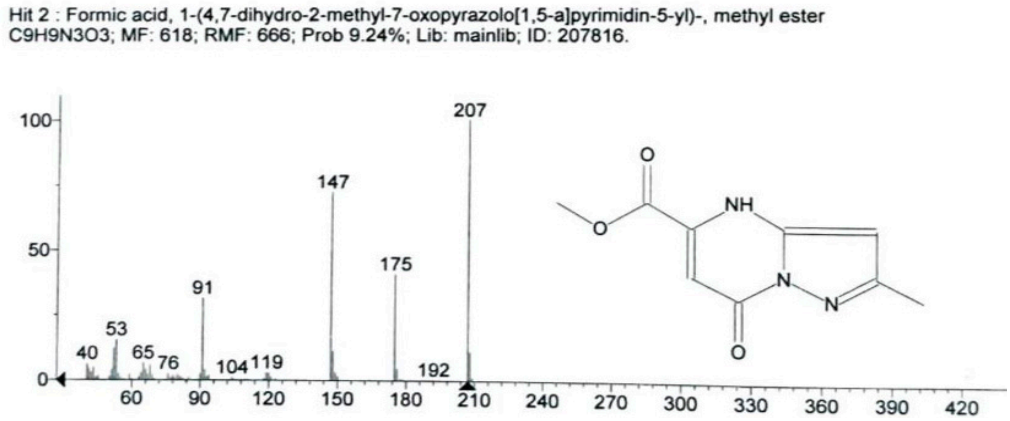

It is also noteworthy as a substance with a nitrogenous heterocyclic system, 1-(4,7-didro-2-methyl-7-oxopyrazolo[1,5-a] pyrimidine-5-yl)-, methyl ether, which is a derivative of formic acid. Compounds in this class have been reported in most literature as having antitumor, antifungal, and cytotoxic activity. Their presence suggests that the species F. oxysporum has the ability to form pyrozolo and pyrimidine rings during the process of secondary metabolite biosynthesis.

Figure 4. *Spectrum of Galactose, 4,6-O-nonydene obtained by GC–MS method*

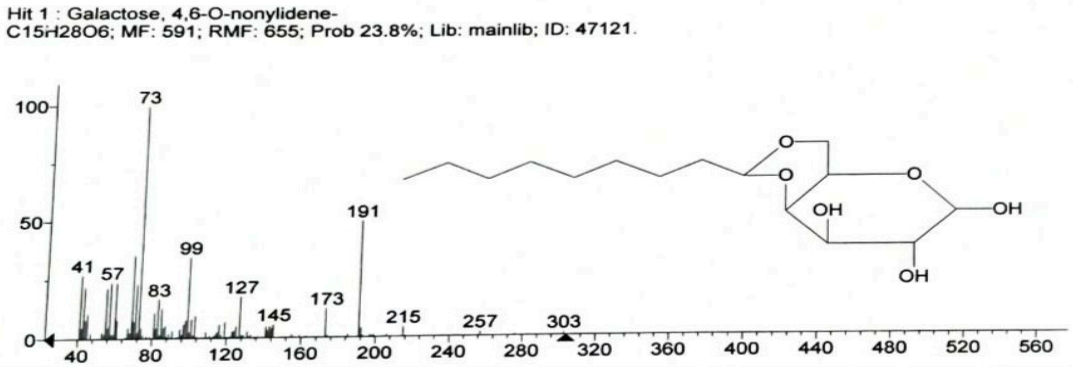

Galactose, 4,6-O-nonidene, is a carbohydrate complex substance that performs protective functions in connection with glycosides and polysaccharides. Compounds of this type play an important role in maintaining the stability of the fungal cell wall, as well as in regulating metabolic balance.

Figure 5. *Spectrum of L-(+)-Ascorbic acid, 2,6-dihexadecanoate, obtained by GC–MS method*

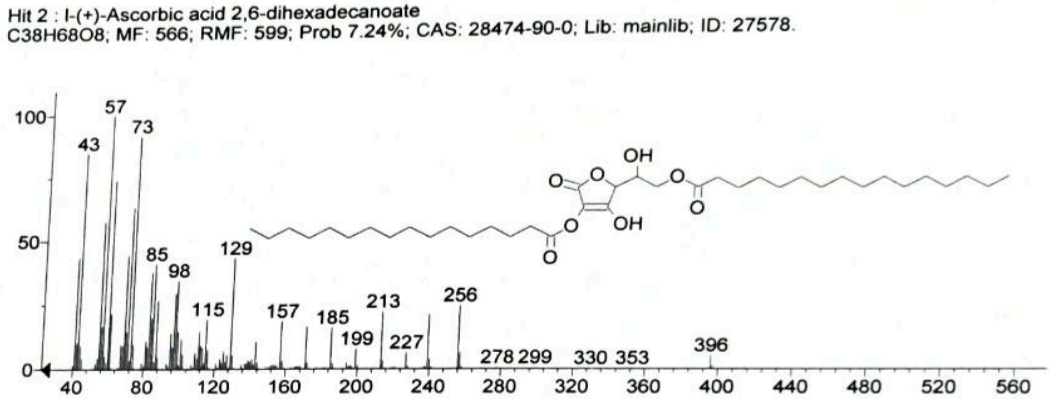

The 2,6-di-hesadekanoate ether of L-(+)-ascorbic acid is an ascorbate derivative of lipid nature and is characterized by its strong antioxidant and membrane-protecting activity. Such compounds confirm that it was formed as a natural defense system against oxidative stress in microfungi such as F. oxysporum. This substance is the esterified form of ascorbic acid with fatty acids, which actively functions in the lipophilic environment in the cell membrane.

Table 1. *Extracts from the hexane extract of the grown biomass of Fusarium oxysporum Schlecht fungus in 6–7 days*

No	Substance Name	Chemical formula	Molecular mass (g/mol)	RT (min)
1.	4-(1,1,3,3-tetramethylbutyl)-phenol	C14H22O	206.32	11.635
2.	Methylcis-3-[p-anisido]acrylate	C11H13NO3	205,9	13,928
3.	Formic acid, 1-(4,7-dihydro-2-methyl-7-oxopyrazolo[1,5-α]pyrimidine-5-yl)-, methyl ester	C9H9N3O3	206,1	13,951
4.	Galactose, 4,6-O-nonydene	C15H28O6	302,5	14,090
5.	L-(+)-Ascorbin acid, 2,6-dihexadecanoate	C38H68O8	648,2	14,114

In Table 1, the increase in the RT value shows a delay in the release time as the mass and nonpolarity of the molecules increase. Therefore, among the substances in the table, phenols and ethers are eliminated more quickly, and shaker and ascorbin derivatives are more slower. Overall, the identified metabolites indicate that the fungus F. oxysporum has high biochemical adaptability and the potential to form a second-second metabolite. The diversity of the composition of these substances opens promising areas for their pharmacological application. In particular, phenolic and ascorbate derivatives can be used in the development of antimicrobial, antioxidant and antitumor drugs, and acrylate and pyrosolo-pyrimidine derivatives in the study of bioactive synthesis pathways. The results indicate that Fusarium oxysporum fungus is a potential biotechnological facility capable of synthesizing complex, biologically active metabolites. Therefore, future research should be directed towards identifying the bioactivity, toxicological properties and pharmaceutical value of these compounds.

Conclusion

The detection of bioactive metabolites belonging to the phenolic, indolic, phosphonate, and ester class in the hexane extract of Fusarium oxysporum Schlecht fungus showed that these microorganisms have a complex secondary metabolism system. The obtained results confirm the practical value of these compounds as antimicrobial, antioxidant and environmentally stable bioregulators. The results of the research expand the possibility of using fungi of the genus Fusarium as a source of bioactive substances in the pharmaceutical and biotechnology fields.

References

Abdel-Naime, W. A., Mohamed, N. Z., & El-Shiekh, S. M. (2019). Phytochemical and biological study of some Fusarium oxysporum metabolites. Natural Product Research, – 33(18). – P. 2689–2696. URL: https://doi.org/10.1080/14786419.2018.14720233

Azami, S. A., Rafiq, M., & Abbas, S. (2024). Volatile organic compounds derived from Fusarium oxysporum and their role in plant defense mechanisms. Journal of Plant Pathology, – 106(2). – P. 145–159. URL: https:// doi.org/10.1007/s42161–024–01356–7

Davis, N. D., Diener, W. L., & Eldridge, D. W. (1997). Production of toxic metabolites by Fusarium oxysporum. Applied Microbiology, – 15(3). – P. 781–784. URL: https:// doi.org/10.1128/aem.15.3.781–784.1997

4.Ding, T., Yang, Y., & Zhao, J. (2019). Characterization of bioactive fatty acids produced by Fusarium oxysporum. Microbiological Research, – 227. – P. 126–134. URL: https:// doi.org/10.1016/j.micres.2019.126294

Druzhinina, I. S., Shelest, E., & Kubicek, C. P. (2011). Novel traits of plant-associated Trichoderma species: Evidence for genetic exchange with plant pathogenic Fusarium. BMC Genomics, – 12. – 485 p. URL: https:// doi.org/10.1186/1471–2164–12–485

El-Hassan, S. A., & Gowen, S. R. (2006). Formulation and delivery of the bacterial antagonist Bacillus subtilis for management of lentil vascular wilt caused by Fusarium oxysporum f. sp. lentis. Journal of Phytopathology, – 154(3). – P. 148–155. URL: https:// doi.org/10.1111/j.1439–0434.2006.01075.x

Al-Hassan, S. A., Al-Habbash, M. R., & Ibbini, J. H. (2024). Eco-safe biofertilizer formulations from Fusarium-derived metabolites for sustainable agriculture. Environmental Sustainability, – 7(2). – P. 225–238. URL: https:// doi.org/10.1016/j.envsus.2024.225

Ghavam, M., Esfandiari, M., & Mousavi, S. (2021). Evaluation of cytotoxic and antimicrobial activities of Fusarium oxysporum metabolites. Microbial Pathogenesis, – 152. – 104770 p. URL: https:// doi.org/10.1016/j.micpath.2021.104770

Guo, X., Li, H., & Zhang, C. (2010). Fatty acid profiles of Fusarium species associated with plant defense responses. Journal of Agricultural and Food Chemistry, 58(19), 10469–10475. URL: https:// doi.org/10.1021/jf102144z

Mishra, A., Sharma, R., & Tiwari, S. (2022). Phenotype microarray analysis reveals the biotransformation of Fusarium oxysporum f. sp. lycopersici influenced by Bacillus subtilis PBE-8 metabolites. FEMS Microbiology Ecology, – 98(6). – fiac102. URL: https:// doi.org/10.1093/femsec/fiac102

Rahman, M., & Singh, P. (2023). Biocontrol potential of Fusarium-associated endophytes for sustainable crop protection. Frontiers in Microbiology, – 14. – 1123456 p. URL: https:// doi.org/10.3389/fmicb.2023.1123456

Raffaele, S., Leger, A., & Kamoun, S. (2009). Fungal effectors and plant susceptibility. Annual Review of Plant Biology, – 60. – P. 373–394. URL: https:// doi.org/10.1146/annurev.arplant.043008.092944

Reghmit, N., Zhang, W., & Kumar, R. (2024). Phenolic volatiles from Fusarium oxysporum with antifungal potential. Environmental Research, – 244. – 118725 p. URL: https:// doi.org/10.1016/j.envres.2024.118725

Singh, A., Patel, H., & Gajera, H. (2021). Secondary metabolites of Fusarium species and their biotechnological applications. World Journal of Microbiology and Biotechnology, – 37(9). – P. 156. URL: https:// doi.org/10.1007/s11274–021–03093–1

Stracquadanio, C., Quiles, J. M., & Masiello, M. (2020). Fusarium oxysporum secondary metabolites: A review of bioactive potential. Applied Microbiology and Biotechnology, – 104. – P. 1377–1395. URL: https:// doi.org/10.1007/s00253–019–10340–8

Zhao, L., Li, P., & Gao, J. (2019). Role of linoleic acid in fungal–plant interaction and defense signaling. Frontiers in Plant Science, – 10. – 1121 p. URL: https:// doi.org/10.3389/fpls.2019.01121

submitted 14.10.2025;
accepted for publication 28.10.2025;
published 26.11.2025

Contact: roziyevazarnigor90@gmail.com

The Austrian Journal of Technical and Natural Sciences, No 9–10
ISSN 2310-5607

PREMIER Publishing
ppublishing.org

DOI:10.29013/AJT-25-9.10-46-50

MASS-CHROMATOGRAPHIC ANALYSIS OF METABOLITES OF THE FUNGUS TRICHOLOMA CALIGATUM

Ruziyeva Zarnigor [1], Kamolov Luqmon[1], Gulboyeva Dilafruz[1], Hasanova Madina[1], Meyliyeva Muxlisa [2]

[1] Faculty of Chemistry and Biology, Karshi State University, Uzbekistan, Karshi

[2] Faculty of Medicine, Turon University, Uzbekistan, Karshi

Cite: *Ruziyeva Z., Kamolov L., Gulboyeva D., Hasanova M., Meyliyeva M. (2025). Tmass-Chromatographic Analysis of Metabolites of the Fungus Tricholoma Caligatum. Austrian Journal of Technical and Natural Sciences 2025, No 9–10.* https://doi.org/10.29013/AJT-25-9.10-46-50

Abstract

In recent years, macrofungi are famous for their unique nutrient retention, moreover, for the production of biologically active substances such as microfungi. In our study, we aimed to study the biologically active substances of the fungus Tricholoma caliogatum and in this study, the insoluble residue GC–MS (gas chromatography — mass spectrometry) was analyzed in organic solvents (hexane, chloromine, methanol) that separated during the last steps of the alcohol (ethanol) extract process of the fungus Tricholoma caligatum. According to the analysis results, the residual revealed the following major components: 1-(3,5-dimethyl-1-adamantanoyl)semicarbazide, Amphetamine-3-methyl cyclobutanol, N-Acetyl-2-methylamphetamine, Amphetamine-3-methyl acetate, N-Acetyl-4-methylamphetamine, Rhodopin, Octadecanoic acid, 2-hydroxy-1,3-propanedilyl di-ester, Hexadecanoic acid, 1-(hydroxymethyl)-1,2-ethanyyl ester and other lipid and carotenoid derivatives of high molecular weight. The different natures of the compounds identified (amine/alkaloid-like, carotenoid pigments, fatty acid esters, and semicarbazide derivatives) indicate that the residue is a complex organic polymer-and-conjugate mixture.

Keywords: *Tricholoma caligatum; alcohol extract; GC–MS; a secondary metabolite; lipid esters; Chromatographic*

Log in

In recent years, the secondary metabolites in macrofungs have been studied extensively as they are considered as an important resource in pharmaceuticals, food industry, and biotechnology. Fungi belonging to the conslog Tricholoma, in particular Tricholoma caligatum, are remarkable for the richness of their chemical components. (Erol et al., 2020) have isolated substances such as lascivol, trametenolic acid, ergosterol, and ergosterol peroxide from the fruit body of T. caligatum. The anti-inflammatory effects of these compounds and the possibility of sup-

pressing the NF-κB signaling pathway have been established. This case forms the basis for considering T. caligatum as a source of pharmacologically active molecules. (Taşkın et al., 2019) compared the volatile substances of T. caligatum and T. anatolicum species, noting that terpenes are higher in T. caligatum and alcohol and esters are relatively low. These findings explain the odor and taste profile unique to this species. In a study conducted by Gillardoni et al., 2023, novel triterpenoid structures from the genus Tricholoma were identified, and their structure was confirmed using NMR and MS techniques. This result further enriches the diversity of metabolites in the constellation Tricholoma. Zhao et al., 2024) analyzed studies between 2018 and 2023 and summarized that more than 100 different metabolites from Tricholoma species had been identified. Among them, steroids, terpenoids, phenolics, polysaccharides and alkaloids indicate the chemical diversity of the species of Tricholoma. (Stojek et al., 2024) analyzed the fatty acid content in wild mushrooms and noted that linoleic, oleic, and palmitic acids are found as the main components in the genus Tricholoma. These lipids are significant in cell membrane stability and biological activity. Research by Yu et al., 2023 shows that Tricholoma species has a balanced amino acid and fatty acid profile. It is one of the factors that increase the nutritional value of piglets. (Broser et al., 2023) Having discovered the presence of rhodopsin-cyclase enzymes in the type Tricholoma, they have shown that it is important in the synthesis of pigment and light-sensing molecules. Studies (led by Qin and Pandey., 2023–2024) highlight the presence of melanin and other pigment polymers in the genus Tricholoma, which play a key role in protecting fungi from external factors. Saiz-Jimenez et al. 2021) have shown that it is possible to detect the phenolic and aromatic components via pyrolytic analysis of melanin. Such a method is important when chemically characterizing insoluble residues. Gutierrez-Reyes et al., 2025) have provided methods for characterizing biomass-derived substances based on MS. This methodology is useful for the detection of high molecular components in Tricholoma extracts. Sun et al., 2022) gave a general analysis of the polysaccharides of edible fungi, highlighting the importance of β-glucan and chitin for the cell wall in Tricholoma species. (Clericuzio et al., 2018) Metabolites isolated from the Tricholoma type have been reported to show pharmacological activity. Among them, the important role of terpenoids and steroids has been noted. Roziyeva et al., 2025), while describing novel metabolites from T. caligatum, confirming their antimicrobial and antioxidant activity. And additional research will further deepen the diversity of the species Tricholoma. (Inside vs. Others, 2023) The Tricholoma section revealed structural differences in the genomes of Caligata, indicating the evolutionary position of T. caligatum. S. et al. (2018) has investigated the antioxidant activity and safety of T. equestre based on the phenolic/flavonoid content. (Benazza-Bouregba et al., 2016) A new find of T. caligatum from North Africa has been confirmed via molecular markers. Metabolome and transcriptome analyses in 2022–2023 have expanded knowledge of the cell wall and metabolite biosynthesis of T. matsutake. (Gamboa-Becerra et al., 2024) described metabolites from T. mesoamericanum and evaluated its antioxidant and nutritional value. In general, the available literature confirms the chemical diversity of the species Tricholoma caligatum and indicates that studying it as a source of bioactive compounds is of scientific and practical importance.

Research methodology

Sample Preparation

Fruit bodies of the fungus Tricholoma caligatum were selected as the object of research. The sample was first thoroughly washed with distilled water, cleaned of surface contamination, and dried at 45–50 °C. The dried material was ground into a fine powder in a lab grinder and prepared for storage in an airtight container.

Extraction Process

The extraction process was carried out using an alcoholic solvent. The cousin powder was extracted in 98% ethanol solution for 8 h in the Soxhlet extraction apparatus. The extraction process has been carried out minimum 6-7 times. In the solvent, the substance was washed out, after which the solvent was removed by a rotary evaporator. This extraction separated the stained at the beginning

and white at the end of the process, the residual part, insoluble in any organic solvent.

Conclusion and discussion

The bleached substance in the last stage of alcohol extract of the litter biomass obtained by the above method was attracted to the chromatographic separation process. The dissociating whitish substance (insoluble in hexane, chloroform, ethyl acetate, and even methanol) at the last step of alcohol extraction of Tricholoma caligatum was analyzed using the GC–MS method, mass chromatogram analysis revealed peaks consistent with a number of important compounds. The chromatographic profile of this extract showed additional cleavage and differentiation of metabolites, and among those dissociated substances the biological importance of rhodopin is great.

Figure 1. *Gas-liquid chromatogram of extract (Rhodopin) in an alcohol-solvent system*

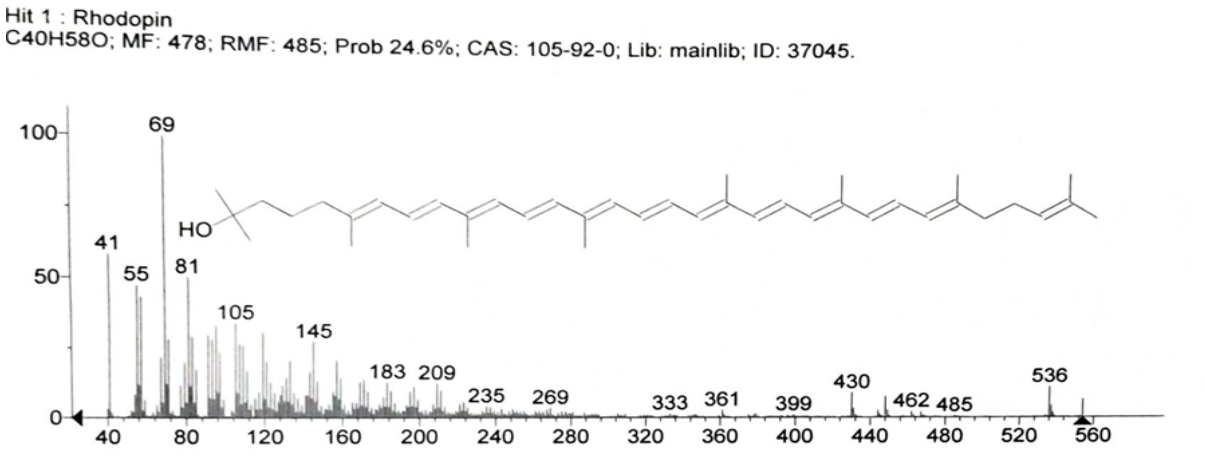

The volatile metabolites detected by GLX (gas-liquid chromatography) chromatogram of the resulting extract were identified through the MC database. The substance belongs to the group of carotenoids. Carotenoids are pigments found in many organisms, and they play photoprotection, light harvesting, and antioxidant roles. Rhodopin (1,2-dihydro-ψ, ψ-caroten-1-ol) is a C40H58O-formulated oxycarotene and is also found in purple bacteria (e.g. Rhodopseudomonas acidophila, Rhodomicrobium vannielii), and several other microorganisms.

Figure 2. *Gas-liquid chromatogram of extract (Octadecanoic acid, 2-hydroxy-1,3-propanedilyl di-ester (C39H76O5)) in an alcohol-solvent system*

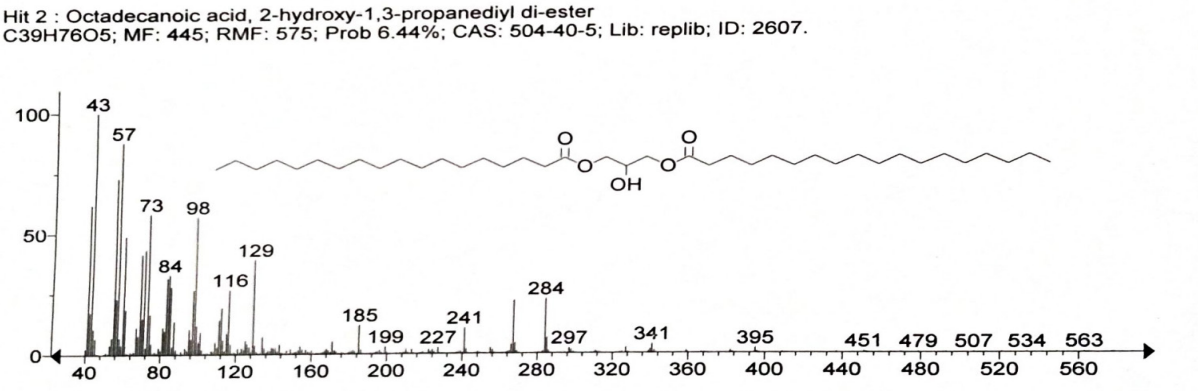

The 2nd substance is Octadecanoic acid, 2-hydroxy-1,3-propanedilyl di-ester (C39H76O5), better known as glyceryl distearate (GDS), among the mono- and di-esters

of natural fatty acids. This substance is used as an excipient component in many pharmaceutical products. The main composition is stearic acid, which in the body is hydrolyzed and broken down into stearic acid and glycerin. Glyceryl distearate is not an active substance as a drug, but its pharmacological importance is manifested in its helpful properties: Improve the bioavailability (absorption of drugs). Being a carrier of fat-soluble vitamins (A, D, E, K) and lipophilic drugs. Application in fat-based adjuvant systems for antigens and vaccines. Its use as a transport system for lipid-based drugs. Glyceryl distearate is recognized by FDA and European pharmacopoeia as a GRAS (Generic Safe Substance). Its toxic effect has not been determined and is widely used in medicines, cosmetics. The biological activity of most of the decaying substances is considered to be high.

Conclusion

As a result of GC–MS analysis, the substances identified and their biological activity were evaluated as: 3-Methylamphetamine – has stimulant effect on the central nervous system, increases attention, but has toxic effect. N-Acetyl-2-methylamphetamine – is a metabolite of amphetamine, which forms in the body during the process of suppressing the action of the drug. Amphetamine is a powerful psychostimulant that increases alertness, but can cause addiction. Benzeneethanol,α-(1-aminoethyl)-, hydrochloride–is a derivative of phenethylamine, generally showing psychotropic property by influencing neurotransmitters. D-Mannitol – used for medicinal purposes; As an osmotic diuretic, it reduces swelling, stimulates kidney function. 1-Octadecanamine, N-methyl – a long-chain amine, may exhibit antimicrobial properties by interacting with biological membranes and lipid layers. 9,10-Secocholesta-5,7,10(19)-triene-3,24,25-triol – a compound of steroidal nature, is among the derivatives of cholesterol, is involved in hormonal and metabolic processes. Cyclotrisiloxane, hexamethyl – generally not biologically active; these substances are mainly technical mixtures and come from the GC-MS hardware. In general, among the substances identified: - Biologically active amines (1–4) are mostly psychotropic and have stimulant effects. Mannitol (5) is used in medicine as a diuretic and detoxifier.- Lipid/steroid derivatives (6–7) play an important role in metabolic and hormonal processes. Siloxane (8) is a technical mixture and is considered to be lower in biological value.

References

Erol, E., Ali, Z., Öztürk, M., Khan, S., Khan, I. Inhibition of iNOS Induction and NF-κB Activation by Taste Compounds from the Edible Mushroom Tricholoma caligatum. Records of Natural Products, – 14(1). DOI http://doi.org/10.25135/rnp.139.19.04.1263

Taşkın, H., Çelik, Z. D., Bozok, F., Cabaroğlu, T., & Büyükalaca, S. First Report on Volatile Composition of Tricholoma anatolicum in Comparison with Tricholoma caligatum. Records of Natural Products, – 13(6). DOI: http://doi.org/1025135/rnp.122.18.12.1095

Gillardoni, G., et al. New Tricholomalides D–G from the Mushroom Tricholoma. Natural Product Research, – 37(5). DOI: http://doi.org/10.3390/molecules28217446

Zhao, M., Yuan, S., Li, Z., Liu, C., & Zhang, R. Review of the Structural Characteristics and Biological Activities of Tricholoma Secondary Metabolites (2018–2023). DOI: Molecules, – 29(19). DOI: http://doi.org/10.3390/molecules29194719

Stojek, K., et al. Factors affecting composition of fatty acids in wild-growing macrofungi. Mycologia. DOI: http://doi.org/10.1080/00275514.2024.23250456

Yu, C. X., et al. Composition and contents of fatty acids and amino acids in edible mushrooms. Foods, – 12(16). DOI: http://doi.org/10.3390/foods12162985

Broser, M., et al. Diversity of rhodopsin cyclases in zoospore-forming fungi. PNAS, – 120(23). DOI: http://doi.org/10.1073/pnas.2310600120

Qin, Y., et al. Melanin in fungi: Advances in structure, biosynthesis and potential applications. Microbial Cell Factories, – 23. DOI: http://doi.org/10.1186/s12934024026148

Pandey, S., et al. Efficient production and characterization of melanin from fungal sources. Frontiers in Microbiology, – 14. DOI: http://doi.org/10.3389/fmicb.2023.1320116

Saiz-Jimenez, C., et al. Analytical Pyrolysis of the Fungal Melanins from Ochroconis spp. Applied Sciences, – 11(3). DOI: http://doi.org/10.3390/app11031198
Yu, W., et al. Metabolomic profiling of fungal extracts by GC-MS: methodology and pitfalls. Foods. DOI: http://doi.org/10.3390/foods12162985
Gutierrez-Reyes, C. D., et al. MS-based characterization of biomass-derived materials. Polymers, – 17(5). DOI: http://doi.org/10.3390/polym17050856
Sun, Y., He, H., Wang, Q., Yang, X., Jiang, S., & Wang, D. A Review of Development and Utilization for Edible Fungal Polysaccharides. Polymers, – 14(20). DOI: http://doi.org/10.3390/polym14204454
Clericuzio, M., et al. Secondary Metabolites Isolated from Tricholoma Species (Basidiomycota). Natural Product Communications, – 13(9). DOI: http://doi.org/10.1177/1934578X18013009266
Roziyeva, Z. Q. Secondary metabolites of the fungus Tricholoma caligatum. Web of Journals.
Ichida, H., et al. (2023). Near-complete de novo assembly of Tricholoma bakamatsutake chromosomes. G3: Genes|Genomes|Genetics, – 13(11). DOI: http://doi.org/10.1093/g3journal/jkad198
Muszyńska, B., Kała, K., Radović, J., Sułkowska-Ziaja, K., et al. (2018). Study of biological activity of Tricholoma equestre fruiting bodies and their safety for human. European Food Research and Technology, – 244. – P. 2255–2264. DOI: http://doi.org/10.1007/s00217-018-3134-0
Benazza-Bouregba, M., Savoie, J.-M., Fortas, Z., & Billette, C. (2016). A new record of Tricholoma caligatum from North Africa. Phytotaxa, – 282(2). – P. 119–128. DOI: http://doi.org/10.11646/phytotaxa.282.2.3
PubMed (2022–2023). Quantitative transcriptomic and metabolomic analyses of Tricholoma matsutake fruiting bodies. Pub Med Central.
Gamboa-Becerra, R., Montoya, L., Bandala, V. M., Monribot-Villanueva, J. L., Guerrero-Analco, J. A., Ramos, A. (2024). Metabolomic profiling of Tricholoma mesoamericanum. International Journal of Food Science & Technology, – 59(6). – P. 4348–4358. DOI: http://doi.org/10.1111/ijfs.17121

submitted 28.09.2025;
accepted for publication 12.10.2025;
published 26.11.2025

Contact: roziyevazarnigor90@gmail.com

The Austrian Journal of Technical and Natural Sciences, No 9–10
ISSN 2310-5607

PREMIER Publishing
ppublishing.org

DOI:10.29013/AJT-25-9.10-51-57

DETERMINATION OF THERMAL STABILITY OF POLYMERIC MATERIALS BASED ON RECYCLED POLYETHYLENE

Safarova Matluba Alimkulovna [1], ***Shakhnoza Mamatova Berdikobilovna*** [1], ***Davranova Guzal Turdievna*** [1], ***Kurbanov Mingnikul Jumagulovich*** [1], ***Dilnoza Shavkatova*** [1]

[1] Karshi State University

Cite: *Safarova M.A., Shakhnoza M.B., Davranova G.T., Kurbanov M.J., Dilnoza Sh. (2025). Determination of thermal stability of polymeric materials based on recycled polyethylene. Austrian Journal of Technical and Natural Sciences 2025, No 9–10.* https://doi.org/10.29013/AJT-25-9.10-51-57

Abstract

The purpose of this article is to obtain lightfast, resistant to oxidation, aggressive environments and heat-resistant polymeric materials based on low-pressure polyethylene waste by adding chemical binders and fillers. The analysis of heat resistance of polymeric materials modified with chemical binders and fillers is carried out.

Keywords: *polyethylene, polypropylene, oligomer, sulfur, melamine, sodium acetate, extruder, derivatogram, thermogravimetry*

Introduction

Today, the world's population is growing exponentially. This growth leads to the fact that humanity's need for modern equipment and materials is growing every day. As a result, the globalization of large cities, the development of production and industry lead to the formation of a large amount of industrial harmful gases, solid and household waste. This will lead to serious environmental problems for humanity and the environment in the future. Currently, the use of disposable polyethylene packaging is growing rapidly. The disposal of these wastes and their economic use have become one of the main problems of our time. In the field of recycling polyethylene packaging waste, a number of authors describe numerous recycling methods in the scientific works of a number of authors (Mamatova Sh.B., Qurbonov M. J., Safarova M. A., 2024; Mamatova Sh.B., Kurbanov M.Zh., 2022; Mamatova Sh.B., Kurbanóv M. J., Safarova M. A., Izbasarova G., 2024; Mamatova, Sh.B., Kurbanov, M.Zh., 2023).

It is known that polyethylene waste, although withdrawn from consumption, loses its original properties, but these materials are not considered obsolete. The efficiency of recycling of waste from these polymer products depends not only on the technology of their processing, but also on the quality of the material involved in processing, its homogeneity, as well as the quantitative content of contaminating mechanical and organic impurities. During operation, plastics lose elasticity and

become brittle under the influence of heat, moisture, stress, radiation (α, β and γ radiation), as well as oxygen in the air. As a result, the mechanical and electrical properties of products made of polymeric materials deteriorate. In particular, the effect of temperature adversely affects most of the physical and mechanical properties of polymer materials. Lowering the temperature increases the brittleness of most polymer materials, while heating reduces properties such as coefficient of linear expansion and viscosity. High temperatures also lead to changes in the mechanical properties of polymeric materials (tensile, bending, compressive strength, etc.) (Mamatova Sh.B., Qurbonov M. J., 2023; Mamatova Sh., Safarova M., Davronova G., Raxmatova G., Makhmayorov J., Abdullayev B., Kurbanov M. 2024; Mamatova Sh.B., Qurbanov M. J., To ʻrayeva M., 2024).

Research methods

For the study, the waste of low-density polyethylene of PY-456 grade produced by the Shurtan Gas Chemical Complex, which had served its service life, was sorted, cleaned of mechanical impurities, washed repeatedly and the purified product was dried in a special dryer. After that, the purified product was crushed in a special device. A certain amount of the resulting product was taken and placed in the extruder. Also, to obtain a heat-resistant polymer material, a certain amount of sodium acetate, sulfur, melamine and polypropylene oligomer was added to the crushed secondary polyethylene. To obtain a mixed polymer mass, the extruder operating mode was set at 60 rpm and the temperature was 115–140^{0}C. To form a homogeneous mixture in the extruder, the product was passed through the extruder 2 times.The resulting hot mixture was cooled and placed in a granulator. During the granulation process, the hot mixture was transferred to the forming head. Passing through the head, the mass was continuously squeezed out in the form of a wire, cooled and cut into granules with a special knife. The size of the samples was 3–5 mm. These granules served as the main raw material for further research.

All studies of polymer materials obtained from secondary polyethylene waste were carried out in accordance with the requirements of the State Standard for Polymer Materials. In particular, the data of thermogravimetric analysis of the obtained polymer materials were carried out in accordance with the requirements of GOST-12423. Samples for thermogravimetric analysis were identified by the difference between the initial temperature and the rate of decomposition.

The results of a thermogravimetric study of polymeric materials based on recycled polyethylene were calculated on the basis of the rate of mass loss of the samples taken for the experiment according to the following formula:

$$\upsilon m=\Delta m/\Delta \tau$$

here: Δm is the decrease in the weight of the weight, mg; $\Delta \tau$ is the time interval, minutes.

Discussion of the results

At present, industrialized countries pay special attention to the production of modified polymer materials. This is achieved by adding various organic modifiers to obtain new types of materials based on recycled polyethylene and organic modifiers. The use of materials based on recycled polyethylene as various consumer products is considered to be very promising and economically beneficial for the national economy. Two methods of modifying polymer materials are used. The first method is structural modification of polymers, the second is chemical modification. Modification of polymeric materials with chemical reagents and agents is carried out by adding chemical reagents that process chemical bonds with macromolecules of the original polymer raw materials.

The main goal of this work is to obtain a new type of heat-resistant modified polymer materials. It is known that nitrogen-containing organic modifiers increase plasticizing properties, and salts of organic acids increase the flame-retardant properties of polymeric materials. From this point of view, samples of the following composition were taken for the study: polyethylene (PE), sulfur (S), sodium acetate (CH3COONa), melamine and polypropylene oligomer (o-PP) in accordance with the quantitative ratios of 50:1:1:1:1 (SMA-1 (from primary polyethylene)), 50:1:1:1:1 (SMA-2), 50:0.5:0.5:0.5 (SMA-3) and 50:1.5:1.5:1.5 (SMA-4). The heat resistance of the obtained polymer materials was studied. Below is the DTA analysis curve of the SMA-1 sample.

Figure 1. *Derivatogram of a sample containing CMA-1*

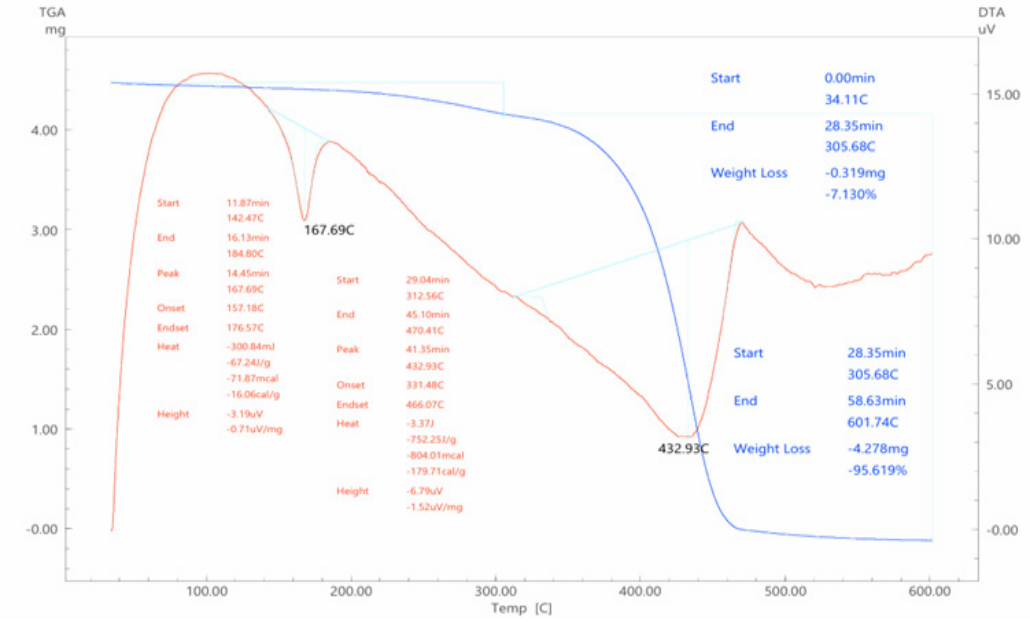

According to the data obtained, the initial decomposition temperature of the sample is 34.11 ºC, and the final temperature is 305.68 ºC. Mass loss under the influence of temperature for the CMA-1 sample was 7.13%. The quantitative weight loss during the initial degradation period of this CMA-1 sample is 0.319 mg in the range from 0.00 minutes to 28.35 minutes. The second temperature decomposition period of the sample was 28.35 minutes and the temperature reading was 305.68 °C. The final temperature of this second decomposition period was 601.74 °C. The time required for this decomposition was 28.35 minutes and 58.63 minutes. The mass loss of the CMA-1 sample during this second degradation period was 4.278 mg, or 95.61%. In the course of the study, two heat absorption curves are observed on the derivatogram of this sample containing CMA-1. These absorption curves have been found to be at temperatures of 167.69 °C and 432.93 °C.

Similarly, the analytical DTA curve of a sample containing CMA-2 was studied. Figure 2 shows the derivatogram of the CMA-2 sample.

Figure 2. *Sample CMA-2 Derivatogram*

According to the data of Figure-2, it was determined that the initial decomposition temperature of the CMA-2 sample was 34.95 ºC, and the final temperature was 303.89 ºC. It was established that during the decomposition of the CMA-2 sample at this temperature, a mass loss of 3.84% was observed. The quantitative weight loss of the same sample was 0.242 mg between 0.00 min and 27.91 min. The start time of the second decomposition period under the influence of temperature for this CMA-2 sample was 27.91 minutes, and the temperature reading was 303.89 °C. The final temperature of this second decomposition period was 540.59 °C. The decomposition time was found to start after 27.91 minutes and end after 52.05 minutes. The weight loss at the second stage of decomposition was 6.01 mg, or 95.53%. As can be seen from the derivatogram of this CMA-2 sample obtained during the study, two heat absorption lines are observed during the decomposition period under the influence of temperature. These absorption curves were found to correspond to temperatures of 115.11 °C and 470.72 °C.

The analytical curve of the DTA of the CMA-3 sample was also studied below.

Figure 3. *CMA-3 Sample Derivatogram*

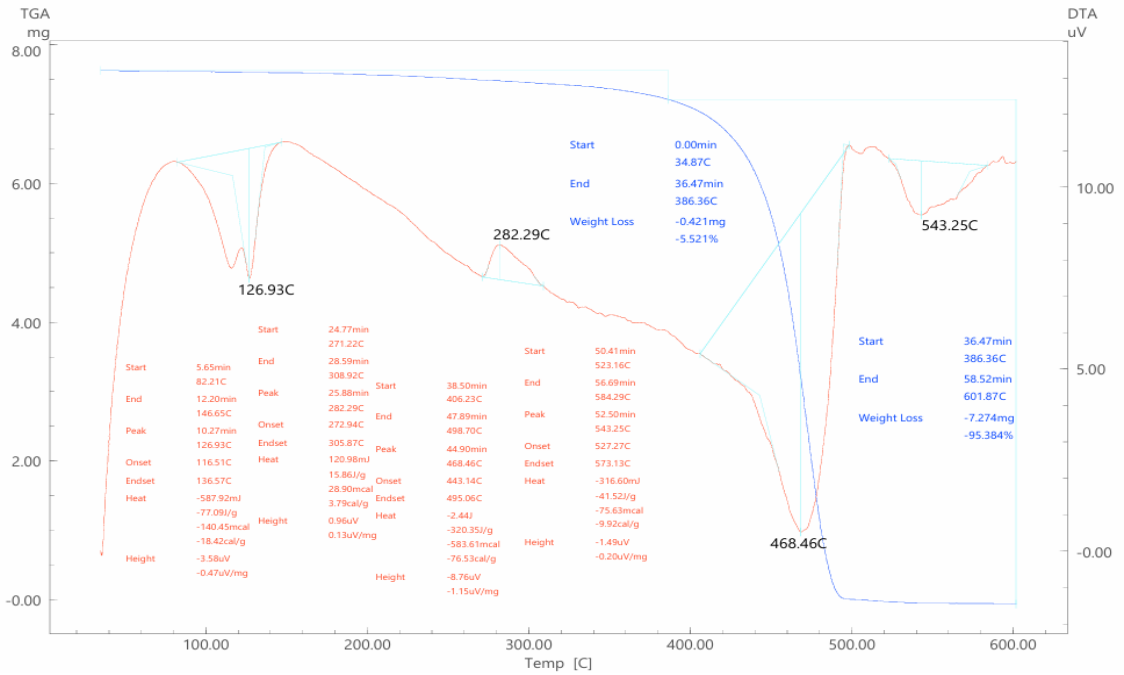

According to the data obtained, the initial decomposition temperature of the CMA-3 sample was 34.87 ºC, and the final temperature was 386.36 ºC. Mass loss during decomposition of the CMA-3 sample at this temperature was 5.521%. It was found that the mass loss during the initial period of decomposition of the same sample containing CMA-3 was 0.242 mg in the range from 0.00 minutes to 36.47 minutes. The second decomposition period of this sample under the influence of temperature was 36.47 minutes, and the temperature reading was 386.36 °C. The final temperature of this second decomposition was 601.87 °C. It was found that the time required for this decomposition, It started after 36.47 minutes and ended after 58.52 minutes. It was found that the weight loss of the CMA-3 sample during this period was 7.27 mg or 95.38%. In the course of the study, four heat absorption curves are observed on the derivatogram of this sample. These curves have been found to correspond to temperatures of 126.93 °C, 282.29 °C, 468.46 °C and 543.25 °C.

The analytical DTA curve of the CMA-4 sample was also studied.

According to the data obtained, the initial decomposition temperature of the CMA-4 sample was 37.24 ºC, and the final temperature was 395.29 ºC. Mass loss in this temperature range was 12.78%. The quantitative weight loss during the initial decomposition period of the same CMA-4 sample was 0.696

mg in the range from 0.00 minutes to 36.97 minutes. It was found that the time of the beginning of the second decomposition period under the influence of the temperature of this sample was 36.97 minutes, and the temperature index was 395.29 °C. The final temperature of the second decomposition period was 532.02 °C. It was found that the decomposition time was 36.97 minutes and 50.87 minutes. The loss of mass and time of the second resolution period was 4.57 mg, 84.06%. In the course of the study, two heat absorption curves were obtained during the decomposition period of a sample containing SMA-4 under the influence of temperature. These absorption curves were found to correspond to temperatures of 115.36 °C and 473.87 °C.

Figure 4. *Sample CMA-4 Derivatogram*

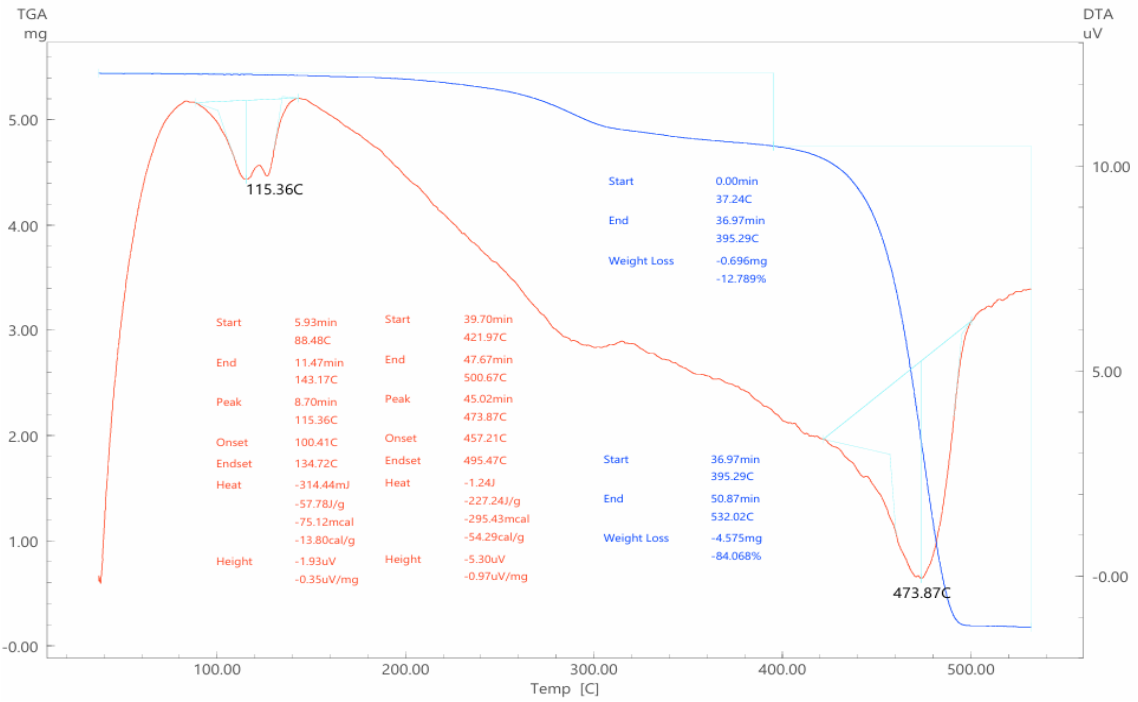

The results from the data analysed above are summarized in tables 1 and 2 below.

Table 1. *Results of Thermogravimetric Analysis of Polymer Material Based on Secondary Polyethylene Matrix (1st Decomposition Period)*

Temperature range. °C	Duration of decay. min.	Loss weight. mg	Loss Weight. %
SMA-1 ratio: 50:1:1:1:1			
34.11–305.68	0.00–28.35	0.319	7.13
CMA-2 ratio: 50:1:1:1:1			
34.95–303.89	0.00–27.91	0.242	3.84
CMA-3 ratio: 50:0.5:0.5:0.5:0.5			
34.87–386.36	0.00–36.47	0.242	5.52
CMA-4 ratio: 50:1.5:1.5:1.5:1.5			
37.24–395.29	0.00–36.97	0.696	12.78

As can be seen from the data presented in Table 1, there is no significant difference between the initial decomposition temperatures and decomposition time of the CMA-1 sample and the CMA-2 sample. However, it can be noted that the difference in weight loss between these samples has changed significantly. Comparing the results of the

CMA-1 and CMA-2 samples presented above with the results of the CMA-3 sample, a significant difference can be noticed. that the temperature in the first period of decomposition (386.36^{0}C) is higher, and the duration (36.47 minutes) is slightly longer. Similarly, the results of the three above samples were compared with those ofCMA-4. The results show that the initial decomposition temperature of the CMA-4 sample (37.24–395.29 °C) is higher, and the decomposition time is also longer. However, it was found that the mass loss of this CMA-4 sample was slightly higher than that of the three samples mentioned above.

Table 2 shows the results of the second decomposition of these samples.

Table 2. *Results of thermogravimetric analysis of polymeric material based on secondary polyethylene matrix (2nd decomposition period)*

Temperature range, °C	Duration of decay, min.	Loss weight, mg	Loss Weight, %
	SMA-1 ratio: 50:1:1:1:1		
305.68–601.74	28.35–58.63	4.278	95.61
	CMA-2 ratio: 50:1:1:1:1		
303.89–540.59	27.91–52.05	6.01	95.53
	CMA-3 ratio: 50:0.5:0.5:0.5:0.5		
386.36–601.87	36.47–58.52	7.27	95.38
	CMA-4 ratio: 50:1.5:1.5:1.5:1.5		
395.29–532.02	36.97–50.87	4.570	84.06

Analysis of the data presented in Table 2 shows that the difference between the temperature and duration of secondary degradation of the CMA-1 sample derived from virgin polyethylene and the CMA-2 sample derived from recycled polyethylene has not changed significantly, i.e. the temperature in the CMA-2 sample has decreased. When comparing the results of the CMA-1 and CMA-2 samples presented above with the CMA-3 sample, there is a significant difference. that the temperature in the second decomposition period (601.87^{0}C) is higher and the duration (58.52 minutes) is slightly longer. Similarly, comparing the results of the above three samples with those of CMA-4, it can be observed that the temperature of the second decomposition period (532.02^{0}C)and the decomposition time of theCMA-4 sample also decreased. However, it can be observed that the mass loss of this CMA-4 sample is slightly lower compared to the CMA-2 and CMA-3 samples.

Findings. As a result of the destruction of recycled polyethylene, carbon-carbon bonds arise in some parts of the chain due to the disproportion of hydrogen atoms from methylene groups that are part of the polymer chain. As a result, chemical bonds are formed between the macromolecules of the thermally destructed polymer material and chemically binding reagents polypropylene due to the breaking of the π bonds of double bonds. In addition, the modified sulfur contributes to the vulcanization of the polyethylene product by forming sulfide bridges between the macromolecules of recycled polyethylene. Such polymeric materials have increased heat resistance, reduced flammability, increased resistance to oxidation, as well as increased resistance to weathering, aggressive environments and light compared to products made of pure polyethylene.

References

Mamatova Sh.B., Qurbonov M.J., Safarova M.A. Modification and study of the properties of recycled polyethylene // Development of science. 2024. – No. 1. – P. 157-164.

Mamatova Sh.B., Kurbanov M.Zh. Production of building materials from polyethylene waste on the basis of secondary processing // Proceedings of KarSU, 2022. – No 5/1. – P. 71–75.

Mamatova Sh. B., Kurbanóv M. J., Safarova M. A., Izbasarova G. Modification of Secondary Polyethylene on the Basis of Sulfur and Melamine // Collection of Scientific Articles on the Results of the Work of the International Scientific Forum “Science and Innovations: Modern Concessions” – Moscow. – 2024. – P. 129-135. DOI 10.34660/INF.2024.38.92.018.

Mamatova, Sh. B., Kurbanov, M. Zh. Study of Physicochemical Properties of Melamine Modification of Secondary Polyethylene//Universum: Chemistry and Biology. – 2023. – No. 10-2 (112). – P. 33-39. URL: https://7universum.c om/en/нature/archive/item/16027

Mamatova Sh.B., Qurbonov M.J. Study of Thermogravimetric Analysis of Secondary Polyethylene and Melamine Modification // Modern Problems of Theoretical and Experimental Chemistry and Chemical Technology. Scientific and Practical Materials of the International Conference. – Karshi, 2023. – October 20. – P. 217-218.

Mamatova Sh., Safarova M., Davronova G., Raxmatova G., Makhmayorov J., Abdullayev B., Kurbanov M. Determination of the Time of Induction Oxidation of a Secondary Polyethylene Composition // New Materials, Compounds and Their Applications. – 2024. – 8(2). – P. 223-232. URL: https://doi.org/10.62476/nmca82223

Mamatova Sh.B., Qurbanov M.J., To ʻ rayeva M. Determination of the flammability of modified secondary polyethylene // Actual problems of chemistry. Republican Scientific and Practical Conference. – Urganch, 2024. – 21iyun. –B. 402-403.

submitted 08.10.2025;
accepted for publication 22.10.2025;
published 26.11.2025

Contact: safarovamatluba86@gmail.com; davranovaguzal1988@gmail.com;
mengniqulqurbonov@gmail.com; dilnozashavkatova@gmail.com

The Austrian Journal of Technical and Natural Sciences, No 9–10
ISSN 2310-5607

PREMIER Publishing
ppublishing.org

DOI:10.29013/AJT-25-9.10-58-62

YNTHESIS AND X-RAY DIFFRACTION ANALYSIS OF A HIGH-INTENSITY COPPER PHTHALOCYANINE PIGMENT CONTAINING NITROGEN AND SULFUR

Yusupov Muzafar [1], ***Mukxlisa Robiddinova*** [1], ***Doniyor Sherkuziyev*** [1]

[1] Department of Chemical Engineering, Namangan State Technical University, Republic of Uzbekistan, Namangan region

Cite: *Yusupov M., Mukxlisa R., Doniyor Sh. (2025). Ynthesis and X-ray diffraction analysis of a high-intensity copper phthalocyanine pigment containing nitrogen and sulfur. Austrian Journal of Technical and Natural Sciences 2025, No 9–10.* https://doi.org/10.29013/AJT-25-9.10-58-62

Abstract

The synthesis and characterization of a novel high-intensity copper phthalocyanine (CuPc) pigment incorporating nitrogen and sulfur within its molecular framework are presented in this study. The pigment is distinguished by the formation of chelate complexes that contribute to the stabilization of the macroheterocyclic structure and enhance its optical performance. The synthetic approach employed a carefully controlled process, ensuring the incorporation of heteroatoms into the phthalocyanine ring system.

Comprehensive structural analysis was conducted using advanced physicochemical methods, with a particular focus on X-ray diffraction (XRD) techniques. The diffraction peak profiles revealed well-defined crystalline features, accompanied by amorphous domains, confirming both the successful integration of heteroatoms and the composite nature of the synthesized pigment. These findings indicate that nitrogen and sulfur substitution significantly influences the crystallographic arrangement and electronic distribution within the macrocyclic lattice.

The study further highlighted the contribution of organic components that coexist within the pigment, providing insight into their role in stability and spectral behavior. The presence of nitrogen- and sulfur-containing moieties was shown to play a pivotal role in modulating the electronic transitions, as supported by spectroscopic evaluations. These structural modifications have a direct impact on the pigment's optical intensity, chemical stability, and potential multifunctionality.

Overall, this work not only advances the understanding of copper phthalocyanine derivatives but also opens new perspectives for their practical use in high-performance functional materials. Potential applications include optoelectronic devices, heterogeneous catalysis, photovoltaic systems, and advanced pigment technologies, where enhanced structural integrity and tunable electronic properties are of critical importance.

Keywords: *copper phthalocyanine, nitrogen-sulfur pigments, chelate complexes, X-ray diffraction, optical properties, functional materials*

Introduction

Colorants, including dyes and pigments, have been utilized extensively since ancient times for decorative, protective, and functional purposes. Their application spans a wide range of fields, from art and textiles to construction and industrial manufacturing. In recent decades, the demand for paints and coatings has grown substantially in response to the rapid pace of construction and infrastructural development both worldwide and within our Republic. This increasing demand has consequently intensified the need for high-quality raw materials, particularly pigments, which serve as the essential coloring agents in paint and coating formulations (Yusupov M., Kayumjanov O., 2024).

Pigments play a crucial role not only in imparting color but also in enhancing the durability, weather resistance, and overall performance of paint products. The advancement of pigment chemistry has allowed for the creation of materials with improved optical properties, higher stability, and multifunctionality, thus expanding their role in modern coating technologies. As the construction industry continues to expand, the strategic importance of developing efficient, sustainable, and cost-effective pigment systems becomes increasingly evident (Yusupov, M., & Kadirkhanov, J., 2023).

Phthalocyanines (Pcs) are planar, highly conjugated macroheterocyclic compounds that exhibit strong structural and functional resemblance to porphyrins. Their discovery in the early 20th century revolutionized the pigment industry, and since then, phthalocyanines have been established as one of the most stable classes of synthetic dyes (Lever, A. B. P., 1990). The unique physicochemical properties of these molecules-such as intense absorption in the visible region (Q-band), high molar extinction coefficients, and remarkable thermal and chemical stability – have positioned them as versatile candidates in both traditional and emerging technological domains (Linstead, R. P., 1934; Kadish, K. M., & Smith, K. M. (Eds.). 2003).

Among metallophthalocyanines, copper phthalocyanines (CuPcs) stand out as industrially significant pigments due to their vivid blue-green coloration and resistance to photobleaching. Beyond their conventional use in paints, inks, and coatings, CuPcs have attracted growing interest in advanced applications, including organic photovoltaics, gas sensing, and electrocatalysis (Bottari, G., et al., 2010). Recent advances in coordination chemistry and synthetic design have facilitated the incorporation of heteroatoms such as nitrogen and sulfur into the phthalocyanine macrocycle. These modifications have been shown to profoundly influence the electronic distribution within the macrocycle, enhancing intermolecular π–π stacking, tuning HOMO–LUMO energy levels, and improving solubility and processability (Dini, D., & Hanack, M., 2006; Han, J., et al., 2024).

The structural elucidation of such heteroatom-modified CuPcs often relies on X-ray diffraction (XRD), which provides critical insights into crystallinity, molecular packing, and polymorphic phases. For example, nitrogen-substituted phthalocyanines typically adopt more ordered packing arrangements, whereas sulfur-substituted analogues introduce distortions that modulate intermolecular interactions and lead to changes in optical and catalytic properties (Claessens, C. G., et al., 2002). Complementary spectroscopic techniques such as infrared (IR) spectroscopy and UV–Vis absorption further confirm the presence of characteristic functional groups and conjugated electronic systems (Dinçer, H. A., et al., 2007).

Several studies have emphasized the synergistic role of nitrogen and sulfur atoms in improving both the optical intensity and the structural rigidity of copper phthalocyanines. Zhan et al. (2014) demonstrated that simultaneous substitution of these heteroatoms significantly enhances the material's applicability in optoelectronic devices, owing to improved electron mobility and tailored absorption profiles (Zhan, R., et al., 2014). Moreover, Claessens et al. (2002) highlighted that such structural modifications not only enrich the optical features but also contribute to catalytic activity in redox reactions, making these pigments multifunctional materials.

Despite these advancements, gaps remain in fully understanding the correlation between structural modifications and functional performance. While nitrogen and sulfur substitution has been proven to alter crystallinity and intermolecular interactions,

systematic studies linking these modifications to large-scale performance in device applications are still scarce. Hence, further exploration of the structure–property relationship in heteroatom-containing copper phthalocyanines is essential for advancing their practical utility in optoelectronics, catalysis, and next-generation pigment technologies (Abbaspour, A., et al., 2013).

Research method

For the high-temperature synthesis, 1 mol of phthalic anhydride and 5 mol of urea were placed into a 250 mL heat-resistant beaker and heated in an HP-550-S electric furnace under a fume hood at approximately 140 °C until complete melting occurred. Subsequently, 1 mol of copper(I) chloride was added at the same temperature. Upon stirring, the mixture changed its color to light blue. Continuous stirring was maintained, followed by the addition of 1 mol of ammonium sulfate and ammonium heptamolybdate as a catalyst. The reaction mixture was thoroughly homogenized with a glass rod and heated until a uniform mass was obtained.

Initially, the reagents fully liquefied and then transformed into a viscous mass. The reaction was interrupted, cooled to room temperature, and then maintained in a SNOL furnace for 3 h at a temperature up to 260 °C. This treatment yielded a dark-blue porous powder. Concentrated sulfuric acid (<90%) was gradually added at 80 °C under a fume hood until a paste-like consistency was achieved. During this stage, irritating and suffocating gaseous by-products were released, at which point the process was halted and hot water was carefully introduced. As a result, unreacted starting materials and intermediate products were transferred into the aqueous phase.

After standing, a dark bluish precipitate together with a partially blue solution was observed. The precipitate was collected into a larger vessel, and the acidic medium was neutralized with distilled water. The pigment was then filtered through a Büchner funnel and dried at 80 °C in a ШС-8001 ШСУ dryer.

Results analysis

Thus, the exothermic reaction leading to the formation of the phthalocyanine pigment containing nitrogen, sulfur, and copper (CuSPc) was completed. The target pigment was synthesized with a theoretical yield of 69.3%. Single-crystal X-ray diffraction (SCXRD) is a powerful and widely applied analytical technique for determining the three-dimensional atomic structure of crystalline materials. This method has become indispensable across multiple disciplines, including chemistry, biology, physics, and materials science, due to its ability to reveal the precise atomic arrangement within molecules, minerals, metals, and complex biological macromolecules such as proteins and DNA.

The primary strength of X-ray crystallography lies in its ability to provide accurate structural information at the atomic scale. This makes the technique essential not only for molecular characterization but also for the discovery and development of new compounds. The principle of the method is based on the diffraction of X-rays by the periodic array of atoms within a crystal lattice. The diffraction pattern produced carries detailed information about the internal crystal structure. Through mathematical modeling and computer-assisted analysis, the atomic positions can be precisely determined. Figure 1 presents the results of the X-ray analysis, showing the presence of functional groups in the structure of the synthesized copper phthalocyanine pigment.

The diffractogram displays several distinct peaks corresponding to both the target product and residual secondary phases.

At lower diffraction angles (7–10°), intense peaks corresponding to ammonium heptamolybdate $(NH_4)_6Mo_7O_{24}$ were observed, indicating the partial retention of the catalyst within the pigment matrix. In the region between 15–40°, characteristic reflections assigned to intermediate organic compounds such as $C_8H_{10}O_3$ and $CH_4N_2O_2$ were detected. These signals suggest that certain organic precursors or by-products were not fully decomposed during the synthesis.

At higher angles (>40°), diffraction peaks corresponding to copper sulfate ($CuSO_4$) were identified, together with minor contributions from residual organic species. The presence of $CuSO_4$ implies that a portion of copper remained bonded in the form of sulfate salts rather than being completely integrated into the phthalocyanine framework.

Figure 1. *X-ray diffraction (XRD) analysis of the synthesized copper phthalocyanine pigment (CuSPc)*

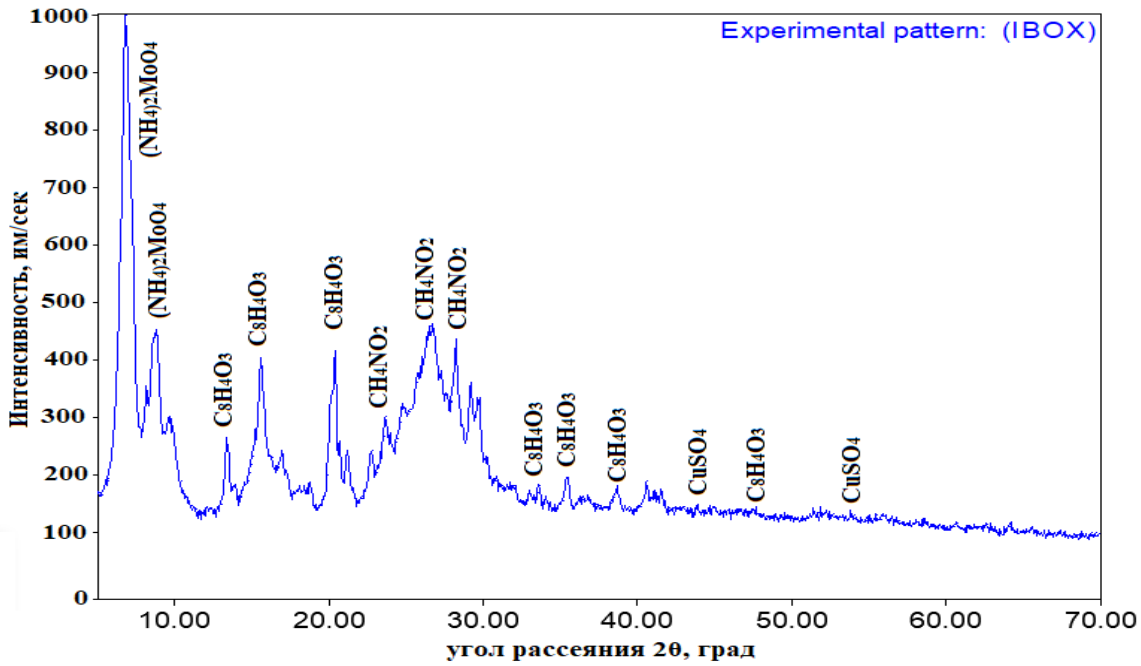

Overall, the XRD results confirm the successful formation of copper phthalocyanine (CuPc) pigment, as evidenced by the dominant crystalline features associated with phthalocyanine derivatives. However, the detection of catalyst residues $(NH_4)_6Mo_7O_{24}$, unreacted intermediates, and $CuSO_4$ side phases indicates that the reaction did not proceed to full completion under the applied conditions. Optimization of synthesis parameters, particularly temperature control and purification steps, may further improve the phase purity of the final pigment.

Conclusion (discussion)

The X-ray diffraction (XRD) analysis of the synthesized copper phthalocyanine pigment (CuSPc) clearly demonstrates the successful formation of the target crystalline phase, confirming the efficiency of the applied synthesis approach. Nevertheless, the diffractogram also revealed the presence of several secondary phases, including residual ammonium heptamolybdate, partially undecomposed organic intermediates, and copper sulfate. These findings indicate that the catalytic agent was not completely eliminated, and a fraction of the organic precursors and copper salts persisted in the final product, suggesting that the reaction did not reach full completion under the current experimental conditions.

The coexistence of the desired CuSPc phase with secondary by-products may negatively affect the pigment's structural homogeneity and potentially influence its optical, electronic, and chemical stability characteristics. Therefore, to achieve higher phase purity and enhanced performance, further optimization of the synthesis parameters is required. Particular attention should be directed toward more precise temperature control, extended reaction time, and improved purification protocols. Such refinements are expected to not only eliminate unwanted residues but also promote the complete incorporation of copper into the phthalocyanine framework, thereby ensuring superior functional properties of the resulting pigment for advanced material applications.

References:

Yusupov M., Kayumjanov O. (2024). Synthesis of metal phthalocyanine pigment based on npk and calculation of particle size using the debye-scherrer equation / Scientific and Technical Journal of Namangan Institute – P. 122–126.
Yusupov, M., & Kadirkhanov, J. (2023). In E3S Web of Conferences (Vol. 390). EDP Sciences.
Lever, A. B. P. (1990). Phthalocyanines: Properties and Applications. Wiley-VC H.
Linstead, R. P. (1934). The Phthalocyanines. Journal of the Chemical Society, – P. 1016–1027.
Kadish, K. M., & Smith, K. M. (Eds.). (2003). The Porphyrin Handbook, Vol. 15: Phthalocyanines: Properties and Materials. Academic Press.
Bottari, G., et al. (2010). Functional phthalocyanines in photodynamic therapy, solar cells and nonlinear optics. Chemical Society Reviews, – 39(8). – P. 2900–2933.
Dini, D., & Hanack, M. (2006). Synthesis and properties of substituted phthalocyanines. Chemical Reviews, – 106(5). – P. 1937–1986.
Han, J., et al. (2024). Graphite-conjugated nickel phthalocyanine for efficient CO_2 reduction. Chemical Science.
Claessens, C. G., et al. (2002). Phthalocyanines: From outstanding electronic properties to emerging applications. Chemical Reviews, – 102(4). – P. 835–853.
Dinçer, H. A., et al. (2007). Tuning of phthalocyanine absorption ranges by additional substituents. Dyes and Pigments, – 72(1). – P. 24–30.
Zhan, R., et al. (2014). Sulfur- and nitrogen-substituted metallophthalocyanines for advanced optoelectronic applications. Journal of Materials Chemistry C, – 2(34). – P. 7151–7160.
Abbaspour, A., et al. (2013). Electrocatalytic activity of iron and nickel phthalocyanines supported on carbon nanotubes. Journal of Electroanalytical Chemistry, – 704. – P. 130–136.

submitted 23.09.2025;
accepted for publication 07.10.2025;
published 26.11.2025

Contact: muz.yusupov90@gmail.com; robiddinovamuhlisa@gmail.com;
doniyor_8184@mail.ru

The Austrian Journal of Technical and Natural Sciences, No 9–10
ISSN 2310-5607

PREMIER Publishing
ppublishing.org

Section 2. Computer science

DOI:10.29013/AJT-25-9.10-63-67

THE SYMPHONIC MODEL OF SOFTWARE PRODUCTION: HARMONIZING AI AGENTS IN COMPLEX SYSTEM DELIVERY

Gulyan Vagan Liparitovich [1]

[1] Executive Director of Projects Softorize, Los Angeles, CA

Cite: *Gulyan V.L. (2025). The symphonic model of software production: harmonizing AI agents in complex system delivery. Austrian Journal of Technical and Natural Sciences 2025, No 9–10.* https://doi.org/10.29013/AJT-25-9.10-63-67

Abstract

The integration of artificial intelligence (AI) into software development has fundamentally transformed how complex systems are designed, built, and delivered. This narrative review presents the symphonic model, a cohesive framework inspired by orchestral performance that coordinates specialized AI agents within agile teams to achieve superior efficiency, quality, and adaptability. Through thematic synthesis of multi-agent architectures, sequential collaboration patterns, and real-world implementations, the model demonstrates accelerated development cycles, enhanced code integrity, and proactive risk mitigation. While integration challenges, ethical accountability, and data governance remain critical hurdles, structured adoption yields transformative gains. The discussion explores evolving human roles, emerging AI paradigms, and strategic pathways for responsible, scalable implementation.

Keywords: *symphonic model, AI agents, multi-agent systems, software development, agile methodology, context amplification, Three Amigo Agents, LLM orchestration, development automation, operational intelligence, software quality, ethical AI, governance frameworks, knowledge transfer, ROI in AI adoption*

Introduction

Software development now operates at a scale and velocity that traditional methodologies can no longer sustain. Modern systems demand seamless integration of distributed services, real-time responsiveness, stringent security, and continuous evolution, all under compressed timelines. The symphonic model of software production addresses these pressures by reimagining development teams as orchestras, where human specialists and AI agents perform distinct, interdependent roles under unified direction to produce a coherent, high-quality outcome. Drawing from the dynamics of orchestral performance, the model treats each participant as a musician with a unique instrument. Developers, designers, testers, architects, and AI agents contribute specialized outputs including code, interfaces, validations, and

optimizations, while a conductor (typically a human product owner or AI orchestrator) ensures alignment, tempo, and harmony. This is not merely metaphorical: it reflects a deliberate design of role clarity, transparent communication, adaptive coordination, and iterative refinement.

Agile methodologies form the structural backbone of the symphonic approach. With Scrum widely adopted and hybrid frameworks gaining momentum, agile practices enable the feedback-driven, incremental delivery essential for dynamic synchronization. The integration of AI Himalayan agents elevates this foundation, automating repetitive tasks, enhancing decision accuracy, and amplifying contextual understanding while preserving human judgment for strategic, ethical, and creative direction.

The model rests on interconnected principles: role specialization within a unified framework, radical transparency across all contributors, dynamic responsiveness to change, collaborative interdependence that amplifies collective output, and continuous improvement driven by automated metrics and human reflection. This review synthesizes theoretical foundations, technical implementations, case studies, and governance models to evaluate how AI agents organized into development support and operational assistance systems can be harmonized to deliver complex software with unprecedented efficiency and reliability.

Methods

This study employs a narrative review methodology to consolidate insights from academic literature, industry reports, technical documentation, and documented case studies on AI-augmented software development. A systematic search was conducted across Google Scholar, arXiv, IEEE Xplore, ACM Digital Library, ResearchGate, and practitioner platforms using targeted keyword combinations including “symphonic model software,” “AI agents agile,” “multi-agent software engineering,” “orchestral development framework,” “LLM agent collaboration,” and “context amplification AI.” Publications from 2020 to 2025 were prioritized to capture advancements in large language models and multi-agent systems.

Sources were selected based on their description of structured AI agent roles in development workflows, provision of empirical or demonstrable case studies, discussion of integration or ethical implications, and presentation of architectural patterns such as sequential collaboration or orchestration. Purely speculative or marketing-focused content was excluded, as were studies limited to single-agent AI applications.

Thematic analysis involved qualitative coding to identify recurring concepts including agent categorization, collaboration mechanisms, context propagation, performance benchmarks, ethical risks, and governance structures. Case studies were evaluated for reproducibility, documentation completeness, and measurable outcomes. Cross-validation across independent sources ensured robustness. No primary data was collected; the synthesis focused on constructing a coherent, evidence-based framework for symphonic AI harmonization.

Results

AI Agent Categorization and Capabilities. AI agents within the symphonic model are organized into two complementary domains: development support systems and operational assistance systems. Development support systems operate directly within the codebase and design lifecycle, enhancing precision, consistency, and velocity. These agents leverage transformer-based language models to generate context-aware code, predict and prevent defects through static and dynamic analysis, automatically produce comprehensive test suites covering edge cases and regression paths, evaluate pull requests for style, security, and architectural compliance, and synthesize up-to-date documentation from code and version history.

Operational assistance systems focus on runtime environments, infrastructure resilience, and system health. They employ time-series forecasting and unsupervised learning to detect anomalies in performance or behavior before user impact, use reinforcement learning to optimize resource allocation and autoscaling, automate incident correlation and root-cause suggestion during outages, continuously monitor for security threats including zero-day patterns and cre-

dential misuse, and analyze user interaction data to identify friction points and recommend interface improvements.

The Three Amigo Agents Pattern. A defining mechanism of symphonic execution is the Three Amigo Agents pattern, a sequential, context-amplifying collaboration triad that extends traditional product triads by embedding specialized AI agents. The process begins with the Product Manager Agent, which receives high-level vision, user needs, and business constraints and produces a comprehensive Product Requirements Document, detailed user stories, acceptance criteria, API contracts, data models, and system architecture diagrams, transforming ambiguity into traceable specifications.

The UX Designer Agent then consumes this documentation alongside technical constraints to generate a cohesive design system including color palettes, typography, reusable components, wireframes, high-fidelity mockups, interactive prototypes, and accessibility compliance reports, ensuring visual consistency, usability, and implementation feasibility.

Finally, the Implementation Agent receives the accumulated documentation suite, often exceeding 25 artifacts, and produces a complete, production-ready codebase encompassing frontend and backend services, CI/CD pipelines, deployment configurations, and monitoring instrumentation. This agent operates with full contextual awareness, minimizing integration errors and rework.

The human product owner intervenes at decision gates to refine, approve, or redirect outputs, maintaining strategic control while benefiting from amplified context. The sequential handoff creates a knowledge flywheel: initial inputs of five to seven documents expand progressively, resulting in a richly specified, implementable system.

Case Study 1: AI-Orchestrated Health Analytics Platform. A multi-agent health analysis platform was developed from an empty repository to a fully functional system in under three hours using an orchestrator-worker architecture. The Product Manager Agent first generated a detailed PRD, user stories, OpenAPI specification, and database schema for a multi-domain medical insights engine. The UX Designer Agent then produced a glassmorphic design language, reusable React components, and interactive prototypes supporting real-time physician-agent collaboration.

The Implementation Agent subsequently delivered a FastAPI backend with asynchronous endpoints, eight specialized medical domain agents covering cardiology, oncology, and other fields, Server-Sent Events for live data streaming, PostgreSQL integration with vector embeddings, and a React/TypeScript frontend with dynamic dashboards. The system supported concurrent queries, visualized cross-domain insights, and maintained audit trails compliant with healthcare standards, all without human coding.

Case Study 2: Enterprise-Scale Agile Transformation with AI. An online gaming platform restructured multiple cross-functional teams using symphonic principles and embedded AI agents as fixed-role contributors. Teams were organized into specialized sections for frontend, backend, DevOps, quality assurance, and AI, with Kanban boards enhanced by predictive flow analytics. Daily standups incorporated automated AI status summaries, sprint planning used AI-generated risk forecasts, and retrospectives leveraged defect trend analysis from operational monitoring agents. The transformation resulted in a significant reduction in production defects, faster feature delivery, decreased regression testing time, and high acceptance of AI-generated code suggestions. Transparency, collaboration, and continuous improvement were reinforced through integrated ceremonies and real-time visibility.

Performance Metrics and ROI. Organizations implementing the symphonic model report substantial gains across key indicators. Sprint velocity increases markedly, defect escape rates drop sharply, lead time from idea to deployment is halved, and developer satisfaction rises. A hypothetical return-on-investment model for a ten-developer team shows initial costs for tools, training, and integration offset by annual savings in productivity, rework reduction, and revenue acceleration, yielding a positive first-year net gain, rapid payback, and strong multi-year ROI.

Discussion

The symphonic model redefines software production by positioning AI as

a collaborative ensemble member rather than a standalone tool. The Three Amigo pattern's context amplification eliminates common failure modes such as misaligned requirements, design-implementation gaps, and integration debt. By automating routine synthesis and validation, the model frees human contributors to focus on architecture, innovation, and ethical oversight.

However, harmonization requires more than technical connectivity. Ethical governance is essential: as AI agents exercise increasing autonomy, accountability must remain traceable. Audit trails, decision provenance, and human veto mechanisms prevent diffusion of responsibility. Automation bias, the over-reliance on AI outputs, must be countered through confidence scoring, skepticism training, and mandatory review of high-impact recommendations.

Data quality underpins agent effectiveness. Biased or fragmented training data risks perpetuating legacy anti-patterns or excluding edge cases. Federated learning, synthetic data augmentation, and continuous bias monitoring provide mitigation strategies. The model also accelerates institutional learning: AI agents encode best practices across thousands of projects, mentor junior developers through contextual explanations, and enable senior architects to prioritize system-level trade-offs.

Emerging paradigms such as neural-symbolic integration, autonomous verification agents, and cross-project knowledge graphs promise self-optimizing development ecosystems. Human roles will shift from implementation to system curation: defining constraints, validating outputs, and steering innovation. Current limitations include dependency on high-quality prompts, negotiation latency between agents, limited legacy codebase support, and regulatory gaps in AI-driven production.

Future research should focus on longitudinal studies of team dynamics, standardized interoperability benchmarks, and domain-specific governance frameworks. Strategic adoption pathways include piloting with greenfield services, establishing AI orchestrators for task routing and conflict resolution, implementing progressive autonomy from advisory to supervised execution, building real-time feedback flywheels, forming AI review boards, standardizing knowledge formats, and monitoring agent performance drift.

Conclusions

The symphonic model marks a paradigm shift in software engineering, from fragmented workflows and tribal knowledge to a unified, intelligent, and adaptive production system. By harmonizing specialized AI agents within an agile, human-directed framework, organizations achieve dramatic efficiency in complex system delivery, superior quality through multi-layered validation, resilient knowledge capture that transcends individual contributors, and ethical, governable AI embedded in development culture. When implemented with technical precision, cultural alignment, and ethical foresight, this model enables software teams to transcend traditional coding, composing intelligent, evolving digital symphonies that adapt, improve, and perform at scale.

References

Mennella, C., Maniscalco, U., De Pietro, G., & Esposito, M. (2024). Ethical and regulatory challenges of AI technologies in healthcare: A narrative review. *Heliyon*, – 10(4). URL: URL: https://doi.org/10.1016/j.heliyon.2024.e26297

Symphony Solutions. (2021). Agile Implementation in Team: Methodology, Models, Processes & Tools. Retrieved from URL: https://symphony-solutions.com/insights/agile-implementation-guide

Spitfire Audio. (2025). BBC Symphony Orchestra Discover. Retrieved from URL: https://www.spitfireaudio.com/en-us/products/bbc-symphony-orchestra-discover

Vetticaden, G. (2023). 3 Amigo Agents pattern for complex system development using Claude Code. Retrieved from URL: https://www.linkedin.com/posts/georgevetticaden_claudecode-aiagents-developertools-activity-7349066098316562432–8TTf

Qian, C., Cong, W., Qian, Y., Liu, B., & Yin, H. (2025). LLM-Based Multi-Agent Systems for Software Engineering: A Review. URL: https://arxiv.org/html/2404.04834v4

Wang, Y. (2025). Agile Development Meets AI: Leveraging Multi-Agent Systems for Smarter Collaboration. *ResearchGate*. URL: https://www.researchgate.net/publication/388834810_Agile_Development_Meets_AI_Leveraging_Multi-Agent_Systems_for_Smarter_Collaboration

Li, J. (2025). AI-Driven Automation in Agile Development: Multi-Agent LLMs for Software Engineering. *ResearchGate*. URL: https://www.researchgate.net/publication/388834977_AI-Driven_Automation_in_Agile_Development_Multi-Agent_LLMs_for_Software_Engineering

Zhang, L., et al. (2025). A Comprehensive Review of AI Agents: Transforming Possibilities in Software Development. URL: https://arxiv.org/html/2508.11957v1

Smith, A., et al. (2024). Towards LLM-augmented multiagent systems for agile software development. *Proceedings of the IEEE/ACM 46th International Conference on Software Engineering (ICSE)*. URL: https://dl.acm.org/doi/10.1145/3691620.3695336

Johnson, B., et al. (2023). A multi-agent model for planning hybrid software processes. *Procedia Computer Science*, – 220. – P. 105–114.

submitted 12.10.2025;
accepted for publication 26.10.2025;
published 26.11.2025

Contact: alffanchor@gmail.com

The Austrian Journal of Technical and Natural Sciences, No 9–10
ISSN 2310-5607

PREMIER Publishing
ppublishing.org

DOI:10.29013/AJT-25-9.10-68-74

SPATIO-TEMPORAL LATENT FEATURES FOR SKELETON-BASED HUMAN ACTION RECOGNITION USING GCN+SOFTMAX CLASSIFIER

Avazjon Marakhimov [1], ***Kabul Khudaybergenov*** [2,3], ***Zakhriddin Mominov*** [4]

[1] Tashkent State Technical University, Tashkent, Uzbekistan;

[2] Kimyo International University in Tashkent, Tashkent, Uzbekistan;

[3] Research Institute for the Development of Digital Technologies and Artificial Intelligence, Tashkent, Uzbekistan;

[4] Tashkent State University of Economics, Tashkent, Uzbekistan

Cite: *Avazjon M., Kabul K., Zakhriddin M. (2025). Spatio-temporal latent features for skeleton-based human action recognition using GCN+SoftMax classifier. Austrian Journal of Technical and Natural Sciences 2025, No 9–10.* https://doi.org/10.29013/AJT-25-9.10-68-74

Abstract

Human action recognition through skeletal analysis represents a fundamental challenge with significant implications for real-world applications. Contemporary approaches frequently depend on singular skeletal sequence representations, potentially limiting their capacity to comprehensively encode the multifaceted characteristics inherent in human actions. This work introduces LFHAR (Latent Features for Human Action Recognition), an innovative architectural framework that leverages diverse spatio-temporal latent encodings to enhance action feature extraction. The proposed representations model the temporal progression of skeletal configurations while incorporating both joint-level and limb-level motion patterns. The methodology employs a graph-based transformation for individual skeletal frames within temporal sequences, subsequently organizing the extracted graph features into spatio-temporal matrices. Experiments on benchmark datasets validates the robustness and invariance properties of the LFHAR framework. The approach achieves notable performance gains, with accuracy improvements of 2.7% and 2.1% on the NTU-RGB+D 60 and NTU-RGB+D 120 datasets, respectively, substantiating its effectiveness in advancing skeleton-based action recognition.

Keywords: *Invariant representations, Latent features, Skeleton-based action recognition, Spatio-temporal graph network*

1. Introduction

Human action recognition constitutes a critical component across diverse application domains, encompassing human-computer interaction systems, automated surveillance, robotic systems, medical applications, and immersive virtual environments. Research in this domain has explored

multiple data modalities, spanning RGB video streams, depth-based recordings, and skeletal joint representations (Sun et. al., 2022). The skeleton-based paradigm has emerged as particularly compelling due to its inherent robustness against environmental variations including background clutter, attire differences, and illumination changes, while simultaneously offering high-fidelity 3D spatial coordinates of anatomical landmarks. Historical approaches to skeletal data acquisition relied on motion capture infrastructures employing body-mounted sensors, multi-view camera arrays, or infrared tracking systems within constrained laboratory settings (Ahmad et. al., 2021).

Recent breakthroughs in computer vision methodologies have catalyzed fundamental transformations across diverse sectors, encompassing medical diagnostics, financial modeling, predictive analytics, and visual computing. Deep learning architectures have particularly revolutionized automated hierarchical feature learning from visual data, enabling sophisticated pattern recognition capabilities that obviate traditional manual feature design. These advances have yielded remarkable achievements in visual recognition tasks including categorical classification, object localization, and semantic segmentation, often matching or exceeding human-level accuracy. Consequently, these technological developments have facilitated robust skeletal pose estimation directly from video streams through deep learning pipelines, eliminating dependencies on specialized sensor hardware (Cheng et. al., 2020).

The extraction of discriminative action-specific features from skeletal trajectories constitutes a fundamental challenge in skeleton-based recognition systems. Traditional approaches relied on handcrafted feature engineering, transforming skeletal sequences into compact representations suitable for conventional classifiers including K-Nearest Neighbor algorithms, Random Forest ensembles, or Hidden Markov Models.

2. Related works

To address the aforementioned constraints, this research introduces a novel architectural framework for skeleton-based action recognition, designated as LFHAR (**L**atent **F**eatures for **H**uman **A**ction **R**ecognition). The LFHAR architecture comprises three principal components: action representation, latent feature extraction, and human action prediction modules. Within the action representation component, we formulate five distinct image-based spatio-temporal action latent features that encode action sequences from complementary perspectives, thereby mitigating the inherent limitations associated with singular action representation schemes. Although numerous action representation paradigms exist, our proposed quintet of representations strategically emphasizes fundamental motion dynamics to achieve distinctive characterization of individual actions.

In examining human kinematic patterns, action differentiation emerges through temporal evolution of skeletal configurations and the directional characteristics of articular and limb trajectories. Directional motion attributes can be encoded through two complementary modalities: angular variations between interconnected limb segments and spatial displacement metrics between joint coordinates (Xin et. al., 2022). Furthermore, temporally similar actions executed at varying velocities manifest subtle disparities in both angular measurements and inter-joint spatial relationships, necessitating the development of velocity-invariant representational schemes to ensure robust action characterization across different execution speeds.

For encoding the temporal evolution of skeletal poses, we introduce a spatio-temporal Graph Latent Features (GF) representation, manifested as an RGB feature map derived from a graph matrix wherein columns encode individual skeletal graph representations across the three Cartesian dimensions. This representational scheme achieves coordinate invariance by emphasizing temporal variations in topological joint relationships rather than absolute positional coordinates. The underlying rationale for this approach stems from the over-smoothing phenomenon inherent in GCN-based architectures, where representational efficacy becomes contingent upon network depth (Liu et. al., 2025). In contrast, consolidating the complete graph sequence into a unified,

fixed-dimensional image representation ensures computational stability.

Recognizing that graph representations inadequately capture joint motion dynamics, we propose three complementary distance-based latent features to encode spatio-temporal joint and limb displacement patterns throughout the action sequence. Each descriptor manifests as a single-channel grayscale image derived from distance matrices, with columns encoding inter-joint or inter-limb distances. The Joint Distance Latent Features (JDLF) encode intra-frame joint-to-joint distances across the temporal sequence. The Adjacent Distance Latent Features (ADLF) capture inter-frame joint displacements between consecutive temporal instances, providing visual encoding of action velocity that enables recognition of identical actions performed at varying speeds, thereby conferring velocity invariance. The Limbs Angle Latent Features (LALF) quantify angular variations between adjacent limb segments, additionally encoding joint directional information through temporal angular changes. To construct a comprehensive motion representation, these three distance latent features are integrated into a tri-channel Fusion Distance Latent Feature (FDLF). These four distance-based latent features exhibit view invariance through their exclusive reliance on relative distances between anatomical landmarks. Moreover, they normalize actions of heterogeneous temporal durations into fixed-dimensional image representations, ensuring frame-count invariance.

The feature extraction component employs specialized models for deriving features from the five latent representations (GLF, JDLF, ADLF, LALF, and FDLF). Given that these latent features manifest as texture-patterned feature maps (Fig. 1), we implement a shallow 1D CNN architecture optimized for pattern classification. Feature extraction proceeds independently for each latent representation through dedicated single-descriptor models for action prediction. Furthermore, features from all five representations undergo concatenation to construct a comprehensive and complementary action encoding via a fusion model. The prediction component generates six classification outputs: five from individual descriptor models and one from the fusion architecture. Final class determination employs a voting algorithm that implements majority consensus when multiple models produce concordant predictions.

Figure 1. *Architectural overview of the LFHAR framework, comprising three integrated modules*

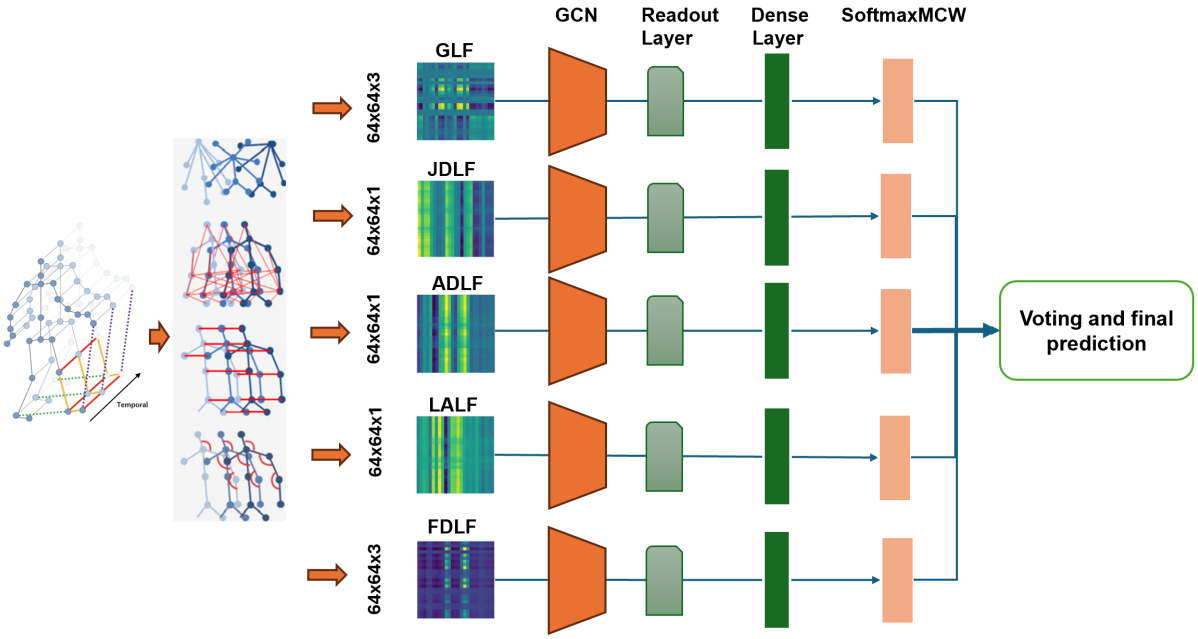

The action representation module performs transformation of input skeletal sequences into five distinct image-based latent representations: Graph Latent Fea-

tures (GLF), Joint Distance Latent Features (JDLF), Adjacent Distance Latent Features (ADLF), Limbs Angle Latent Features (LALF), and Fusion Distance Latent Features (FDLF). The latent feature extraction module employs a GCN architecture followed by Readout layer operations. After then the output from this layer is processed by dense layer and for classification is used SoftMaxMCW (Marakhimov et. al., 2025). *The action prediction module generates classification scores from six feature streams – encompassing the five independent latent representations and their concatenated fusion – utilizing one-dimensional convolutional layers (Conv1D). A voting-based ensemble mechanism subsequently determines the final classification output through consensus aggregation of the multiple prediction streams.*

3. Methodology

The framework of LFHAR-GCN-SoftMaxMCW architecture is depicted in Fig. 1. It mainly consists of three separate stages: human skeleton action representation, latent feature extraction, and action classification.

We use *Human action representation, Skeleton graph matrix* and *Joints distance matrix* from work (Aouaidjia et. al., 2025). However, authors build very heavy models which is impossible to employ in real-time human action recognition. Thus we build our model based on (Marakhimov et. al., 2025) to get the faster human skeleton based action recognition.

3.1. Human action representation

We define the skeleton sequence as $Seq = \{S_k, k = 1,...,T\}$, where T is the number of frames, and the skeleton S_k as a graph $S_k = \{V, E\}, V = \{\{\{J_{i,j}\}_{i=1}^{N}\}_{j=1}^{3}\}, J_{i,j}$ is the coordinate j of the joint i, and N is the number of joints (vertices). We normalize the skeleton sequence by considering the "*middle of the spine*" joint of the first frame as the new origin of the coordinates system. In the rest of the coming sections, we use the term "*limb*" to refer to a skeleton bone that forms an angle with its adjacent bone.

3.1.1. Skeleton graph matrix

For each skeleton S_k represented as $N \times 3$ matrix, the symmetric adjacency matrix is defined as $A = \{a_{i,j}, i, j = 1,...,N\}$, where $a_{i,j} = 1$ if the joints i and j are connected, and $a_{i,j} = 0$, otherwise. The normalized adjacency matrix $\mathbf{A}'$ is calculated by dividing each row by the sum of its values. The graph $\mathbf{G}_k$ of a single skeleton $\mathbf{S}_k$ is obtained by:

$$\mathbf{G}_k = \mathbf{S}_k^t \mathbf{A}' = \begin{bmatrix} j_{11}\, j_{21} \cdots j_{N1} \\ j_{12}\, j_{22} \cdots j_{N2} \\ j_{13}\, j_{23} \cdots j_{N3} \end{bmatrix} \cdot \begin{bmatrix} a'_{11} & a'_{12} & \cdots & a'_{N1} \\ a'_{21} & a'_{22} & \cdots & a'_{N2} \\ \vdots & \vdots & \ddots & \vdots \\ a'_{N1} & a'_{N2} & \cdots & a'_{NN} \end{bmatrix} = \begin{bmatrix} g_{11}\, g_{21} \cdots g_{N1} \\ g_{12}\, g_{22} \cdots g_{N2} \\ g_{13}\, g_{23} \cdots g_{N3} \end{bmatrix}, \quad (1)$$

$$a'_{i,j} = \frac{a_{i,j}}{\sum_{j=1}^{N} a_{i,j}}, \quad (2)$$

where t represents the matrix transpose operation. The spatio-temporal graph representation of the sequence is given by the 3D graph matrix $M^{gr} \in R^{N \times 3 \times T}$ as:

$$\mathbf{M}^{gr} = \{\mathbf{G}_k^t\}_{k=1}^{T} = \left\{ \left\{ \left\{ g_{i,j,k} \right\}_{i=1}^{N} \right\}_{j=1}^{3} \right\}_{k=1}^{T} = \begin{bmatrix} g_{1,j,1} & g_{1,j,2} & \cdots & g_{N,j,T} \\ g_{21} & g_{2,j,2} & \cdots & g_{N,j,T} \\ \vdots & \vdots & \ddots & \vdots \\ g_{N1} & g_{N,j,2} & \cdots & g_{N,j,T} \end{bmatrix}, \quad (3)$$

where $j = 1,2,3$, $g_{i,j,k}$ are the features of the joint i of the coordinate k of the skeleton k. $\mathbf{M}_{gr}$ is a 3D matrix consists of three 2D matrices, corresponding to $j = 1,2,3$, which represents the three Cartesian axes. The construction of the graph matrix is illustrated visually in Fig. 2(a).

3.1.2. Joints distance matrix

One of the key factors for a robust motion representation is to capture the inter-joints distance evolution over time. For example, in the action '*clapping*', it is important to know how far the left-hand joint is moving from the right-hand joint. To construct a joint distance representation, we selected the 32 most informative pairs that have a higher changeable rate during the motion than the other pairs, where the joints involved in the selected pairs.

Given a skeleton S_k, we define the set of the selected pairs as: $Pair = \{p_i, i = 1,...,P\}$, where P is the total number of selected pairs, and $p_i = (J^a, J^b)$ is the pair of the joints J^a and J^b. For each pair p_i, the Euclidean distance d_i is calculated between its two joints as: $d_i = \left\| J^a - J^b \right\|_2$. However, the distance between two joints in a skeleton of a shorter person is less than that of a taller person, due to the difference in limbs length. To normalize the distance d_i of the pair p_i for all body sizes, we divide the distance d_i by the body size z, where the normalized distance $d'_i = d_i / z$, and the body size $z = \sum_{i=1}^{N-1} L_i$, which is the sum of the lengths of all the skeleton limbs L_i, and the limb length is the distance between its joints. The joints distance matrix $M_{jdis} \in R^{P \times T}$ is defined as:

$$\mathbf{M}^{jdis} = \left\{ \left\{ \frac{d_i}{z} \right\}_{i=1}^{P} \right\}_{k=1}^{T} = \left\{ \left\{ d'_{i,k} \right\}_{i=1}^{P} \right\}_{k=1}^{T} = \\ = \begin{bmatrix} d'_{11} & d'_{12} & \cdots & d'_{P1} \\ d'_{21} & d'_{22} & \cdots & d'_{P2} \\ \vdots & \vdots & \ddots & \vdots \\ d'_{P1} & d'_{P2} & \cdots & d'_{PN} \end{bmatrix}, \quad (4)$$

where $d'_{i,k}$ is the normalized distance of the pair p_i of the skeleton S_k.

3.1.3. Adjacent distance matrix

The adjacent distance matrix represents the temporal change in the joint coordinates values between each two consecutive frames. In other words, the distance between the joint in a frame k and its new position in the frame $k+1$. It also represents action velocity, where larger distances indicate faster movement of the joints. Given two consecutive skeletons S_k and S_{k+1} of the sequence, the adjacent Euclidean distance $a_{i,k}$ of a joint i between two consecutive frames k and $k+1$ is written as: $a_{i,k} = \left\| J_{i,k} - J_{i,k+1} \right\|_2$. The Adjacent Distance Matrix $\mathbf{M}^{adis} \in R^{N \times (T-1)}$ is defined as follows:

$$\mathbf{M}^{adis} = \{\{a_{i,k}\}_{i=1}^{N}\}_{k=1}^{T-1} = \{\{\left\| J_{i,k} - J_{i,k+1} \right\|_2\}_{i=1}^{N}\}_{k=1}^{T-1} \quad (5)$$

$$\begin{bmatrix} \left\| J_{1,1} - J_{1,2} \right\|_2 & \left\| J_{1,2} - J_{1,3} \right\|_2 & \cdots & \left\| J_{1,T-1} - J_{1,T} \right\|_2 \\ \left\| J_{2,1} - J_{2,2} \right\|_2 & \left\| J_{2,2} - J_{2,3} \right\|_2 & \cdots & \left\| J_{2,T-1} - J_{2,T} \right\|_2 \\ \vdots & \vdots & \ddots & \vdots \\ \left\| J_{N,1} - J_{N,2} \right\|_2 & \left\| J_{N,2} - J_{N,3} \right\|_2 & \cdots & \left\| J_{N,T-1} - J_{N,T} \right\|_2 \end{bmatrix}$$

4. Experiments

Table 1 presents the comparative results between LFHAR and state-of-the-art approaches on the NTU-RGB+D 60 dataset. The proposed LFHAR method achieves superior recognition accuracy on benchmark datasets and outperforms existing methods that integrate GCN with attention mechanisms. The results indicate a 1.5% improvement over 2s-AGCN, which employs reinforcement learning for dynamic joint selection. In contrast, our approach utilizes multiple invariant representations that offer comprehensive action encoding, enabling adaptation to dynamic variations without requiring complex training procedures.

Table 1. *Comparison of accuracy between LFHAR-GCN-SoftMaxMCW and the other human action recognition methods on the NTU-RGB+D 60 and NTU-RGB+D 120 dataset*

Method	Accuracy	
	NTU-RGB+D 60	NTU-RGB+D 120
ST-GCN	87.2	88.3
AS-GCN	95.2	94.2
EfficientGCN	92.8	96.1
RA-GCN	93.5	93.6
AGC–LSTM	92.1	95.0
2s-AGCN	95.4	95.1
LFHAR-GCN-SoftMaxMCW	96.9	97.2

Table 2 presents a computational complexity analysis comparing the proposed LFHAR-GCN-SoftMaxMCW framework with existing action recognition methods, evaluated using Floating Point Operations Per Second (FLOPS) and inference time measured in sequences per second. The computational efficiency assessment reveals that

the single-descriptor configuration achieves 7.8 FLOPS, positioning it as the second most efficient model in the comparison. The model, which processes the concatenated representations of all five descriptors, demonstrates a computational requirement of 31.6 FLOPS. This represents approximately a five-fold increase compared to the single-descriptor variant, which can be attributed to the additional computational overhead of processing the combined feature representations. Given that the complete framework employs multiple models operating in parallel, the overall computational cost is determined by aggregating the FLOPS values of all constituent models, yielding a cumulative value of 25.3 FLOPS for the entire system.

These computational metrics indicate that while the fusion approach incurs higher computational costs due to feature concatenation, the overall framework maintains reasonable efficiency when considering the performance gains achieved through multi-descriptor integration. The inference time measurements further support the practical viability of the proposed method for real-world action recognition applications.

Table 2. *Comparison of FLOPS and Inference time.*

Method	FLOPS	Inference time
ST-GCN	16.3	42.91
AS-GCN	14.5	18.50
EfficientGCN	17.5	23.4
RA-GCN	22.4	19.52
AGC–LSTM	9	30.3
2s-AGCN	11	12.90
LFHAR-GCN-SoftMax-MCW	25.3	17.50

5. Conclusion

This study presents a novel framework for skeleton-based action recognition that comprises three main components: action representation, feature extraction, and action prediction modules. The action representation module employs five image descriptors to encode skeleton sequences. One descriptor captures the spatio-temporal relationship variations among joints throughout the temporal dimension, while the remaining four descriptors encode the distance variations between joints and limbs over time. These descriptors function as latent features that maintain consistency across different poses, viewing angles, and movement velocities, thereby ensuring robust action representation. For the feature extraction component, we implement a GCN+SoftMaxMCW architecture that processes both individual descriptors and their combined representations to extract relevant features and perform classification. The action prediction module generates six class predictions, which are subsequently processed through a voting mechanism to determine the final action category.

We evaluated the proposed framework using four standard benchmark datasets. The experimental results, along with comprehensive ablation studies, confirm the efficacy of our approach. The comparative analysis with existing methods demonstrates that our framework achieves competitive performance in skeleton-based action recognition tasks. These findings suggest that the integration of multiple image descriptors with graph-based feature extraction provides an effective solution for robust action recognition.

Acknowledgements

The research is supported in part by Grants No. IL-5421101773 of the Uzbekistan Ministry for Innovative Development.

References

Sun Z., Ke Q., Rahmani H., Bennamoun M., Wang G., Liu J. (2022). Human action recognition from various data modalities: A review IEEE Trans. Pattern Anal. Mach. Intell.

Ahmad T., Jin L., Zhang X., Lai S., Tang G., Lin L. (2021). Graph convolutional neural network for human action recognition: A comprehensive survey. IEEE Trans. Artif. Intell., – 2 (2). – P. 128–145

Cheng K., Zhang Y., He X., Chen W., Cheng J., Lu H. (2020). Skeleton-based action recognition with shift graph convolutional network, in: Proceedings of the IEEE/CVF Conference on Computer Vision and Pattern Recognition, – P. 183–192.

Xin W., Liu Y., Liu R., Miao Q., Shi C., Pun C.-M. (2023). Auto-learning-gcn: An ingenious framework for skeleton-based action recognition. Chinese Conference on Pattern Recognition and Computer Vision, PRCV, Springer, – P. 29–42.

Liu R., Liu Y., Wu M., Xin W., Miao Q., Liu X., Li L. (2025). SG-CLR: Semantic representation-guided contrastive learning for self-supervised skeleton-based action recognition. Pattern Recognit., – 162. – Article 111377.

Marakhimov, A.R., Khudaybergenov, K.K. (2025). Softmax Regression with Multi-Connected Weights. Computers, accepted.

Aouaidjia K., Zhang C. and Pitas I. (2025). Spatio-temporal invariant descriptors for skeleton-based human action recognition, Inf Sci (NY), – 700. – 121832p. Doi: 10.1016/j.ins.2024.121832

submitted 23.09.2025;
accepted for publication 07.10.2025;
published 26.11.2025

Contact: kabul.kudaybergenov@gmail.com

The Austrian Journal of Technical and Natural Sciences, No 9 – 10
ISSN 2310-5607

PREMIER Publishing
ppublishing.org

Section 3. Food processing industry

DOI:10.29013/AJT-25-9.10-75-78

IMPROVING THE TECHNOLOGY OF BAKERY PRODUCTS PRODUCTION IN ORDER TO ENSURE FOOD SECURITY OF THE POPULATION

Sattarov Karim Karshievich [1], ***Jankurazov Abror Mamarazhab ugli*** [1]

[1] Gulistan State University

Cite: *Sattarov K. K., Jankurazov A. M. (2025). Improving the technology of bakery products production in order to ensure food security of the population. Austrian Journal of Technical and Natural Sciences 2025, No 9 – 10.* https://doi.org/10.29013/AJT-25-9.10-75-78

Abstract

Bakery products occupy one of the leading places in the diet of the population and are an important source of carbohydrates, proteins, vitamins and minerals. Modern trends in the development of bakery involve the use of food additives that improve nutritional value, functional properties, shelf life and organoleptic characteristics of products. The paper considers the classification of food additives, their technological significance and impact on the quality of bakery products. The problems of using additives and the prospects for improving technology, taking into account the requirements of safety and healthy nutrition, are outlined.

Keywords: *bakery products, food additives, functional products, nutritional value, baking technology*

Introduction

The modern food industry is focused not only on providing the population with mass-consumption products, but also on the production of functional and specialized food products. Bread, as one of the most consumed products, plays a key role in ensuring food security. However, traditional bakery products do not always fully satisfy the physiological needs of the body for the necessary nutrients.

One of the ways to increase the nutritional value of bread is the use of food additives and enriching components: protein concentrates, dietary fiber, vitamins, minerals, enzyme preparations, as well as natural vegetable ingredients (pumpkin, soy, flaxseed flour, vegetable and fruit powders). Their use allows not only to improve the quality of products, but also to give them functional properties, which corresponds to global trends in healthy eating. Proteins are an essential component of food, with their deficiency, hematopoiesis decreases, the development of a growing organism is delayed, the metabolism of fats and vitamins, the activity of the nervous system, liver and other organs is disrupted, and cell recovery slows down after severe diseases.

Protein deficiency is one of the serious problems in the nutrition of the population, especially socially vulnerable groups. Protein deficiency in the country is 30–40% and increases annually, therefore, along with the use of ready-made protein preparations, it is necessary to use non-traditional protein sources (Erashova L. D., Pavlova G. I., Ermolenko R. S., 2009).

Fortified bakery products with protein-containing additives from non-traditional vegetable raw materials are one of the promising ways to increase nutritional value.

Legumes are often used as a source of cheap vegetable protein, since, in addition to their unique chemical composition, they are characterized by their availability and availability of sufficient raw materials. A large number of plant-based proteins and relatively low production costs make it possible to significantly compensate for the protein deficiency in human nutrition. Chickpeas are one of the oldest crops that have been cultivated in the Middle East and other tropical and subtropical countries since time immemorial (Klochkova I. S., Davydovich V. V., 2018). All additives used in the bakery industry can be divided into several groups:

The structure – forming and dough improvers are enzyme preparations (amylases, xylanases), emulsifiers (lecithin, mono- and diglycerides of fatty acids), oxidants (ascorbic acid, Enriching additives – mineral salts (iron, calcium, zinc), B vitamins, vitamin D, dietary fiber, Functional ingredients – protein concentrates from legumes, whey, seeds; powders of vegetables, fruits, herbs; prebiotics, Stabilizers and preservatives – organic acids (sorbic, propionic), essential oils and natural extracts with antimicrobial action. All these additives affect the quality of bread in different ways: Enzymes and emulsifiers improve the gas-holding capacity of the dough, increase the volume and porosity of the bread. Protein concentrates increase the content of essential amino acids, especially lysine, which is deficient in wheat flour. Dietary fiber (bran, fiber, pectin) normalizes digestion and reduces the glycemic index of bread. Mineral supplements make it possible to create preventive products (for example, bread fortified with iron to prevent anemia). Vegetable and fruit powders give products new flavors and increase the content of biologically active substances (Pashchenko L. P., Kurchaeva E. E., Kulakova Yu.A., Yakovleva.E.A., 2004).

The purpose of the study is to analyze the technological and physiological features of the use of food additives in the production of bakery products.

Materials and methods

This study examined the classification of additives by functional purpose, the effect of protein, mineral and vitamin additives on bread quality, the role of enzyme preparations and dough improvers, the use of vegetable powders and dietary fibers, and the safety assessment and regulations for the use of additives in baking. Data from open sources, including scientific articles, books and publications, were used as materials. related to the topic of food additives in bakery. A search was conducted for sources using the electronic databases Google Scholar, Scopus and Web of Science to identify relevant research.

Results and discussion

During the work, five experimental bread samples were prepared with a mixture of chickpea and barley flour from 1 to 5% by weight of wheat flour. The products were made using a non-stick method according to a unified formulation (Ershov P. S., 2001).

The mixture used in the research process had a humidity of 15% and an acidity of 1.8 degrees. At the first stage of production, the mixture was mixed with wheat in appropriate proportions and added to the dough, the dough was kneaded at a temperature of 30–320 C for 40 minutes, the final moisture content of the dough was 42%, which met the requirements of the technological instructions (dough moisture 42–45%).

The kneaded dough of the control sample was left to ferment at a temperature of 32–34^{0}C for 3.5 hours, and then divided into pieces of a given mass and sent for proofing. The fermentation time of the test samples at a temperature of 32–340 °C was 2.5 hours, since the addition of a flour mixture accelerates the maturation process of the dough due to the intensification of its fermentation and accumulation of organic acids, as well as the

presence in the additive of a large amount of minerals that give an acidic reaction. For this reason, a safe method of dough preparation was chosen (Jankorazov A. M., Sattarov K. K., 2024). Thus, the introduction of a mixture of chickpea and barley flour allowed not only to enrich bakery products with vegetable protein, but also to speed up the production process. The molded bread was baked at 180–200^0 C for 50 minutes in a moistened baking chamber until the crust color changed from golden yellow to golden brown. The quality indicators of the prototypes were determined after cooling in accordance with GOST 5667–65 "Bread and bakery products. Acceptance rules, sampling methods, methods for determining organoleptic parameters and weight of products" During the trial baking, organoleptic studies of the products were performed Table 1.

Table 1. *Organoleptic characteristics of bakery products using a mixture of chickpea and barley flour*

Indicators	Control	The content of a mixture of chickpea and barley flour,%	
Appearance:			
Form	Correct, without pretensions (5)		
Surface	Smooth, without cracks or explosions, with oblique cuts (5.0)		With oblique cuts and small cracks (4.0)
Color	Light yellow uniform (5.0)	Yellow with a small amount of dark spots (4.5)	Brown, large number of dark spots (3.5)
Crumb condition:			
Baking	Baked, not moist to the touch, elastic (5.0)		
Promes	Without lumps and traces of non-wood (5.0)		
Porosity	Uniform, developed, without voids and seals (5.0)		Uneven, undeveloped (3.5)
Taste	Pleasant, without an extraneous taste, characteristic of this type of product (4,5)	Pleasant, with a slight hint of nuts (5.0)	With an unpleasant taste of legumes (3.0)
Smell	Pleasant, odorless, characteristic of this type of product (4,5)	Pleasant light smell of nuts (5.0)	Pronounced unpleasant odor of legumes (3.0)

As a result, Table 1 revealed that with an increase in the amount of a mixture of chickpea and barley flour to 5%, the crumb color deteriorates due to dark inclusions of a mixture of chickpea and barley flour, as well as the color of the upper crust darkened much faster. In addition, there was a negative effect on the taste and aroma of bread, as there was a pronounced taste and smell of legumes. When adding a mixture of chickpea and barley flour in an amount from 1 to 3%, the color does not change much compared to the control, with a flour content of 4%, a light pleasant aroma of nuts appears, which is typical for chickpea and barley flour. Thus, an increase in the amount of a mixture of chickpea and barley flour to 5% of the total amount of flour is impractical, since it leads to a deterioration in the organoleptic characteristics of the product, in particular, a pronounced smell and taste of legumes appears, the color and surface of the finished products change. The results of the physico-chemical parameters of samples with different ratios of a mixture of chickpea and barley flour are presented in Table 2.

Table 2. *Physico-chemical parameters of samples with different ratios of a mixture of chickpea and barley flour*

Indicators	Control	The content of a mixture of chickpea and barley flour,%				
		1	2	3	4	5
Crumb moisture,%	40.7	40.8	40.8	41.0	41.0	41.4
Crumb moisture,%	1.8	2.0	2.2	2.4	2.4	2.7
Porosity,%	78	80	80	82	82	64

A study of the physico-chemical quality indicators (Table 1) of molded bread showed that all indicators are within the limits of the norms established in the standard, with the exception of acidity (no more than 2.5 degrees) and porosity for a sample with a mixture content of 5% of the total amount of flour. The increased acidity is due to the fact that when the dough is fermented using a mixture of chickpea and barley flour, the acid accumulation process is faster. Porosity does not correspond to the indicators of GOST 31805–2018 bakery products. General specifications (at least 65%), since the gluten content in the dough when adding a mixture of chickpea and barley flour over 5% of the weight of wheat is not enough.

As a result of organoleptic and physico-chemical studies of samples of bakery products containing mixtures of chickpea and barley flour, it was concluded that it would be advisable to add it in an amount of no more than 4% by weight of wheat flour.

Conclusions

In the course of the study, a recipe for molded bread was developed with the addition of mixtures of chickpea and barley flour in an amount of 4% by weight of wheat flour. A technology for the production of molded bread with mixtures of chickpea and barley flour has been developed, the use of which has reduced the fermentation time of the dough by 30%. The amount of protein in molded bread added to a mixture of chickpea and barley flour was determined, which increased by 18% compared with bread produced according to the control recipe. The nutritional and energy value (250 kcal) of the developed product is calculated. The shelf life of molded bread with mixtures of chickpea and barley flour (48 hours) has been established, during which the product has high organoleptic and physico-chemical properties, and microbiological parameters comply with these requirements “On Food Safety”

References

Erashova L. D., Pavlova G. I., Ermolenko R. S. (2009). The use of non-traditional sources of protein of plant origin // Food Industry Magazine. – P. 14–15.

Klochkova I. S., Davydovich V. V. (2018). Technology of bakery products using protein-containing vegetable raw materials // Scientific papers of Dalrybetuz. – No. 3. – Vol. 46.

Ershov P. S. (2001). Recipes for bread and bakery products. – St. Petersburg, – 155 p.

Pashchenko L. P., Kurchaeva E. E., Kulakova Yu.A., Yakovleva.E.A. (2004). Some information about chickpeas and its use in food.//Storage and processing of agricultural products. Raw materials – No. 4. – P. 59–62.

Jankorazov A. M., Sattarov K. K. (2024). Flour mixtures from wheat and pea flour for bread production. Machinery and technology of food production. Abstracts of the XIII International Scientific Conference of Students and Postgraduates. – Mogilev. – 97 p.

submitted 28.09.2025;
accepted for publication 12.10.2025;
published 26.11.2025

Contact: doctor-sattarov@ mail.ru

The Austrian Journal of Technical and Natural Sciences, No 9–10
ISSN 2310-5607

PREMIER Publishing
ppublishing.org

DOI:10.29013/AJT-25-9.10-79-82

DEVELOPMENT OF METHODS FOR THE DETERMINATION OF TIN IN FOOD

Sobirova Zilola [1], ***Yakhshieva Zukhra*** [1]

[1] Jizzakh State Pedagogical University, Uzbekistan

Cite: *Sobirova Z., Yakhshieva Z. (2025). Development of methods for the determination of tin in food. Austrian Journal of Technical and Natural Sciences 2025, No 9–10.* https://doi.org/10.29013/AJT-25-9.10-79-82

Abstract

This article presents the results of an analysis of canned products to determine the content of tin ions.

The time of complex formation was studied using inversion voltamperometric methods. For tin (II) ions, the maximum signal was observed at 0.260 V in 10 seconds, and these time values were determined as optimal.

The detection limits of tin (II) ions were recorded at 1.33×10^{-8} M ($R^2 \approx 0.991$) for the presented electrochemical methods, and the reliability and sensitivity of the developed method were confirmed in practice

Keywords: *electrochemical methods of analysis, tin ions, food products, metrological characteristics*

Due to the intensive development of industry, transport, industrialization and the chemicalization of agriculture, as well as the acceleration of scientific and technological progress, the release of heavy metals of technogenic origin into the environment has significantly increased in recent years and continues to grow.

Pollution of the biosphere (air, water, soil) with heavy metals leads to their accumulation in food raw materials of plant and animal origin, sometimes in quantities exceeding sanitary and hygienic standards.

The complexity of modern ecological-analytical monitoring of toxic heavy metals and the protection of public health has led to the involvement of researchers worldwide in developing highly sensitive methods of analysis. Monitoring of environmental objects, which includes the analysis of food products for toxic heavy metals, inorganic and organic substances, is carried out using various physical and chemical methods. Among these, electrochemical methods occupy a special place due to their high sensitivity, simplicity, low cost, and suitability for computerization and automation.

Modern requirements for environmental analysis demand new, highly sensitive and rapid methods for determining toxic trace metals. The multicomponent nature of analytical objects and the low concentrations of metallic pollutants require combined methods, including a preconcentration stage.

The rapid development and wide application of electrochemical methods in the last decade are explained by their high accuracy, sensitivity, selectivity, and speed, which allow reliable analytical control of technological processes, environmental samples, biological products, clinical materials, and industrial substances.

Inversion voltamperometric is widely used to determine both metal ions and various compounds. Its efficiency is increased by preliminary adsorption or electrochemical concentration of the analyte on the electrode surface.

Further development of inversion voltamperometric methods is connected with the creation of modified sensor electrodes with unique properties. Chemical modification of sensor surfaces allows the addition of new functional capabilities, enhancing both reactivity and selectivity. Indicator electrodes based on macrocyclic compounds significantly expand the potential of inversion voltamperometric as a highly sensitive and selective method of analysis.

The selectivity of the sensor we developed is ensured by modification with hydrazine sulfate and thioacetamide, which greatly improves both the sensitivity and selectivity of the method and allows for low detection limits of the studied metal ions.

Environmental Safety Related to Tin and Its Analytical Determination

In recent years, the range of objects requiring determination of heavy toxic metals has expanded, including tin, which is one of the priority environmental pollutants. Tin contamination of natural objects and industrial materials has been reported in many regions of the world. Its presence in food products is also well established, and therefore its concentration must be strictly controlled.

According to sanitary and epidemiological regulations of the Ministry of Health of the Republic of Uzbekistan, the concentration of tin in natural waters and soils should not exceed 0.2 and 0.5 mg/L, respectively.

Therefore, it is important to describe and predict the main toxic properties of these metals, assess their increasing levels in food products, and ensure strict analytical control of their content. This is essential for evaluating risks to human health and the environment, making it a highly urgent problem in modern ecological-analytical chemistry.

In this context, the urgent goal of our work was to modify sensors and develop analytical methods for determining tin. Improving electrochemical methods with better metrological characteristics remains a key challenge in food analysis. These requirements are best met by inversion voltamperometric, one of the most powerful electrochemical techniques in terms of sensitivity, selectivity, and information content.

Experimental Methods

Standard solutions were prepared gravimetrically using methods described in the literature. Exact concentrations of stock solutions and standards were determined titrimetrically. Dilute solutions (1×10^{-3} – 2×10^{-8} M) were obtained by successive dilution with triple-distilled water immediately before use.

During the analysis of canned products, we found that by varying the background electrolyte and buffer mixture, high selectivity for tin determination can be achieved. The possibility of using inversion voltamperometric for tin determination under optimized conditions of concentration and background composition was demonstrated.

For food safety monitoring, it is crucial to ensure timely control of maximum permissible concentrations (MPC) of toxic trace metals in canned goods and food products. This monitoring must be carried out by sanitary and epidemiological services across Uzbekistan.

Electrochemical methods, particularly inversion voltamperometric, meet modern requirements for analytical methods: rapid, selective, highly sensitive, accurate, inexpensive, and easy to automate.

Analytical Procedure

Before analysis, the electrolyzer was rinsed with triple-distilled water and filled with 20 ml of background electrolyte (buffer mixture). Indicator, auxiliary, and reference electrodes were inserted, and optimal electrolysis conditions were set: accumulation potential of –0.45 V, accumulation time of 60 s, current range of –1.0 μA, and appropriate

amplitude and potential sweep rate. A voltammogram was recorded at least four times, with only the fourth measurement used for analysis, since the first three serve to condition the electrode and improve reproducibility.

For sample preparation, 5–10 g of solid product (or 10–15 ml if liquid) was weighed into a heat-resistant beaker. Then 4–5 ml of concentrated HCl and the same volume of 5% H_2O_2 were added. The mixture was heated under a watch glass at 80–90 °C for 15–20 min. The solution was diluted to 100 ml with triple-distilled water and filtered if necessary. An aliquot (e.g., tomato juice, cottonseed oil, canned fish, beef) was taken, background electrolyte was added, and the total volume was brought to 20 ml before recording a voltammogram.

The selectivity of the electroanalytical method – that is, the reliable separation of the ion being determined even in the presence of other cations – is one of the important criteria for its practical application. Therefore, in order to evaluate the selectivity of the developed inversion voltammetric method, the effect of foreign metal ions (Cu(II), Fe(III), V(III), Ba(II), Fe(II), Pb(II), Mn(II), Cd(II)) on the voltammetric determination of tin (II) ion was studied. For this, solutions with a total volume of 25 ml were prepared. 2 ml of 0.1 M acetate buffer solution (pH = 5.1), 2.0 μM organic reagent solution, tin (II) ion and foreign metal ions in a certain ratio were added to each solution. The volume of the solution was made up to 25 ml with distilled water. Measurements were carried out by method IV. The collection time for the determination of tin (II) ion was set to 90 seconds. The accumulation potential was 50 mV, and the accumulation potential was applied to the electrode at a scan rate of 25 mV/s.

The results confirmed that the measured concentrations of tin in canned products were consistent with certified reference values and remained within the confidence interval, demonstrating the high accuracy and reproducibility of the developed inversion voltamperometric method. Analysis was carried out using carbon-paste electrodes modified with hydrazine sulfate, which significantly improved the sensitivity and selectivity of tin detection.

Conclusion

The study demonstrated that modified sensor electrodes combined with inversion voltamperometric provide a highly sensitive, selective, and reliable method for determining tin in food products. The results showed good agreement with reference values, confirming the method's accuracy and reproducibility.

The analytical parameters of the method were the correlation coefficient R = 0.991 for tin (II) ions; the lower detection limit was 1.33×10^{-8} M; the quantitative detection limit was 4.00×10^{-8} M. The stability constants of the complexes were calculated as Kf = 4.11 for tin (II) ions.

The metrological parameters of the inversion voltamperometric method, such as accuracy, sensitivity and lower detection limit, developed on the basis of metrological analysis and competitiveness, were compared with physicochemical methods. The proposed method in some cases showed high sensitivity and selectivity compared to the methods used in production laboratories. The developed voltamperometric detection methods are characterized by speed, low detection limit and high selectivity and have been successfully applied in the analysis of food products.

References

Ivanov V. M. (1990). Electroanalytical methods in environmental monitoring. Moscow; Chemistry. – 240 p. – P. 23–28.

Li Y., Chai Y., Yuan R., Liang W., Zhang L. (2008). Aluminum(III) selective electrode based on a newly synthesized glyoxal-bis-thiosemicarbasone shiffbase // Journal. analyte chemistry – V. 63. – P. 1193–1196.

Mohamad Ali A. S., Razak N. A., Ab Rahman I. (2012). Study on the preparation of sol-gel sorbent based thiosemocarbazone for selective. removal of heavy metal ions // World Applied Sciences Journal. – V. 16. – P. 1040–1047.

Budnikov G. K., Maistrenko V. N., Evtyugin G. A. (2010). Modified electrodes for voltamperometric in chemistry, biology and medicine. – M. Binom. Laboratory of knowledge. – 416 p.
Snell K. D., Keenan A. G. (1989). Development of chemically modified electrodes and investigation of their electroanalytical parameters // Chem. Soc. Rev. – V. 8. – 259 p.

submitted 02.09.2025;
accepted for publication 15.09.2025;
published 26.11.2025

Contact: yaxshiyeva67@mail.ru

The Austrian Journal of Technical and Natural Sciences, No 9–10
ISSN 2310-5607

PREMIER Publishing
ppublishing.org

Section 4. Machinery construction

DOI:10.29013/AJT-25-9.10-83-87

ABOUT THE ESTIMATION OF THE MEAN SQUARE VALUE OF A CIRCULAR PLATE IN RANDOM PROCESSES

Xasanov J.A. [1]

[1] Samarkand State University, Samarkand, Uzbekistan

Cite: *Xasanov J.A. (2025). About the estimation of the mean square value of a circular plate in random processes. Austrian Journal of Technical and Natural Sciences 2025, No 9–10.* https://doi.org/10.29013/AJT-25-9.10-83-87

Abstract

This work deals with the problem of investigating the dynamics of transverse vibrations of a circular plate of hysteresis type in random processes, the dissipative characteristics of which are determined by the mean square values. When calculating the dynamic characteristics, a probabilistic approach was used based on the average energy distribution, taking into account the physical and geometric parameters of the circular plate, dissipative coefficients, spectral density and resonance properties. In general, the expression of the mean square values of the slope was determined.

Keywords: *random process, dissipative, hysteresis, elastic, dissipative, mean square value, circular plate*

Introduction

In all areas of modern engineering and technology, including machines and mechanisms, devices and their elements, taking into account nonlinear elastic and dissipative properties of random vibrations, the correct determination of their dynamic characteristics – optimal design, ensuring long-term perfect operation at a high level of reliability is one of the urgent problem.

In the work (Itao K., Crandall S. H., 1978), it was shown that the transverse vibrations of each point of a circular plate of constant thickness under the influence of stationary wide-band random excitations are also a wide-band random process. The root mean square values were determined and their changes were numerically analyzed. In this case, analytical and experimental analyses were carried out for an aluminum plate on a free support with a thickness of 0.16 cm and a diameter of 0.91 m, and conclusions were drawn on reducing the root mean square values.

In the work (Yaping Zhao, Ming Li., 2016), the vibrations of a circular plate subject to Kirchhoff's theory under the influence of random excitations were mathematically modeled. In this case, the random excitations were white noise, including a distributed

load and a concentrated force. Two types of absorber mechanisms, namely internal and external viscous absorbers, were simultaneously taken into account in damping the vibrations. When solving boundary problems, the boundary conditions were fixed, freely supported, and mixed conditions. The eigenfrequencies were determined using the separation of variables method.

The dynamics of systems protected from distributed parameter vibrations under the influence of random motions were studied in the works (Dusmatov O. M., Khodjabekov M. U., 2013; Dusmatov O. M., Khasanov J. A., 2025). The issue of checking the stability of combined nonlinear vibrations of a plate with elastic dissipative characteristics of the hysteresis type and a dynamic absorber was considered.

The work (Amabili M., Pierandrei R. and Frosali G., 1997) studied the free vibrations of a circular plate with variable thickness using the Rayleigh-Ritz method, developed a methodology for examining its dynamics, and provided recommendations.

The work (Afsharmanesh B., Ghaheri A. and Taheri-Behrooz F., 2014) deals with the forced vibrations of circular plates mounted on a Winkler-type base. Parametric studies are mainly conducted under various boundary conditions.

In the works (Bahrami A. and Teimourian A., 2015; Arshid E. and Khorshidvand A. R., 2018; Vinyas M., Sandeep A., Nguyen-Thoi T., Ebrahimi F. and Duc D., 2019; Yalamanchili Swapna, Harsha K Sri., 2021), the direction of wave propagation was taken into account to analyze the free vibrations of annular and circular plates. Methods for mathematical modeling and solving problems were developed. The free vibrations of annular and circular elastic plates were studied using the finite element method and its combination, and conclusions were given.

One of the important issues is the study of the vibrations of circular plates under the influence of random excitations, taking into account the elastic dissipative characteristics of the hysteresis type, and the optimal design as a result of determining their dynamic characteristics in various processes and boundary conditions.

Materials and methods

This work addresses the issue of determining the mean square values of circular plates with hysteresis-type elastic dissipative characteristics under the influence of random excitations based on the generalized spectral density of the base acceleration.

According to the theory of random processes, the following relation is appropriate for the expression of the mean square values:

$$\sigma_T^2 = \int_{-\infty}^{+\infty} \left|A(\omega)\right|^2 S_{W_0}(\omega)\, d\omega. \qquad (1)$$

where $A(\omega)$ is the amplitude-frequency characteristics; $S_{W_0}(\omega)$ is the spectral density of the base acceleration.

A mathematical model of nonlinear transverse vibrational motion of a circular plate with hysteresis-type elastic dissipative characteristics was obtained in (Dusmatov O., 2025). The amplitude-frequency characteristics of the circular plate under consideration is as follows:

$$A(\omega) = \frac{d_*}{\left(1-\eta_{1t}R_{1t}-\nu_{1t}R_{2t}\right)\omega_{01}^2 - \omega^2 + j\left(\eta_{2t}R_{1t}+\nu_{2t}R_{2t}\right)\omega_{01}^2}, \qquad (2)$$

where η_{1t}, η_{2t}, ν_{1t}, ν_{2t} are statistical linearization coefficients; $j^2 = -1$; ω is frequency of vibrations; ω_{01} is the natural frequency of the plate;

$$R_{1t} = \frac{3D}{\omega_{01}^2 \rho h d_1} \sum_{i_1=0}^{k_1} C_{i_1} \frac{h^{i_1}}{2^{i_1}(i_1+3)} \left|\sigma_{T_a}\right|^{i_1} G_{i_1};$$

$$G_{i_1} = \iint_s PQ \left[\frac{\partial^2}{\partial r^2}\left(\beta_1 \left|\beta_1\right|^{i_1}_{\sigma_{\xi_0}}\right) + \left(\frac{1}{r}\frac{\partial}{\partial r} + \frac{1}{r^2}\frac{\partial^2}{\partial \theta^2}\right)\beta_2 \left|\beta_2\right|^{i_1}_{\sigma_{\xi_0}} \right] ds;$$

$$R_{2t} = \frac{6D(1-\mu)}{\omega_{01}^2 \rho h d_1} \sum_{i_2=0}^{k_2} C_{i_2} \frac{h^{i_2}}{2^{i_2}(i_2+3)} \left|\sigma_{T_a}\right|^{i_1} H_{i_2};$$

$$H_{i_2} = \iint_s PQ\left(\frac{1}{r}\frac{\partial^2}{\partial r \partial \theta} - \frac{1}{r^2}\frac{\partial}{\partial \theta}\right)\left(\beta_3 \left|\beta_3\right|^{i_2}_{\sigma_{\xi_0}}\right) ds;$$

$P = P(r)$ and $Q = Q(\theta)$ are functions of radius r and angle θ, respectively;

$D = \frac{Eh^3}{12(1-\mu^2)}$ is cylindrical stiffness; E is

Young's modulus; h is plate thickness; μ is Poisson's ratio;

$$d_\star = \frac{d_2}{d_1}; \qquad d_1 = \int_0^{2\pi} Q^2 d\theta \int_{r_0}^{R_0} P^2 dr;$$

$$d_2 = \int_0^{2\pi} Q d\theta \int_{r_0}^{R_0} P dr;$$

R_0 is radius of circular plate; r_0 is radius of the inner sphere given the boundary conditions; ρ is density of the plate material; σ_{T_a} is absolute value of the mean square; $C_{i_1}\left(i_1 = 0,\ldots,k_1\right)$, $K_{i_2}\left(i_2 = 0,\ldots,k_2\right)$ are α_{1i}, α_{2i}, α_{3i} and z_i hysteresis parameters determined from experimentally selected lines $\alpha_1 = f_r(z)$, $\alpha_2 = f_\theta(z)$, $\alpha_3 = g(z)$ at points corresponding to the coordinates of the cyclic deformations of the material; $f_r(z)$, $f_\theta(z)$ are functions of the maximum values of relative deformation in general form, representing the decrement of vibrations, $g(z)$ is the decrement of vibrations in terms of the values of relative deformation in displacement:

$$f_r(z) = \sum_{i_1=0}^{k_1} C_{i_1} \left|V_1\right|^{i_1}_{\sigma_{\xi_0}} |z|^{i_1}; f_\theta(z) = \sum_{i_1=0}^{k_1} C_{i_1} \left|V_2\right|^{i_1}_{\sigma_{\xi_0}} |z|^{i_1};$$

$$g(z) = \sum_{i_2=0}^{k_2} K_{i_2} \left|V_3\right|^{i_2}_{\sigma_{\xi_0}} |z|^{i_2};$$

$$V_1 = \frac{\partial^2 w}{\partial r^2} + \mu\left(\frac{1}{r}\frac{\partial w}{\partial r} + \frac{1}{r^2}\frac{\partial^2 w}{\partial \theta^2}\right);$$

$$V_2 = \frac{1}{r}\frac{\partial w}{\partial r} + \frac{1}{r^2}\frac{\partial^2 w}{\partial \theta^2} + \mu\frac{\partial^2 w}{\partial r^2};$$

$$V_3 = \frac{1}{r}\frac{\partial^2 w}{\partial r \partial \theta} - \frac{1}{r^2}\frac{\partial w}{\partial \theta};$$

$$\beta_1 = Q\frac{\partial^2 P}{\partial r^2} + \mu\left(\frac{1}{r}Q\frac{\partial P}{\partial r} + \frac{1}{r^2}P\frac{\partial^2 Q}{\partial \theta^2}\right);$$

$$\beta_2 = \frac{1}{r}Q\frac{\partial P}{\partial r} + \frac{1}{r^2}P\frac{\partial^2 Q}{\partial \theta^2} + \mu Q\frac{\partial^2 P}{\partial r^2};$$

$\beta_3 = \frac{1}{r}\frac{\partial P}{\partial r}\frac{\partial Q}{\partial \theta} - \frac{1}{r^2}P\frac{\partial Q}{\partial \theta}$; with bending of the plate.

Let's obtain the spectral density of the base acceleration in the following form (Pavlovsky M. A., Ryzhkov L. M., Yakovenko V. B., Dusmatov O. M., 1997):

$$S_{W_0}(\omega) = \frac{D_{W_0}\alpha\omega_c^3}{\pi\left(\omega_c^2 - \omega^2 + i\alpha\omega_c\omega\right)\left(\omega_c^2 - \omega^2 - i\alpha\omega_c\omega\right)}, \qquad (3)$$

where D_{W_0} is dispersion of the base acceleration; α is parameter characterizing the width of the vibration spectrum; ω_c is the frequency at which the vibration probability is highest in the spectrum of vibrations.

If we substitute the expressions (2) for the amplitude-frequency characteristics and (3) for the spectral density of the base acceleration into the expression (1) for the mean square values, we obtain:

$$\sigma_T^2 = \frac{1}{\pi}\int_{-\infty}^{+\infty} \frac{d_\star^2 D_{W_0}\alpha\omega_c^3}{\left[\left(1-\eta_{1t}R_{1t}-\nu_{1t}R_{2t}\right)\omega_{01}^2 - \omega^2\right]^2 + \left[\left(\eta_{2t}R_{1t}+\nu_{2t}R_{2t}\right)\omega_{01}^2\right]^2} \times \frac{1}{\left[\omega_c^2-\omega^2\right]^2 + \left[\alpha\omega_c\omega\right]^2} d\omega. \qquad (4)$$

We calculate the resulting integral expression using the method presented in (Roberts J. B., Spanos P. D., 1990). To do this, we write it as follows:

$$\sigma_T^2 = \frac{d_\star^2 D_{W_0}\alpha\omega_c^3}{\pi}\int_{-\infty}^{+\infty} \frac{Z_4(\omega)}{X_4(i\omega)X_4(-i\omega)} d\omega, \qquad (5)$$

where

$$Z_4(\omega) = b_3\omega^6 + b_2\omega^4 + b_1\omega^2 + b_0;$$

$$X_4(i\omega) = a_4(i\omega)^4 + a_3(i\omega)^3 + a_2(i\omega)^2 + a_1(i\omega)^1 + a_0;$$

$$a_4 = 1; a_3 = -\alpha\omega_c - p_1\omega_{01};$$

$$p_1 = \left(2\left(p_2 - \left(1-\eta_{1t}R_{1t}-\nu_{1t}R_{2t}\right)\right)\right)^{\frac{1}{2}};$$

$$p_2 = \left(\left(1-\eta_{1t}R_{1t}-\nu_{1t}R_{2t}\right)^2 + \left(\eta_{2t}R_{1t}+\nu_{2t}R_{2t}\right)^2\right)^{\frac{1}{2}};$$

$$a_2 = \alpha p_1\omega_c\omega_{01} + p_2\omega_{01}^2 + \omega_c^2;$$

$$a_1 = -\alpha p_2\omega_c\omega_{01}^2 - p_1\omega_{01}\omega_c^2; a_0 = p_2\omega_c^2\omega_{01}^2;$$

$$b_5 = b_4 = b_3 = b_2 = b_1 = 0; b_0 = 1.$$

We express the value of the integral in expression (5) as follows:

$$I = \frac{\pi}{a_4} \frac{\begin{vmatrix} b_3 & b_2 & b_1 & b_0 \\ -a_4 & a_2 - a_0 & 0 \\ 0 & -a_3 & a_1 & 0 \\ 0 & a_4 & -a_2 & a_0 \end{vmatrix}}{\begin{vmatrix} a_3 & -a_1 & 0 & 0 \\ -a_4 & a_2 - a_0 & 0 \\ 0 & -a_3 & a_1 & 0 \\ 0 & a_4 & -a_2 & a_0 \end{vmatrix}}. \quad (6)$$

If we calculate the determinants in expression (6), we get

$$I = \frac{\pi\left(-p_1\alpha^2\omega_{01}\omega_c^2 - \alpha\left(p_1^2\omega_c\omega_{01}^2 + \omega_c^3\right) - p_1p_2\omega_{01}^3\right)}{p_2^2\omega_{01}^4 + \alpha p_1p_2\omega_c\omega_{01}^3 + \left(\alpha^2p_2 - 2p_2 + p_1^2\right)\omega_{01}^2\omega_c^2 + \alpha p_1\omega_{01}\omega_c^3 + \omega_c^4} \times \frac{1}{\alpha p_1p_2\omega_c^3\omega_{01}^3}. \quad (7)$$

If we substitute the value of the defined integral expression (7) into the mean square expression (5), we get:

$$\sigma_T^2 = \frac{d_*^2 D_{W_0}\alpha\omega_c^3}{\pi\alpha p_1p_2\omega_c^3\omega_{01}^3} \times \frac{\pi\left(-p_1\alpha^2\omega_{01}\omega_c^2 - \alpha\left(p_1^2\omega_c\omega_{01}^2 + \omega_c^3\right) - p_1p_2\omega_{01}^3\right)}{p_2^2\omega_{01}^4 + \alpha p_1p_2\omega_c\omega_{01}^3 + \left(\alpha^2p_2 - 2p_2 + p_1^2\right)\omega_{01}^2\omega_c^2 + \alpha p_1\omega_{01}\omega_c^3 + \omega_c^4}. \quad (8)$$

After some simplifications, expression (8) can be written as follows:

$$\sigma_T^2 = \frac{1}{\alpha p_1p_2\omega_{01}^3} \times \frac{d_*^2 D_{W_0}\left(-p_1\alpha^2\omega_{01}\omega_c^2 - \alpha\left(p_1^2\omega_c\omega_{01}^2 + \omega_c^3\right) - p_1p_2\omega_{01}^3\right)}{p_2^2\omega_{01}^4 + \alpha p_1p_2\omega_c\omega_{01}^3 + \left(\alpha^2p_2 - 2p_2 + p_1^2\right)\omega_{01}^2\omega_c^2 + \alpha p_1\omega_{01}\omega_c^3 + \omega_c^4}. \quad (9)$$

The expression of the mean square values determined (9) allows us to analyze the dynamics and stability of vibrations of a circular plate with hysteresis-type elastic dissipative characteristics under the influence of random excitations at different values of the parameters.

Conclusion

The mean square values of the nonlinear vibrations of a circular plate with hysteresis-type elastic dissipative properties under the influence of random excitations were obtained in an analytical form depending on the system parameters. This expression allows us to evaluate the influence of random excitations on the vibrations of a circular plate, to check their dynamics and stability under various boundary conditions.

References

Itao K., Crandall S. H. (1978). Wide-band random vibration of circular plates. Journal of Mechanical design, October, – Vol. 100. – P. 690–695.

Yaping Zhao, Ming Li. (2016). Random vibration analysis of viscoelastic circular thin plates. Intertional Conference on theory and application of random vibration (ICTARV).

Dusmatov O. M., Khodjabekov M. U. (2013). Checking the stability of the vibration protected plate in case of random vibrations. Jizzakh State Pedagogical Institute Newsletter., – No. 1. – P. 8–12.

Dusmatov O. M., Khasanov J. A. (2025). Random nonlinear vibrations of an imperfectly elastic circular plate with a dynamic absorber. International Scientific Journal Theoretical & Applied Science., – 05. – Vol 145. – P. 364–368.

Amabili M., Pierandrei R. and Frosali G. (1997). Analysis of vibrating circular plates having non-uniform constraints using the modal properties of free-edge plates: application to bolted plates. Journal of Sound and Vibration, – Vol. 206. – No. 1. – P. 23–38.

Afsharmanesh B., Ghaheri A. and Taheri-Behrooz F. (2014). “Buckling and vibration of laminated composite circular plate on Winkler-type foundation,” Steel and Composite Structures, – Vol. 17. – No. 1. – P. 1–19.
Bahrami A. and Teimourian A. (2015). “Free vibration analysis of composite, circular annular membranes using wave propagation approach”. Applied Mathematical Modelling, – Vol. 39. – No. 16. – P. 4781–4796.
Arshid E. and Khorshidvand A. R. (2018). “Free vibration analysis of saturated porous FG circular plates integrated with piezoelectric actuators via differential quadrature method”. GinWalled Structures, – Vol. 125. – P. 220–233.
Vinyas M., Sandeep A., Nguyen-Thoi T., Ebrahimi F. and Duc D. (2019). “A finite element-based assessment of free vibration behaviour of circular and annular magneto-electro-elastic plates using higher order shear deformation theory”. Journal of Intelligent Material Systems and Structures, – Vol. 30. – No. 16. – P. 2478–2501.
Yalamanchili Swapna, Harsha K Sri. (2021). Random vibration analysis of composite plate. IOP Conf. Series: Materials Science and Engineering – 1185. – 012035 p.
Dusmatov O. (2025). Khasanov J. Transverse vibrations of a circular plate taking into account the imperfect elasticity of the material. Samarkand university scientific bulletin, – No. 1. – P. 91–95.
Pavlovsky M. A., Ryzhkov L. M., Yakovenko V. B., Dusmatov O. M. (1997). Nelinejnye zadachi dinamiki vibrozashitnyh sistem (Nonlinear problems of the dynamics of vibration protection systems). – Kiev, Technique, – 204 p.
Roberts J. B., Spanos P. D. (1990). Random Vibration and statistical linearization. Chichester etc., John Wiley & Sons XIII, – 407 p.

submitted 08.09.2025;
accepted for publication 22.09.2025;
published 26.11.2025

Contact: xasanovjaxongir089@gmail.com

The Austrian Journal of Technical and Natural Sciences, No 9–10
ISSN 2310-5607

PREMIER Publishing
ppublishing.org

Section 5. Medical science

DOI:10.29013/AJT-25-9.10-88-93

ASSESSMENT OF THE ROLE OF COSMETOLOGIST AND PARENTS IN THE FORMATION OF PROPER SKIN CARE HABITS IN ADOLESCENTS

Azarenkova Yuliia [1]

[1] Owner, Skin Care Pro LLC, USA, Charlotte

Cite: *Azarenkova Y. (2025). Assessment of the role of cosmetologist and parents in the formation of proper skin care habits in adolescents. Austrian Journal of Technical and Natural Sciences 2025, No 9–10.* https://doi.org/10.29013/AJT-25-9.10-88-93

Abstract

The article discusses the significance of parents and professional cosmetologists in shaping proper skin care habits among adolescents. It highlights the main issues related to adolescent skin, such as emotional support, and emphasizes the influence of cosmetologist advice on developing a healthy attitude towards skincare. The article emphasizes the need for a comprehensive approach that includes training, motivation, and psychological support in order to strengthen self-esteem and prevent skin-related issues.

Keywords: *teenagers, skin care, parents, cosmetologist, healthy habits, emotional support, adolescent skin, prevention, psychology of care, skin diseases*

Introduction

Adolescence is a time of significant physiological and psychological changes, which directly affect the skin and emotional well-being. During this period, young people often experience problems such as acne, oily or dry skin, which can lead to decreased self-esteem and increased stress.

Parents play an important role in supporting their teenagers by helping them establish a proper skincare routine and develop healthy habits that they can maintain throughout their lives. The role of a professional cosmetologist is particularly significant, as they are able to provide not only effective skincare recommendations but also emotional support, increasing motivation, and helping teenagers cope with any psychological difficulties related to their appearance.

The article explores various approaches to collaboration between parents, adolescents, and cosmetologists to foster a comprehensive and thoughtful approach to skin care.

Parents are the first teachers who can teach teenagers about the basics of hygiene and skin care. It's important to create a positive environment at home where teenagers feel comfortable discussing their skin concerns and emotional state openly. Parents should encourage their teenagers by helping them find the right products for their skin,

explaining the significance of regular routines and a healthy lifestyle (good nutrition, enough sleep, minimizing stress).

Professional cosmetologist assistance is essential to accurately determine skin type, diagnose potential issues, and select personalized care. The cosmetologist educates teenagers on proper washing techniques, product usage, and prevents incorrect actions that could worsen skin conditions. Additionally, a specialist can assist a teenager in addressing psychological aspects related to appearance, increasing self-confidence, and motivating them to care for themselves.

Skincare is not merely a physical process but also a significant aspect of a teenager's emotional well-being. Parental and cosmetologist psychological support reduces anxiety associated with appearance, prevents complex development, and fosters a positive image formation. Joint efforts enable a teenager to cultivate healthy habits and a positive attitude towards their body and self-image (Table 1).

Table 1. *Features of baby skin care*

No.	Indicator	Characteristic
1.	Skin sensitivity	Children's skin is delicate and sensitive, so it can easily become irritated or have allergic reactions. Therefore, it is important to use soft and hypoallergenic products.
2.	Humidification	Regular skin hydration is essential for maintaining healthy skin. It is recommended to use creams and lotions specifically designed for children. It is best to apply moisturizers immediately after bathing, as this will help lock in moisture and prevent dryness.
3.	Sun protection	Children's skin is particularly sensitive to UV radiation, so it's important to use special high-SPF sunscreen starting at 6 months old. Also, it's best to avoid direct sunlight during the peak hours of the day.
4.	Clothing and textiles	You should choose clothes made from natural fabrics, such as cotton or linen, which are free from hard seams and bright dyes. Before wearing new clothes for the first time, it is recommended to wash them to remove any chemical residues.
5.	Monitoring the changes	It is important to regularly check children's skin for redness, rashes, or any other changes.
6.	Proper nutrition	A healthy diet also has a positive impact on the condition of the skin. Make sure your child gets enough fluids and nutrients in their diet.

The cooperation between parents and a professional cosmetologist is essential for the successful establishment of stable and healthy habits in teenagers and the harmonious development of their emotional well-being.

Discussion

It should be noted that the study of adolescent skin care has evolved in parallel with the advancement of dermatology and cosmetology. In the early XX century, scientists primarily focused on adult skin, while adolescent skin was seen as a transitional phase that did not warrant separate study. However, in the 1930s, observations of acne, which often occurs during adolescence, led experts to recognize the importance of understanding the hormonal and physiological changes that occur during this period. These observations led to the discovery of the link between increased sebaceous gland activity and hormonal fluctuations, marking the beginning of the development of methods for caring for and treating adolescent skin.

In the middle of the XX century, during the 1950 s and 1970 s, with the development of cosmetology and creation of specialized products, the study of adolescent skin began to become more systematic. Scientists started to consider the skin of teenagers as a unique object with special properties, different from those of children and adults. This period was marked by the emergence of the first dedicated cosmetic lines and recommendations for

hygiene aimed at reducing acne and preventing skin issues.

From the 1980s to the 2000s, researchers focused not only on the physical aspects of adolescent skincare, but also on its psychological aspects. Understanding that quality of life and emotional well-being affect skin health led to the development of holistic care programs. Research into skin physiology, external factors, and lifestyle has intensified.

Nowadays, adolescent skin care is considered an interdisciplinary field that integrates dermatology, endocrinology, psychology, and cosmetology. Modern approaches rely on a comprehensive analysis of individual factors, including skin type, hormonal balance, and stress levels, to develop effective and safe treatments and products that not only address specific concerns but also promote long-term skin health.

It should be noted that pediatric dermatology is a specialized branch of medicine that focuses on the diagnosis, treatment, and prevention of skin conditions in children from birth to adolescence. Unlike adult dermatology, pediatric dermatologists take into account the unique characteristics of the developing skin of children, including its increased sensitivity and susceptibility to infections and allergens.

The skin of children differs from that of adults in several ways. It is thinner, with a more prominent vascular system and an immature epidermal barrier, making it more vulnerable to external factors such as infections, allergens, and irritants. These differences in the structure and function of the skin influence the presentation of diseases and require tailored approaches to treatment.

The most significant objectives of modern pediatric dermatology include the early identification and management of inflammatory skin conditions such as atopic dermatitis, psoriasis, and contact dermatitis, as well as infectious diseases of the skin, including fungal and bacterial infections. Additionally, much attention is given to hereditary conditions and genodermatoses, which include pigmentation disorders, congenital skin abnormalities, and tumor processes (Vygotsky L. S., 1984).

Modern diagnostic methods in pediatric dermatology include dermatoscopy, laboratory tests, and immunological and molecular genetic studies. These methods allow for a more accurate determination of the cause and type of disease. Treatment is based on an integrated approach, combining local and systemic methods, with a focus on minimizing side effects and using safe drugs for children. Topical corticosteroids, immunomodulators, moisturizers, and protective agents are actively used, as well as systemic therapy including biologics if necessary.

Prevention plays an important role, including hygiene, early detection of allergies, and adjustments to diet and lifestyle. Modern pediatric dermatology also takes into account the psychological aspect of skin conditions, as skin problems can significantly impact a child's quality of life and social adjustment.

Results

It should be noted that modern cosmetology for children involves a careful and comprehensive approach to skin care, considering age-related characteristics, high sensitivity, and specific needs of children's skin. Cosmetologists primarily address issues related to skin imbalances, inflammatory processes, allergic reactions, and the consequences of conditions such as atopic dermatitis, juvenile acne, and pyoderma (Pozdnyakova M. A., Krasilnikova O. N., 2016).

The first stage of a cosmetologist's work involves taking a detailed medical history and assessing the skin condition to identify any possible contraindications. Special attention is given to the individual tolerance of cosmetic ingredients and the state of a child's immune system.

Daily practices include gentle cleansing procedures to remove sebum, allergens, and impurities while preserving the protective barrier. For example, using soft foams, gels, and milks containing natural ingredients like chamomile extract, aloe vera, and calendula helps prevent over-dryness and irritation.

Topical cosmetics containing anti-inflammatory and soothing ingredients such as panthenol, dexpanthenol, and allantoin help combat inflammation and redness. For acne or comedones, gentle exfoliants like enzyme peels with low-concentrated fruit acids are used to gently exfoliate keratinized cells

without harming the sensitive skin of children.

Modern cosmetologists use physiotherapy methods, such as LED therapy, to promote wound healing, reduce inflammation, and improve microcirculation, without the risk of skin injury. In some cases, they may also use hardware procedures, such as ultrasound cleaning or low-intensity microcurrent therapy. However, these procedures are only recommended after consultation with a pediatrician and dermatologist, and only for children of a certain age.

It is also important for cosmetologists to educate parents about the rules of home care for their children. This includes teaching them about proper selection of cosmetics, such as hypoallergenic products free from parabens and dyes, as well as controlling the environment, such as nutrition, humidity, and elimination of allergens. The cosmetologist will also inform parents that any application of products or procedures should be done gently and only after consulting with specialists.

In general, modern child cosmetology aims to maintain the health and natural balance of a child's skin, prevent complications, and form good hygiene habits. This helps to avoid the development of chronic skin conditions and promotes the child's overall health and development. (Fig. 1)

Figure 1. *Formation of proper hygiene habits in children (Bekuzarova N. V., Nazarenko E. M., Teterina A. V., 2023)*

When working with children, a cosmetologist plays a crucial role in not only providing skin care but also in helping to form healthy habits and providing emotional support. However, this can be challenging due to various factors.

One of the main challenges is the lack of motivation and knowledge among children. Many teenagers are not aware of the importance of regular skin care, leading to irregular and improper procedures. This can make it difficult for cosmetologists to convince clients to change their habits, especially when these habits are associated with unhealthy lifestyles such as poor nutrition, lack of sleep, and poor hygiene.

Secondly, emotional support requires psychological skills from a cosmetologist, which may not be developed in specialists with a purely technical background. Many teenage clients have low self-esteem and appearance-related complexes, and require

attention and positive feedback. Lack of empathy and communication skills can make it difficult to establish a trusting relationship, reducing the effectiveness of care and the formation of new habits.

Additionally, there is the challenge of limited consultation time. During a single session, a cosmetologist may not be able to fully discuss all aspects of healthy lifestyles for children, including nutrition and psychological well-being, which can reduce the quality of the overall approach. Young clients may also experience stress due to external factors that can negatively impact skin health and complicate the work of the specialist.

In addition, some children may expect instant results and quickly lose interest in long-term therapy, limiting their ability to form sustainable habits. Due to the fast-paced nature of modern life, it can be challenging people to find time for consistent care, and cosmetologists must strike a balance between a client's real capabilities and necessary recommendations.

To successfully form healthy habits and provide emotional support for children, a cosmetologist needs to take a comprehensive and individualized approach that considers the unique characteristics of the child's psychology and physiology.

Firstly, it is important to adapt communication methods. A cosmetologist should use simple and positive language, avoiding complex terms and eliminating fears associated with the procedures. To achieve this, it can be helpful to incorporate game elements and visuals that make it easier for children to understand information about hygiene and skincare.

Secondly, it is essential to involve parents and other close associates of children in the process of establishing healthy habits. By explaining and teaching adults about the right approaches to taking care of and maintaining a child's emotional well-being, a supportive environment can be created in which new beneficial practices can be consolidated and encouraged. A cosmetologist can suggest simple household routines and regular activities that parents can follow and support.

Thirdly, it's important to develop the cosmetologist's ability to provide psychological support – the skills of active listening, patience, and empathy. This can help establish a trustworthy relationship with the child, reducing anxiety and increasing motivation to follow recommendations. Using praise and encouragement for accomplishments can boost self-esteem and promote the development of positive attitudes.

In addition, the cosmetologist should optimize the time spent with the child by scheduling short but regular sessions in order to avoid tiring the child or causing resistance. It is essential to create a comfortable and relaxed atmosphere in the space where you work with children to minimize stress levels.

Furthermore, it is recommended to engage in preventive conversations and provide accessible advice on topics such as proper nutrition, sleep routines, and hygiene, highlighting the connection between these factors and skin health. The information should be presented in small, easily understandable steps so that the child can gradually incorporate new habits into their daily routine.

Conclusions

Thus, the main challenges for a cosmetologist when it comes to forming healthy habits and providing emotional support for children are low motivation and awareness among parents, lack of psychological skills among professionals, limited time available for complex communication, and high expectations for quick results.

To address these challenges, a systematic approach is required. This includes training cosmetologists in communication skills for working with children, increasing the time available for consultations, and developing customized programs that take into account each child's unique personality and lifestyle.

References

Bekuzarova N. V., Nazarenko E. M., Teterina A. V. (2023). Fostering a value-based attitude to health. The world of science and thought. The World of Science and Ideas, – (2). – P. 113–116.

Vygotsky L. S. (1984). Child psychology: Collected works: In 6 volumes. Vol. 4. / L. S. Vygotsky; Edited by D. B. Elkonin. – Moscow: Pedagogika, – 376 p.
Pozdnyakova M. A., Krasilnikova O. N. (2016). Modern possibilities of cosmetology in the conditions of the regional polyclinic // Bulletin of the RUDN University. Series: Medicine. – No. 3. – P. 143–148.

submitted 16.10.2025;
accepted for publication 01.11.2025;
published 26.11.2025

Contact: azarenkova.yv@gmail.com

The Austrian Journal of Technical and Natural Sciences, No 9–10
ISSN 2310-5607

PREMIER Publishing
ppublishing.org

DOI:10.29013/AJT-25-9.10-94-97

PROGNOSTIC SIGNIFICANCE OF EGFR AND VEGF RECEPTORS IN COLORECTAL CANCER RECURRENCE PREDICTION

Tillyashaykhov Mirzagaleb Nigmatovich[1,2], Karakhodjaev Botir Shokirovich[1]

[1] Republican Specialized Scientific and Practical Medical Center of Oncology and Radiology

[2] Tashkent State Medical University

Cite: *Tillyashaykhov M.N., Karakhodjaev B.Sh. (2025). Prognostic significance of EGFR and VEGF receptors in colorectal cancer recurrence prediction. Austrian Journal of Technical and Natural Sciences 2025, No 9–10.* https://doi.org/10.29013/AJT-25-9.10-94-97

Abstract

The aim of this study was to evaluate the role of growth factor receptors EGFR and VEGF in predicting recurrence of colorectal cancer. The analysis included 103 tissue samples from patients treated at an oncology center between 2016 and 2022. Immunohistochemical methods were used to assess the expression of EGFR and VEGF, and their association with recurrence or non-recurrence was analyzed. The results demonstrated that positive receptor status was significantly associated with an increased likelihood of recurrence (p=0,018 for EGFR and p=0,001 for VEGF). Odds ratio analysis confirmed that negative status of these markers reduces the risk of recurrence. The findings suggest that EGFR and VEGF have high prognostic value and potential as therapeutic targets in personalized treatment of colorectal cancer. The article emphasizes the need for further research to confirm and expand the application of these biomarkers in clinical practice.

Keywords: *Colorectal cancer, EGFR, VEGF, recurrence, prognostic markers*

Introduction

Colorectal cancer (CRC) is one of the leading malignancies worldwide and poses a significant healthcare challenge due to its high morbidity and mortality rates (Ferlay et al., 2019). Despite advances in diagnostics and therapy, disease recurrence remains a significant barrier to improving treatment outcomes (Van Cutsem et al., 2020). Therefore, identifying reliable prognostic markers capable of predicting tumor clinical behavior is a pressing challenge in modern oncology (Menter et al., 2019).

Growth factor receptors, such as epidermal growth factor receptor (EGFR) and vascular endothelial growth factor (VEGF), play a key role in carcinogenesis, including tumor growth and metastasis (Morgillo et al., 2017). EGFR is involved in the regulation of cell proliferation and survival, and its overexpression correlates with the aggressive course of many cancers, including colorectal cancer (Yonesaka et al., 2018). Similarly, VEGF promotes angiogenesis, which is critical for the nutrition and growth of rapidly growing tumors (Abdollahi et al., 2018).

While the role of these receptors in the pathogenesis of colorectal cancer is actively studied, a deeper understanding of their prognostic significance remains necessary. The present study aimed to investigate the relationship between EGFR and VEGF status and the risk of recurrence in patients with colorectal cancer (Jubb et al., 2020). We hypothesize that positive status of these receptors is associated with an increased likelihood of recurrence, thereby confirming their value as therapeutic targets and prognostic markers (Miller et al., 2021).

The aim of the study is to evaluate EGFR and VEGF expression as potential markers of disease progression, which may facilitate the development of more personalized treatment approaches and improved clinical outcomes in patients with colorectal cancer.

Materials and Methods

This dissertation is based on an analysis of 103 patients treated at the Russian Scientific and Practical Medical Center of Oncology and Radiology from 2016 to 2022.

Inclusion Criteria:

1. Patients aged 18 years and older;
2. Confirmed diagnosis of colorectal cancer based on histological examination;
3. Presence or absence of lymph node metastases based on preoperative or surgical examination.

Exclusion Criteria:

1. History of other malignancies or significant comorbidities that may affect study results;
2. Stage IV disease.
3. Patients with incomplete information about the primary tumor, lymph node status, or treatment history.

Study Design and Sample

This study was designed as a retrospective analysis aimed at assessing the prognostic value of EGFR and VEGF growth factor receptors in patients with colorectal cancer. Tissue samples from patients treated at our oncology center between 2020 and 2024 were collected for analysis. Only patients with complete clinical information, including data on disease recurrence and expression levels of the receptors under study, were included.

Immunohistochemical Assessment

EGFR and VEGF expression in tumor tissue samples was assessed using immunohistochemical staining. Antibodies specific to EGFR and VEGF were used in accordance with the protocols provided by the manufacturers. Expression levels were assessed by two independent pathologists blinded to patient clinical information, thereby eliminating bias in the interpretation of results. A positive tumor was defined as intense staining in more than 10% of tumor cells.

Statistical Analysis

Statistical analysis was performed using SPSS software (version XX). The chi-square test and Fisher's exact test were used to compare the frequencies of positive and negative receptor statuses in the recurrence and non-recurrence groups. Differences were considered significant at a p-value of less than 0.05. Odds ratios for receptor negativity were calculated to estimate the likelihood of recurrence in the corresponding patient subgroups.

Results. We analyzed growth factor receptors, such as EGFR and VEGF, in relation to the presence or absence of recurrence in patients with colorectal cancer. The results of the analysis show significant statistical differences, highlighting the importance of these receptors as prognostic factors.

Table 1. *Analysis of growth factor receptors depending on relapse*

Indicators	Category	recurence (yes-1, no 0)		p
		absence of relapse	Presence of relapse	
EGFR	EGFR positive	25 (52,1)	41 (74,5)	0,018*
	EGFR negative	23 (47,9)	14 (25,5)	
VEGF	VEGF positive	24 (50,0)	44 (80,0)	0,001*
	VEGF negative	24 (50,0)	11 (20,0)	

** – the differences in the indicators are statistically significant (p < 0,05)*

EGFR (Epidermal Growth Factor Receptor) is a key receptor that plays a vital role in regulating cell growth, division, and survival. Its activation is associated with various mechanisms of carcinogenesis, including stimulation of tumor cell proliferation, invasiveness, and angiogenesis. EGFR expression is elevated in many tumors, including colorectal cancer, and is associated with more aggressive forms of the disease and worse clinical outcomes. Studies have shown that EGFR positivity correlates with an increased likelihood of metastasis and recurrence, which is confirmed by our data: 74.5% of patients with relapse were EGFR positive, while only 52.1% of patients without relapse were EGFR positive. Statistically significant differences with a p-value of 0.018 highlight the importance of monitoring EGFR levels when planning therapy. Since EGFR is a target for various targeted therapies, the study results indicate the potential clinical significance of this receptor for personalized treatment of colorectal cancer.

VEGF (Vascular Endothelial Growth Factor), in turn, is a key factor regulating angiogenesis—the process of forming new blood vessels from existing ones. This is particularly important for tumors, as they require and enhance vascularity for growth and spread. Increased VEGF expression is associated with tumor aggressiveness and poor survival rates. The results of our analysis show that 80.0% of patients with relapse have a positive VEGF status, compared with 50.0% of patients without relapse (p=0.001). These data highlight the association between high VEGF status and disease recurrence, suggesting that angiogenesis may be an important mechanism in colorectal cancer progression. Given these results, VEGF may serve not only as a prognostic marker but also as a potential target for therapies aimed at inhibiting angiogenesis, thereby limiting tumor growth and metastasis.

A comparative analysis of the odds ratios for EGFR and VEGF statuses shows that negative status of these receptors reduces the likelihood of recurrence in patients with colorectal cancer. The odds of EGFR-negative tumors in the recurrence group were 2.694 times lower, while for VEGF-negative tumors in the same group, the odds were 4.000 times lower. These significant differences highlight how biological markers can predict tumor behavior and recurrence.

Thus, these data highlight the importance of EGFR and VEGF as prognostic markers in clinical practice, as well as their potential as targets for new therapies in the management of colorectal cancer. Research into these factors could provide the basis for developing more effective and personalized treatment approaches that can improve quality of life and patient survival. Further in-depth studies are needed to confirm these findings and identify optimal treatment strategies based on tumor marker characteristics.

Conclusion

This study confirmed a significant association between the expression of the growth receptors EGFR and VEGF and the risk of colorectal cancer recurrence. The statistically significant differences detected indicate the high prognostic value of these biomarkers for assessing the likelihood of disease recurrence. Their use in clinical practice may facilitate more accurate patient stratification and the selection of personalized therapeutic strategies aimed at reducing the risk of recurrence and improving survival. Further multicenter and prospective studies are needed to confirm these findings and develop standards for the use of these markers in oncology practice.

References

Ferlay J, et al. Global cancer statistics 2019: GLOBOCAN estimates of incidence and mortality worldwide for 36 cancers in 185 countries. CA Cancer J Clin. 2019.

Van Cutsem E, et al. Updates on colon and rectal cancer treatment in 2020: a decade in review. Lancet Oncol. 2020.

Menter D.G., et al. Targeting pathways of resistance to antiangiogenic therapy in colorectal cancer: a focus on VEGF and EGFR. Am J Clin Oncol. 2019.

Morgillo F., et al. Mechanisms of resistance to EGFR-targeted drugs: lung cancer and other solid tumors. Crit Rev Oncol Hematol. 2017.
Yonesaka K., et al. The role of EGFR mutation and ALK gene rearrangement in lung cancer. Exp Biol Med (Maywood). 2018.
Abdollahi A., et al. Regulation of angiogenesis by bFGF and VEGF in patients with lung cancer. Clin Canc Res. 2018.
Jubb A.M., et al. Impact of VEGF on survival in colorectal cancer patients. Ann Oncol. 2020.
Miller K.D., et al. Cancer treatment and survivorship statistics, 2021. CA Cancer J Clin. 2021.
Bensi M., et al. Advances in personalized therapy in colorectal cancer: focus on targeted therapy. J Clin Med. 2022.
Gray R., et al. Treatment of metastatic colorectal cancer with anti-EGFR therapy and KRAS mutation status. J Clin Oncol. 2021.

submitted 14.10.2025;
accepted for publication 28.10.2025;
published 26.11.2025

Contact: djumaniyazova.gulnoza@bk.ru

The Austrian Journal of Technical and Natural Sciences, No 9–10
ISSN 2310-5607

PREMIER Publishing
ppublishing.org

Section 6. Technical sciences in general

DOI:10.29013/AJT-25-9.10-98-101

INNOVATIVE TOOL OF TECHNOLOGICAL INTEGRATION (Composite Technical Solutions as an Inevitable Foundational Component for the Creation of Integrative Inventions and as the Main Instrument of Technological Integration)

Aleksandr Mikhalevich [1]

[1] Company RENTON

Cite: *Mikhalevich A. (2025). Innovative tool of technological integration. Austrian Journal of Technical and Natural Sciences 2025, No 9–10.* https://doi.org/10.29013/AJT-25-9.10-98-101

Abstract

The introduction of new technologies, the use of new materials, and the replacement of traditionally accepted production methods with unconventional ones that contribute to and are an essential prerequisite for a technological leap or breakthrough, as well as for improving production efficiency, are today referred to as the innovation process. This process, under conditions of diverse technical and technological cultures and varying initial levels for the commencement of initiated innovation processes, may differ significantly; however, the acute necessity for the initiation of such processes is undeniable. Psychological barriers associated with the need to combine classical solutions with the latest developments within an innovative project, and classical composite technical solutions serve as an inevitable fundamental component for the creation of integrative inventions that utilize composite technical solutions as the principal instrument of technological integration.

Keywords: *Technological integration; Composite technical solutions; Innovative integration tool; Traditionally accepted production methods; Various technical and technological cultures; Psychological barriers; Technological breakthrough; Initiated innovation process; Main instrument of technological integration; Thermodynamic cycle; Optimization of the thermodynamic cycle*

Change in the Rules and Criteria of Industrial Design

The first quantum computer has been introduced, joining the global race for *quantum supremacy*. The innovative 20-qubit computer utilizes advanced superconducting technology. *Quantum supremacy* refers to the level of performance achieved by a quantum computer that enables it to solve problems requiring computational power practically unattainable by conventional supercomputers. As of today, quantum supremacy has been achieved only

for specific model tasks by several quantum computers, yet the development of quantum computing continues worldwide. All developed nations participate in this global competition, with the United States and China being recognized leaders. Israel has now joined this race as well.

The development of quantum computing encompasses not only the creation of quantum computers but also the establishment of infrastructure for access to computational capacities, the development of software, and the capability to use quantum computers in conjunction with conventional supercomputers.

"Quantum technologies must fundamentally expand human capabilities across a wide range of fields. In recent years, the United States has advanced initiatives in robotics, autonomous systems, cybersecurity, and artificial intelligence, integrating them into business domains, including cooperation with startups and academic institutions."

"The presentation of the first quantum computer is an important milestone. This is not a standalone initiative but part of a broad strategy to promote breakthrough technologies across various sectors. All these efforts are elements of a strategic plan for the development of quantum computing, aimed at maintaining technological leadership, preserving the competitiveness of the high-tech industry, and ensuring sustainable economic growth."

Laboratories engaged in quantum computer development are now focusing on the design, modeling, integration, and adaptation of practical applications for superconducting quantum computers. This work implies close cooperation with companies and research institutes worldwide, positioning the developer as a leader in the field of quantum computing.

This honorable status, which provides a significant competitive advantage, is reinforced by close coordination among government institutions, academia, and industry.

"The research team working on this ambitious project is among the best. The collaborative and interdisciplinary nature of this project will yield significant research outcomes and strengthen scientific and technological standing."

"Quantum technologies are intended to fundamentally enhance human capabilities in a wide spectrum of areas," stated the CEO of the developing company.

In recent years, the company has advanced a number of initiatives in robotics, autonomy, cybersecurity, and artificial intelligence, integrating them into business directions – some in cooperation with startups and academic institutions.

The strength of industry depends on partnerships between academia, startups, industry, and government institutions.

Technologies are studied in academic circles and applied in industry, serving as a powerful multiplier.

Experts have noted that the quantum computer continues to evolve and possesses enormous technological potential.

It should be recalled that the smallest unit of information storage in a traditional computer is the bit, which can take on only one of two values: 0 or 1.

When solving a problem, a conventional computer performs a large number of sequential operations with bits.

For complex tasks, this process can take a considerable amount of time.

Quantum computers, on the other hand, operate with qubits (quantum bits), which, in addition to 0 or 1, can assume both values simultaneously.

In performing computations, quantum computers do not sequentially iterate through all possible combinations, as conventional computers do, but rather execute calculations instantaneously.

The introduction of new technologies, the use of new materials, and the replacement of traditionally accepted production methods with unconventional ones that facilitate and are an indispensable condition for a technological leap or breakthrough and an increase in production efficiency are now commonly referred to as the innovation process.

This process, under conditions of differing technical and technological cultures and varying levels of starting positions for the initiation of innovation processes, may differ significantly; however, the acute need to begin such a process is beyond question.

In recent years, the economies of nearly all industrially developed countries have acquired and continue to exhibit an increasingly pronounced innovative character.

While at the early stages of this trend technological breakthroughs had a local character and were observed mainly in high-tech fields, microelectronics, and so-called nanotechnologies, today the innovation process has become increasingly directed toward classical, fundamental technologies – energy, medicine, and transport – thus encompassing all key areas of human activity.

Entrepreneurs, in order to enhance the competitiveness of their products and technologies, are compelled to continuously seek new paths to improve efficiency, reduce energy consumption and intensity, increase environmental safety, and achieve economic stability within each enterprise or company. New opportunities in the design and testing of technical solutions have also introduced elements of composite design approaches, which are becoming key criteria for tools and methodologies in industrial design.

The situation has changed fundamentally with the use of artificial intelligence and artificial neural networks.

Scientists at **Intel Corporation** have developed algorithms that allow different AI models to work together. The elimination of the "language barrier" between systems accelerates performance by a factor of 2.8. Until recently, each AI model used its own unique set of tokens, understandable only to itself. This created a barrier to interoperability among systems developed by different companies.

Major technology corporations had previously employed the *"on-the-fly decoding"* method, in which a small, fast model makes an initial assessment of a request, while a larger and slower model verifies and corrects the response. However, this approach only works with models that "speak" the same digital language.

The new solution consists of two main algorithms.

The first allows models to translate their output data into a universal format understandable by all systems. The second forces models to focus on tokens with identical meaning across different systems – similar to words such as "banana" or "internet," which sound nearly identical in various human languages. These shared tokens become the starting point for decoding. The results exceeded researchers' expectations. Instead of information loss during "translation," the new algorithms accelerated the performance of large language models by an average of 1.5 times, and in the best cases – by 2.8 times. The algorithms have already been made publicly available on the **Hugging Face Transformers** platform and have become part of the standard toolkit for efficient AI performance.

This solution is particularly important for **edge devices** – smartphones, drones, and autonomous vehicles – that must rely on limited computing power in the absence of an Internet connection.

In the case of a self-driving vehicle, faster data processing can prevent a catastrophe. The study marks a new stage in the development of **collaborative AI**, where developers can freely combine the best features of different models, creating more efficient and accessible solutions for millions of users worldwide.

Not long ago, product durability was considered one of the most important criteria defining its commercial value. Today, with the constant reduction of time between the release of a new product and the introduction of an even newer one, this period has become so short that, within the framework of the innovation process, it often makes little sense to focus efforts and resources on excessive durability – whose lifespan would exceed the interval between the start of production and the market launch of its next-generation successor.

Which exceeds the period between the start of operation of an existing product and the market release of a newer or upgraded one. Since this period may vary significantly for different types of products, the very concept of durability becomes temporally blurred and, as an inventive objective, is no longer a critical factor.

There is also a subjective aspect of durability that must be taken into account.

Established perceptions of product longevity across various product types determine many commercial factors, including the quantity of goods demanded – and therefore sold – as well as their actual market price.

Imagine that a technical solution has been found that significantly increases a product's durability. In this case, such a factor would reduce the quantity of products required while maintaining the existing price level that consumers are willing to pay. This, in turn, leads to decreased sales volumes for manufacturing companies, placing them in a position where

they must choose – either to accept the innovation or to do everything possible to block its implementation and adoption.

As practice shows, these companies most often choose the latter, blocking the innovation; and in this process, the only party that loses is the inventor, the one who has created something that the market itself refuses to accept.

References

Yakus, Adam et al., November 9, 2006. U.S. Patent Application № 20060250934
Dresdner Jr., Karl P. et al., November 5, 2020. U.S. Patent Application № 20200345585
Bayramijamal, Faramarz, September 10, 2020. U.S. Patent Application № 20200283920
Mykityuk, Alexander Yurievich, August 20, 2020. U.S. Patent Application № 20200262728
James, Patrick Ismail, May 14, 2020. U.S. Patent Application № 20200147553.

List of References and Patent and Licensing Materials:

Appendix 1.

United States Patent Application **20060250934**
Kind Code **A1**
November 9, 2006

Three-dimensional optical information carrier and a method of manufacturing thereof

Abstract

A three-dimensional optical information carrier is presented. The information carrier comprises formatting marks disposed on the nodes of a three-dimensional lattice formed by the intersection of equiangular spaced radial planes, equidistantly spaced cylindrical spiral tracks and virtual recording planes.

Appendix 2.

United States Patent Application **20070288947**
Kind Code **A1**
December 13, 2007

SWING ARM OPTICAL DISC DRIVE

Abstract

Disclosed is a swing type optical disc drive. The drive includes a disc rotating on a disc support and a swing arm pivoted at one of its ends and having a distal end communicating with an encoder. The pivot point and a point on distal end define a swing axis of the arm. The disc further includes an optical system mounted on the arm such that optical axis of the system is parallel with the swing axis and both axes lie in the same plane. A cam actuator imparts a swinging motion to the arm. The swinging motion of the arm positions the plane with the optical axis and the arm axes such that the plane is always tangent to a reading/recording track of the disc.

submitted 14.10.2025;
accepted for publication 28.10.2025;
published 26.11.2025

Contact: sedova.alina7810@gmail.com

The Austrian Journal of Technical and Natural Sciences, No 9–10
ISSN 2310-5607

PREMIER Publishing
ppublishing.org

DOI:10.29013/AJT-25-9.10-102-106

OPTIMIZATION OF INDUSTRIAL ADIABATIC COOLING SYSTEMS TO REDUCE ENERGY CONSUMPTION AND CARBON DIOXIDE EMISSIONS

Nikitin Vitaliy Vyacheslavich [1]

[1] Founder & CEO, Asvi Group Services LLC, Houston, USA

Cite: *Nikitin V.V. (2025). Optimization of industrial adiabatic cooling systems to reduce energy consumption and carbon dioxide emissions. Austrian Journal of Technical and Natural Sciences 2025, No 9–10*. https://doi.org/10.29013/AJT-25-9.10-102-106

Abstract

The article discusses the urgent task of improving the energy and environmental performance of industrial facilities through the optimization of adiabatic cooling systems. It analyzes the basic principles of adiabatic system operation and their advantages over traditional compressor units. The focus is on the development and analysis of optimization techniques aimed at achieving a balance between maximum cooling capacity, minimal water consumption, and, consequently, reduced electricity usage. The paper presents mathematical models and control algorithms that allow the system to adapt to changing climate conditions and thermal loads in real-time. It also justifies the direct link between reduced energy consumption and reduced indirect carbon dioxide (CO_2) emissions associated with electricity generation. The results of the study show that the introduction of intelligent adiabatic cooling systems can significantly reduce the operating costs and carbon footprint of industrial facilities and data centers.

Keywords: *adiabatic cooling, energy efficiency, optimization, reduction of CO_2 emissions, industrial cooling, energy saving, evaporative cooling, control algorithms, carbon footprint, sustainable development*

The relevance of research

Modern industrial enterprises are striving to reduce the energy intensity and environmental impact of their production processes. Adiabatic cooling systems, used for air conditioning in process rooms and equipment, represent an energy-efficient alternative to traditional compression systems. However, the use of these systems can sometimes lead to the irrational use of water and energy resources.

Optimizing these systems can significantly reduce electricity consumption and direct and indirect CO_2 emissions, in line with global trends towards sustainable development and international energy efficiency standards.

The purpose of the study

The main goal of the research is to develop and scientifically justify a methodology for optimizing industrial adiabatic cooling systems, aiming to simultaneously reduce electricity consumption and indirect carbon dioxide emissions while maintaining the necessary cooling capacity.

To achieve this goal, a number of tasks must be completed. First, existing systems must be analyzed to identify key performance indicators. Then, a mathematical model must be developed to describe the thermodynamic, energy, and water processes within the system. Based on this model, a multi-criteria optimization algorithm must be created that can find the best balance between cooling efficiency, water use, and energy use in real time. Finally, the system's performance must be simulated numerically for various conditions, and the potential for energy savings and CO_2 reductions compared to traditional or unoptimized systems must be quantified.

Materials and methods of research

The current industrial adiabatic cooling systems used in the food, chemical, and metallurgical industries are the focus of this research. During the study, methods of thermodynamic analysis, energy and exergy balances, mathematical modeling of mass and heat transfer processes, as well as computer simulation tools such as CFD modeling, are employed.

The experimental component involves collecting data on actual operating conditions of the equipment, measuring temperatures, humidity, airflow, and water flow. To evaluate the environmental impact, a method for calculating the carbon footprint is used, based on CO2 emission factors calculated from electricity consumption. Based on the collected data, recommendations are developed for technological and design improvements aimed at enhancing the energy efficiency of these systems.

The results of the study

The idea of adiabatic cooling, which is based on using water evaporation to reduce air temperature, dates back to ancient times. In ancient Egypt and Persia, simple evaporation devices such as vessels with a porous surface were used, through which air passed and was cooled by the evaporation of moisture. This principle was also applied in architecture, with wind towers and fountain systems creating natural cooling for rooms.

Since the early XX century, as industry developed and the need for air conditioning increased, adiabatic systems began to receive engineering attention. The first industrial installations, used in textile and food manufacturing, employed direct water evaporation in air streams. However, these systems were limited by climate conditions, so further development focused on improving control over heat and mass transfer processes.

In the second half of the XX century, new indirect adiabatic cooling systems were developed, which did not require water to enter the working airflow. Instead, cooling occurred through heat exchange surfaces, making it possible to use these systems over a wider range of temperatures and humidities, including areas with high relative humidity (Fig. 1).

Figure 1. *Indirect adiabatic cooling scheme*

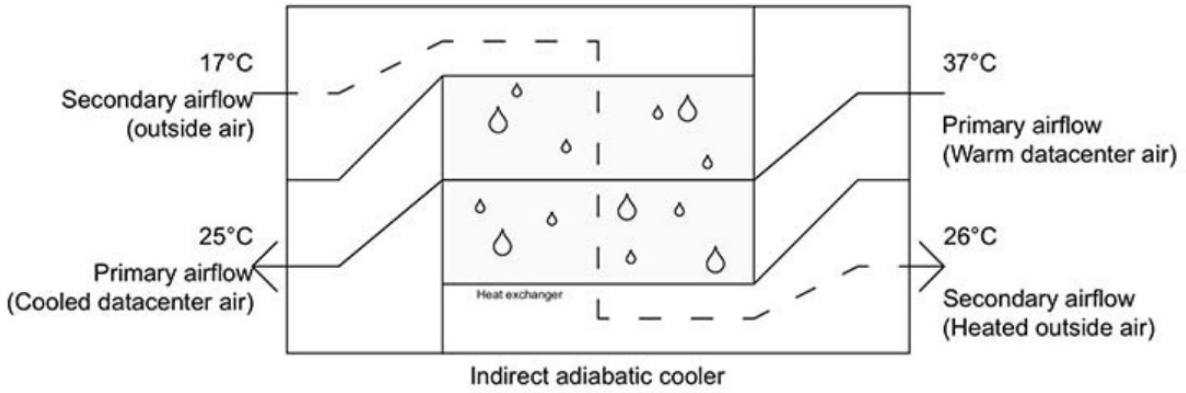

Since the 1980s and 1990s, computer technology has played a significant role in the design of more efficient adiabatic systems using computational fluid dynamics (CFD) techniques. During this time, combined systems that combine adiabatic cooling with mechanical cooling or heat recovery have

emerged, increasing their overall energy efficiency (Tarabarin L.I., 2023).

In the XXI century, researchers and industry have focused on increasing environmental sustainability and reducing energy consumption. This has led to the introduction of intelligent control systems and automatic water and air flow optimization, which have significantly reduced operating costs and the carbon footprint.

Modern adiabatic systems, such as those used in data centers and logistics complexes, are an integral part of the "smart" and energy-efficient industry. These systems have evolved from simple evaporative technologies to more complex, integrated solutions that meet today's environmental and energy-saving standards (Tab. 1).

Table 1. *Evolution of adiabatic cooling systems*

No.	Name	Characteristic
1.	Traditional technologies	In the early days, simple methods such as fans and natural convection were used to cool the air. However, these systems were not very effective and consumed a significant amount of energy.
2.	Use of water	The introduction of water-cooling, where water is evaporated to lower air temperature, has significantly increased efficiency. However, this process requires a significant amount of water.
3.	Adiabatic coolers	The development of adiabatic coolers, which use the principle of evaporative cooling, has led to a reduction in energy consumption and an increase in efficiency.
4.	Modern technologies	The introduction of microcontrollers and sensors has allowed us to automate cooling processes and make them more adaptable to environmental conditions.
5.	New materials	The use of modern thermal insulation and water-resistant materials to enhance the efficiency of systems.
6.	Integration with sustainable energy sources	Modern adiabatic systems are often combined with solar panels and other renewable energy sources, which makes them more environmentally friendly.
7.	Smart technologies	Implementation of the IoT (Internet of Things) for monitoring and control of cooling systems, which allows optimizing their operation in real time.

It should be noted that, in recent decades, the development of industrial adiabatic cooling systems has focused on improving energy efficiency and reducing environmental impact. Modern solutions incorporate automated control systems, innovative heat exchange materials, and a comprehensive analysis of air and moisture flow (Dolgov A.I., 2012).

One of the key areas of focus is the use of intelligent control systems. These systems allow for real-time monitoring and control of water flow, fan speed, and incoming air temperature. By taking into account weather data, heat load, and indoor conditions, these systems can optimize water and energy consumption. Thanks to adaptive algorithms, electricity consumption can be reduced by 20–40%, compared to traditional systems. In addition, water consumption can also be optimized.

Another significant area is the development of hybrid adiabatic systems. These systems combine evaporative cooling with either mechanical (compressor) cooling or regenerative heat exchange, ensuring stable air parameters and minimal energy consumption. These hybrid schemes are particularly useful in data centers, where equipment temperature directly affects work efficiency. In some European data centers, the use of adiabatic cooling has resulted in a 30–50% reduction in carbon footprint compared to traditional air conditioning systems.

Innovative materials also play a significant role in this process. Modern evaporation

units, made from cellulosic, nanostructured, or ceramic materials, offer a higher evaporation rate and reduce the risk of bacterial growth. This not only reduces maintenance costs but also increases the longevity of the equipment (Yang Yu., Chen S.-S., 2010).

An important aspect of aerodynamics is digital modeling and optimization, which allows for the design of systems with minimal pressure loss and even airflow distribution. The use of computational fluid dynamics (CFD) models helps adjust the geometry of channels and nozzle placement, improving heat and mass transfer efficiency.

One promising solution is the recovery of moisture and energy through two-stage cooling systems and exhaust air recycling. These systems can reduce energy consumption by up to 60%, compared to traditional air conditioning units. These technologies are actively being implemented in logistics facilities, the food industry, and large-scale ventilation systems.

Optimization of industrial adiabatic cooling systems relies on digital technologies, intelligent controls, hybridization, and new high-performance materials. These technologies not only significantly reduce energy consumption but also contribute to reducing CO_2 emissions, promoting the development of a more sustainable and environmentally friendly industry.

Despite their energy efficiency and environmental advantages, modern industrial cooling systems face several challenges that limit their potential for optimization. The main challenge is the instability of performance depending on climatic conditions. During high humidity, water evaporation intensity decreases, leading to a reduction in cooling efficiency and a need for additional mechanical cooling. This increase in energy consumption indirectly increases carbon emissions.

Another significant issue is the high water consumption. Intense evaporation requires a substantial amount of liquid, particularly with high system efficiency. An inefficient water circuit and lack of a closed water loop increase resource scarcity and impact operational sustainability. Additionally, when salts and contaminants accumulate in the water, heat transfer decreases, and frequent cleaning or replacement of the evaporation panels becomes necessary.

The correct configuration of automated control systems can be difficult. To achieve maximum energy efficiency, a precise interaction between temperature, humidity, pressure sensors, and fan and pump controllers is necessary. Even small errors in the algorithms can lead to energy wastage or unstable microclimate parameters. Additionally, the introduction of intelligent systems requires capital investment and staff training, which can hinder the widespread adoption of innovation.

The reliability and durability of the components remain a significant challenge. Adiabatic cooling, while effective, is associated with high humidity, which can lead to corrosion of metal elements and reduce the service life of fans, pumps, and panels. This requires the use of expensive anti-corrosive materials and regular maintenance, which adds to the cost of the system.

Another issue is the lack of advanced digital modeling tools. Despite the availability of CFD (computational fluid dynamics) analysis systems, detailed simulations of evaporation and turbulent flow are not commonly used in practical applications. This can lead to design errors and unnecessary energy losses, as well as increased maintenance costs.

The main challenges in optimizing adiabatic cooling systems include climate-dependent efficiency, water scarcity, complex control, technical reliability, and insufficient digitalization in design. Addressing these issues requires an integrated approach that includes implementing intelligent monitoring systems, utilizing sustainable materials, establishing closed water supply cycles, and adapting technologies to regional climate conditions.

We believe that optimizing industrial adiabatic cooling systems requires a multilayered process aimed at enhancing energy efficiency, minimizing water consumption, and ensuring reliable operation of equipment across diverse climates.

The basis of the modern approach is the integration of engineering solutions, automation, and digital control technologies. This involves adapting the operating modes of a system to changes in temperature and humidity using intelligent control algorithms. These algorithms regulate the speed of fan rotation, water spray intensity,

and pump performance, based on machine learning principles. This allows the system to learn and predict future climate conditions, optimizing resource allocation for maximum efficiency.

A significant role is played by reducing water consumption with closed water circulation systems, filtration, and recirculation, which prevent excessive moisture loss. The building uses materials with increased corrosion resistance and hydrophilic coatings, which promote uniform evaporation and the durability of the building's elements.

CFD models and digital twins are used to improve the efficiency of airflow, allowing for the prediction of temperature and humidity distribution at all stages of design and operation. Automated monitoring systems connected to cloud platforms collect real-time data from temperature, humidity, and vibration sensors, enabling proactive maintenance and emergency prevention.

Energy saving is achieved through the introduction of frequency-controlled engines, optimization of duct aerodynamics, and the use of renewable energy sources. In the future, the development of these systems will involve the use of neural networks for integrated climate management, intelligent equipment diagnostics, and the complete digitalization of design and operational processes.

The detailed optimization of industrial adiabatic cooling systems ensures a high level of energy efficiency, environmental sustainability, and reliability at minimal operating costs.

Conclusion

Optimization of industrial adiabatic cooling systems is a crucial aspect in the development of modern energy-efficient technologies and the enhancement of environmental sustainability in production processes.

The use of intelligent control algorithms, digital twins, and automated monitoring ensures the flexibility and accuracy of equipment operation, while minimizing energy and water consumption. Increased efficiency is achieved through an integrated approach that includes engineering improvements to the design, optimization of aerodynamics, and the introduction of adjustable drives and recirculation systems.

Digitalization of the design and operation processes is essential, as it enhances transparency, predictability, and reliability of integrated systems. The development of adiabatic cooling helps reduce the carbon footprint by minimizing the impact on urban energy systems, while also increasing the competitiveness of businesses.

In the future, the integration of artificial intelligence, the Internet of Things, and sustainable engineering solutions will form the basis for establishing new standards in the field of industrial climate systems. These systems will ensure a balance between production efficiency and conservation of natural resources, leading to a more sustainable future.

References

Dolgov A.I., On the issue of optimizing gas turbine cooling systems // Technological audit and production reserves. – No. (1 (7)). 2012. – P. 7–8.

Tarabarin L. I. Optimization of the exhaust gas treatment plant of industrial and energy enterprises from harmful emissions, including greenhouse gases // Innovations and investments. – No. (10). 2023. – P. 188–192.

Yang Yu., Chen S.-S. Thermodynamic modeling of CO_2 solubility in aqueous solutions of NaCl and Na2SO_4 // Investigation of supercritical fluids. 2010. – No. 55. – P. 623–634.

submitted 14.10.2025;
accepted for publication 28.10.2025;
published 26.11.2025

Contact: Asvigroupservices@gmail.com

The Austrian Journal of Technical and Natural Sciences, No 9–10
ISSN 2310-5607

PREMIER Publishing
ppublishing.org

DOI:10.29013/AJT-25-9.10-107-113

STUDY OF THE EFFECT OF GLAUCONITE AND VERMICULITE ON THE SALINITY OF THE SOIL OF KARAKALPAKSTAN

Ochilov Siroj Urazboy uli [1], ***Allaniyazov Davran Orazimbetovich*** [1], ***Erkayev Aktam Ulashevich*** [2], ***Allaniyazov Davlet Orazimbetovich*** [3], ***Uzakbaeva Mehriban Muratbaevna*** [3]

[1] Chemistry Laboratory, Karakalpak Research Institute of Natural Sciences, Karakalpak branch of Ruz

[2] Department of Chemical Technology of Inorganic Substances, Tashkent Institute of Chemical Technology, Tashkent

[3] Karakalpak Research Institute of Natural Sciences, Karakalpak Branch Academy of Sciences of the Republic of Uzbekistan

Cite: *Ochilov S.U., Allaniyazov D.O., Erkayev A.U., Allaniyazov D.O., Uzakbaeva M.M. (2025). Study of the Effect of Glauconite and Vermiculite on the Salinity of the Soil of Karakalpakstan. Austrian Journal of Technical and Natural Sciences 2025, No 9–10.* https://doi.org/10.29013/AJT-25-9.10-107-113

Abstract

The studies were carried out on saline soils that were taken soil samples on the territory of Mamiy, Shumanai district of the Republic of Karakalpakstan to assess the state of soils and salinization and content of water-soluble salts of this site. All soil samples taken are saline, salinization-sulfate-chloride, chloride-sulfate, sulfate. The degree of salinization varies from medium to very strong in all soil profiles. There are also summarized data on the studied components, the most characteristic soil conditions of the surveyed area.

Keywords: *Karakalpakstan, Shumanai, glauconite, vermiculite, soil salinization, dry residue, agronomists, agriculture, water-soluble salts, adsorption, desorption*

Introduction

Today, increasing soil salinity is one of the pressing problems around the world. This is one of the most common processes that leads to land degradation worsening and determining their fertility. In this aspect, the process of draining and drying the bottom of the Aral Sea led to pollution, environmental pollution, soil salinization, salinity, which depends on the areas of gradual salt formation (Turemuratova A.Sh., Reymov K. D., Allaniyazov D. O., 2022).

Research objects and methods

The object of research in this work is the soils of the Shumanai region: the Mamiy section located 70 km from the center of Nukus Karakalpakstan.

Research material and methodology

The water extract of the selected soils was prepared according to the generally accepted method – soil: water in a ratio of 1:5 (Arinushkina E. V., 1970). The content of chlorine ions was determined by sea argentometric methods; calcium and magnesium trilonometric; sulfate by titration; aqueous extract with sulfuric acid solution in the presence of methyl orange indicator; sodium and potassium ions by difference of sum of anions and cations. The results of the analysis of aqueous extracts were expressed in milligram equivalents per 100 g, air-dry soil, the sum of water-soluble salts in percent.

The results of the aqueous draw analysis were monitored for solids.

The degree of salinization of soils was evaluated on a scale (Arinushkina E. V., 1970; Genkel P. A., 1975; Genkel P. A., 1975; Kovda V. A., 1984). The data obtained are presented in table 1.

Figure 1. *Coordinates of samples obtained in the territories of Mamiy, Shumanai district, Karakalpakstan*

1, (42,6009667, 58,9927549) / Kontr 11/98

2, (42,5963145, 58,9856809) / Kontr 11/76

3, (42,5938604, 58,9859182) / Kontr 17/17

4, (42,5940663, 58,9874199) / Kontr 11/73

Research results

Table 1 shows the content of Cl, SO_4^{2-} – and Na^+ ions in the studied samples in the ranges of 0,75–30,00, 9,43–43.55 and 1,48–42,13 mg-eq per 100 g of dry soil, respectively, so that soils from salinization with sulfates and sodium chlorides.

The dry residue in the samples ranges from 0,750 to 4.800 ml, eq. Based on the value of the dry residue of this sample by the degree of salinity, it belongs to the class; weak, weak and highly saline, respectively.

To study the percentage of adsorption of ions with agronomic ore, first prepared aqueous extracts from the 4th sample at ratios of 1:10 (soil: H_2O). Next, a certain amount of agro or was added to the obtained extract, and after 2 days, the ionic composition of the extract was determined, and the adsorption and desorption rates of Cl, SO_4^{2-}, Na^+ ions from the aqueous extract were calculated.

As follows from the analysis of the result of Table 1, the strongest saline soil sample is the 4th sample containing Cl, SO_4^{2-} and Na^+ ions. It is 30,00;43,55 and 42,13 mg, eq per 100 g of dry sample.

Therefore, the 4 th sample was used in further studies.

The adsorption capacities of glauconite and heat-treated vermiculite of ions: Cl,

Table 1. *Ion composition of soil samples*

No.	Sample №	Color and transparency of the hood	pH	solid residue		NO_2^-	Numerator: mg-eq per 100 g, dry, soil; denominator: % to abs, dry soil												
				experimental	combed		anions						cations					Sum of mg-eq cations	Salinity type
							CO_3^{2-}	HCO_3^-	Cl^-	SO_4^{2-}	NO_3^-	Sum of mg-eq anions	Ca^{2+}	Mg^{2+}	NH_4^+	Na^+		
1.	11/98	Transparent without color	7.10	0.750	0.713	0.01 0.001	No –	0.80 0.049	0.75 0.026	9.43 0.453	0.02 0.001	11.01	7.20 0.144	2.00 0.024	0.33 0.006	1.48 0.034	11.01	–C– weakly
2.	11/76	Transparent without color	6.90	1.780	1.712	0.02 0.001	No –	0.60 0.073	7.75 0.275	18.46 0.886	0.15 0.009	26.98	9.20 0.184	6.40 0.078	0.33 0.006	11.05 0.254	26.98	–C– average
3.	17/17	Transparent without color	7.10	0.940	0.905	0.03 0.001	No –	0.80 0.049	3.25 0.115	10.12 0.485	0.06 0.004	14.26	4.80 0.096	3.40 0.041	0.17 0.003	5.89 0.135	14.26	–C– weakly
4.	11/73	Transparent without color	6.80	4.800	4.662	0.06 0.003	No –	1.00 0.061	30.00 1.064	43.55 2.090	0.65 0.040	75.26	7.80 0.156	25.00 0.304	0.33 0.006	42.13 0.969	75.26	–C– strongly

* *Depth of ignition 0–20 cm*

Table 2. *The influence of temperature on the adsorption capacity of vermiculite and glauconite*

No.	Sample №	Color and transparency of the hood	pH	solid residue		NO_2^-	Numerator: mg-eq per 100 g, dry, soil; denominator: % to abs, dry soil										
				experimental	combed		anions					Sum of mg-eq anions	cations				Sum of mg-eq cations
							CO_3^{2-}	HCO_3^-	Cl^-	SO_4^{2-}	NO_3^-		Ca^{2+}	Mg^{2+}	NH_4^+	Na^+	
1.	Vermiculite 800° C 11/73	Transparent without color	9.20	4.020	3.837	0.02 0.001	0.40 0.012	0.30 0.018	23.75 0.842	35.49 1.704	0.64 0.040	60.60	20.20 0.405	6.60 0.080	0.35 0.006	33.45 0.769	60.60
2.	Vermiculite 600° C 11/73	Transparent without color	6.70	4.700	4.552	0.02 0.001	No —	1.20 0.073	27.50 0.975	44.75 2.148	0.64 0.004	74.11	12.00 0.240	23.50 0.286	0.25 0.004	38.36 0.822	74.11
3.	Vermiculite 400° C 11/73	Transparent without color	7.10	4.600	4.570	0.02 0.001	No —	1.20 0.073	26.25 0.931	45.00 2.160	0.64 0.040	73.11	13.00 0.260	22.00 0.267	0.25 0.004	37.86 0.871	73.11
4.	Vermiculite 11/73	Transparent without color	7.10	4.860	4.737	0.003 0.001	No —	0.90 0.055	27.50 0.975	46.38 2.226	0.64 0.040	75.45	13.80 0.276	20.60 0.250	0.12 0.002	40.93 0.941	75.45
5.	Glauconite 11/73	Transparent without color	6.60	4.560	4.484	0.33 0.015	No —	1.10 0.067	26.25 0.931	43.46 2.086	0.64 0.040	71.78	15.00 0.301	21.00 0.255	0.12 0.002	35.66 0.820	71.78

* *Soil ratio: Agroores 1:1*

SO_4^{2-} and Na^+ of the water extract of the 4th soil sample were studied.

The effects of heat-treated vermiculite temperature, soil: Agro-ore ratio and fraction size were studied.

Calcination temperature The ratio of soil: size fractions of Agro-ore varied from 400 to 800 °C, 5:1–1:3 and 1–7 mm, respectively.

Sieve composition of initial glauconitis and vermiculitis

No.	Name Agro ores	Size fraction, mm					
		– 5 + 3	– 3 + 2	–2 + 1	–1 + 0.5	– 0.5 + 0.25	– 0.25
1.	Vermiculite	40.97	55.52	2.0	0.9	1.6	0.8
2.	Glauconite	–	–	–	–	33.26	66.74

Tables 2 and 3 show the influence of the temperature of the calcination agro-ore and the adsorption capacity of vermiculite and glauconite.

Table 3. *Degree of sorption and desorption (%) of soluble ions of agro-ore*

The sample number corresponds to the numbers table 2.	anions					cations			
	CO_3^{2-}	HCO_3^-	Cl^-	SO_4^{2-}	NO_3^-	Ca^{2+}	Mg^{2+}	NH_4^+	Na^+
1.	No	–70.00	–20.83	–18.36	–1.53	+158.9	–73.60	+6.06	–20.60
2.	No	+20.00	–8.33	+2.75	–1.53	+53.80	–6.00	–24.24	–8.94
3.	No	+20.00	–12.50	+3.32	–1.53	+66.66	–12.00	–24.24	–10.13
4.	No	–10.00	–8.33	+6.42	–1.53	+76.92	–17.6	–63.63	–2.84
5.	No	+10.00	–12.5	–0.20	–1.50	+92.30	–16.00	–63.63	–15.35

4 (11/73) samples were selected as saline soils; Table 3 shows that the adsorption capacity of glauconite relative Cl and Na^+ ions is greater than the capacity of the original vermiculite. When using glauconite 12,5; 11,15; 3,5% Cl and Na^+ are adsorbed and the ions are finally applied.

Vermiculite and adsorption are 8,33 and 2,84% hard 1,5 and 5,40 tons' times lower, however, with increasing calcination temperature, the adsorption capacity of vermiculite increases from 8,33; 2,84 to 20,83 and 20,60, respectively, relative Cl^- and Na^+ ions.

It is necessary to purify the adsorption capacity of the used Agro-ore relative to NH_4^+ is the same and is equal to 63,63%; with increasing temperature, the heat treatment of the wall of adsorption of NH_4^+ ions decreases, and at 800^0C it practically stops; the adsorption capacity of NO_3^- ions is not affected by the type and temperature of the Agro-ore calcination and is 1,53%.

As for the SO_4^{2-}, ion, glauconite slightly sorbs, but the original vermiculite is not sorbed, and with increasing calcination temperature, the pore size increases and at 800 °C it becomes adsorbed as Cl^- and Na^+ ions also to the SO_4^2 and Mg^{2+} ions.

Tables 4 and 5 show the effect of the soil: Agro-ore ratio on the adsorption capacity of Cl^- and Na^+ ions. Based on the results of tables 2 and 3, heat treatment of vermiculite at 800 °C for 30 minutes was used as adsorption.

As the experimental results show in table 5, the influence of the soil: Agro-ore ratio on the adsorption capacity of ions is complex. Therefore, based on the results, we can conclude that the 2nd experiment is optimal, (soil: Agro-ore ratio = 1,67:1) the degree of adsorption of Cl^- and Na^+ ions assigned under these conditions reaches more than 12 and 14%, respectively.

Table 4. *Change depending on the ratio of soil and agro-ore and the ionic composition of the extract*

No.	ratio Soil: Agro-ore,	Color and transparency of the hood	pH	solid residue		NO_2^-	Numerator: mg-eq per 100 g, dry, soil; denominator: % to abs, dry soil										
				experimental	combed		anions					Sum of mg-eq anions	cations				Sum of mg-eq cations
							CO_3^{2-}	HCO_3^-	Cl^-	SO_4^{2-}	NO_3^-		Ca^{2+}	Mg^{2+}	NH_4^+	Na^+	
1.	5:1	Transparent				0.05	No	1.20	30.00	47.41	0.64	79.30	11.20	27.80	0.33	39.97	79.30
		without color	6.00	5.100	4.902	0.002	–	0.073	1.064	2.275	0.040		0.224	0.338	0.006	0.919	
2.	1,67:1	Transparent				0.005	No	1.20	26.25	41.66	0.64	69.80	10.60	23.00	0.33	35.87	69.80
		without color	6.20	4.480	4.328	0.002	–	0.073	0.931	1.999	0.040		0.212	0.279	0.006	0.825	
3.	1:1	Transparent				0.05	No	1.00	28.75	47.49	0.64	77.93	11.40	24.10	0.33	42.10	77.93
		without color	6.20	5.000	4.874	0.002	–	0.061	1.019	2.279	0.040		0.228	0.301	0.006	0.968	
4.	1:2	Transparent				0.06	No	1.00	25.00	37.97	0.64	64.67	9.40	19.60	0.50	34.84	64.67
		without color	6.20	4.180	4.022	0.003	–	0.061	0.886	1.823	0.040		0.188	0.238	0.801	0.015	
5.	1:3	Transparent				0.06		1.00	25.00	37.21	0.64	63.91	11.00	16.00	0.55	36.36	63.91
		without color	6.20	4.080	4.005	0.003		0.061	0.886	1.786	0.040			0.194	0.010	0.836	

Sample 4 (11/73) was selected as saline soils

Table 5. *Changes in the ionic composition of the extract depending on the size of Agro-ore fractions*

No.	Color and transparency of the hood	pH	solid residue		NO_2^-	Numerator: mg-eq per 100 g, dry, soil; denominator: % to abs, dry soil										
			experimental	combed		anions					Sum of mg-eq anions	cations				Sum of mg-eq cations
						CO_3^{2-}	HCO_3^-	Cl^-	SO_4^{2-}	NO_3^-		Ca^{2+}	Mg^{2+}	NH_4^+	Na^+	
1.	Transparent	6.35	3.860	3.730	0.02	No	0.90	23.50	34.72	0.65	59.79	12.50	16.00	0.17	31.12	59.79
	without color				0.001	–	0.055	0.833	1.666	0.040		0.251	0.195	0.003	0.715	
2.	Transparent	5.90	3.720	3.616	0.001	No	1.00	23.50	33.18	0.64	58.32	9.50	17.50	0.50	30.83	58.33
	without color				0.001	–	0.061	0.833	1.592	0.040		0.190	0.213	0.009	0.709	
3.	Transparent	6.20	3.860	3.721	0.03	No	1.00	22.50	35.32	0.64	59.49	12.00	16.00	0.35	31.14	59.49
	without color				0.001	–	0.061	0.798	1.695	0.040		0.240	0.195	0.006	0.716	
4.	Transparent	6.00	4.100	3.964	0.01	No	1.20	23.50	37.97	0.64	63.32	9.50	18.00	0.23	35.59	63.32
	without color				0.001	–	0.073	0.833	1.823	0.040		0.190	0.219	0.004	0.818	
5.	Transparent	6.60	4.100	3.948	0.02		1.00	23.00	38.23	0.64	62.89	11.50	17.00	0.50	33.89	62.89
	without color				0.001		0.061	0.816	1.835	0.040		0.230	0.207	0.009	0.779	

Table 6. *Change (%) in the degree of absorption and desorption of ions from the extract depending on the ratio of soil and agricultural ore*

The sample number corresponds to the numbers in table 4	anions					cations			
	CO_3^{2-}	HCO_3^-	Cl^-	SO_4^{2-}	NO_3^-	Ca^{2+}	Mg^{2+}	NH_4^+	Na^+
1.	No	+20.00	0	+8.86	–1.53	+43.58	+11.20	0	–5.12
2.	No	+20.00	–12.5	+4.33	–1.53	+35.89	–8.00	0	–14.85
3.	No	0	–4.16	+9.04	–1.53	+46.15	–3.60	0	–0.07
4.	No	0	–16.66	–12.81	–1.53	+20.51	–21.60	+51.51	–17.30
5.	No	+0	–16.66	–14.55	–1.53	+41.02	–36.00	+66.66	–13.69

Table 7. *Changes in the degree of absorption and desorption of ions from the extract depending on the size of agro-ore fractions*

The sample number corresponds to the numbers in table 5	anions					cations			
	CO_3^{2-}	HCO_3^-	Cl^-	SO_4^{2-}	NO_3^-	Ca^{2+}	Mg^{2+}	NH_4^+	Na^+
1.	No	–10.00	–21.66	–20.27	0	+60.25	–36.00	– 48.48	–26.13
2.	No	0	–21.66	–23.81	–1.53	+21.79	–30.00	+51.51	–26.82
3.	No	0	–25.00	–18.89	–1.53	+53.84	–36.00	+6.06	–26.08
4.	No	+20.00	–21.66	–12.81	–1.53	+21.79	–28.00	–30.30	–15.52
5.	No	0	–23.33	–12.21	–1.53	+47.43	–32.00	+51.51	–19.55

Tables 5 and 7 show experimental data on studying the effect of fraction size on the adsorption capacity of heat-treated vermiculite for Cl^- and Na^+ ions from the aqueous extract of the 4-th soil (Allaniyazov D. O., 2019; Allaniyazov D. O., Erkaev A. U., 2021; Allaniyazov D. O., Erkayev A. U., Tajibayev T. A., Ochilov S. U., 2023; Allaniyazov D. O., Tazhibaev T. A., Ochilov S. U., 2024; [5–9].

As follows from table 6, at selected intervals of varying the size of fractions 1 = 7 mm, the degree of sorption of Cl^-, SO_4^{2-} and Na^+ ions fluctuates in the ranges of 21,60–24,33; 12,21–23,81 and 15,12–26,82%, respectively.

Figure 2. *Effect of fraction size on the degree of adsorption of ions (Cl, SO_4^{2-}, Na^+) from soil water extract*

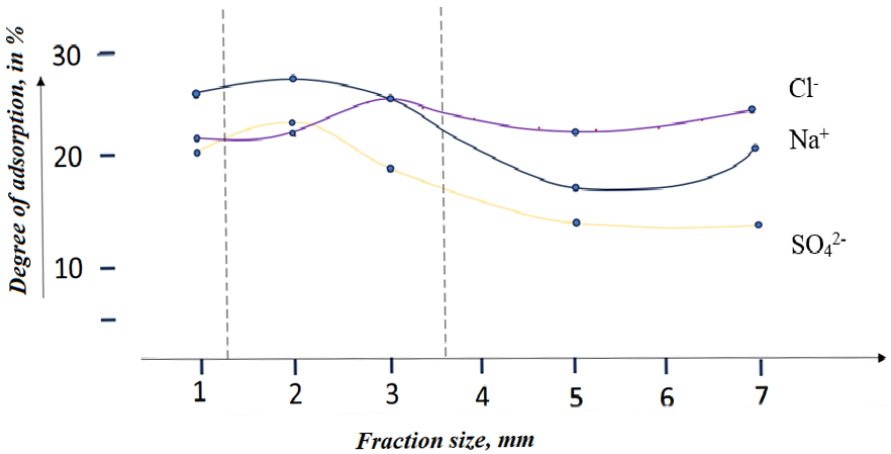

In Fig. 2. The nature of changes in the adsorption properties of ions is presented depending on the size of the fractions; the figure shows that in the intervals of 1,25–3,25 mm of fractions the curves, the adsorption capacity of ions intersects and reach a minimum value, therefore the optimal size of vermiculite should be in the intervals of 1,21–3,25 mm.

Conclusions

The studies have shown that all soil samples are saline, characterized by mixed salinity–chloride–sulfate; sulfate, the degree of salinity varies from medium to very strong across all soil profiles.

Based on the results, we can conclude that of all the experiments carried out, the 2 nd experiment is the most optimal (soil: Agro-ore ratio = 1,67:1), the degree of adsorption of Cl^- and Na^+ ions assigned under these conditions reaches more than 12 and 14%, respectively.

In addition to combating soil salinity by selecting crops and creating salt-tolerant varieties, in relation to certain types of soil salinization, it is necessary to use techniques that increase the salt tolerance and productivity of cultivated plants on saline soils.

References

Turemuratova A. Sh., Reymov K. D., Allaniyazov D. O. (2022). Distribution of salts in groundwater and drained surface of the Aral Sea. Universum: Chemistry and Biology, – No. 6–1. – (96). – P. 31–36.

Arinushkina E. V. (1970). Guide to Chemical Analysis of Soils, Moscow State University Publishing House, – 257 p.

Genkel P. A. (1975). Plant Physiology, M: Enlightenment, – P. 140–208.

Kovda V. A. (1984). Problems of combating desertification and salinization of irrigated soils, – M.: Kolos, – 304 p.

Allaniyazov D. O. (2019). Development of scientific foundations of processes for production and technology of complex fertilizers from glauconites and phosphorites of Karakalpakstan Diss. Ph D. – Tashkent IONH AN RUz, – 123 p.

Allaniyazov D. O., Erkaev A. U. (2021). Enrichment of Karakalpakstan glauconite by dry method. International Scientific Journal "National Association of Scientists" (NAU) ISSN 2413-5291. – Vol. 2. – No. (36_63). – P. 4–8.

Allaniyazov D. O., Erkayev A. U., Tajibayev T. A., Ochilov S. U. (2023). Processing of local agro ores of Karakalpakstan for high-efficiency fertilizer. Journal of Survey in Fisheries Sciences – 10(3S). – P. 1225–1232.

Allaniyazov D. O., Tazhibaev T. A., Ochilov S. U. (2024). Application of agricultural ore of Karakalpakstan as complex fertilizers. Collection of materials of the V International Scientific and Theoretical Conference "Actual Issues of Natural Sciences". – P. 566–569.

Allaniyazov D. O., Erkaev A. U. (2022). Study of agrochemical effect of obtained new types of complex fertilizers based on Karakalpakstan agro-ore with various mineral fertilizers. International Journal of Advanced Research in Science and Technology, Int. J. Adv. Res. Sci. Technol. – Vol. 11. – Issue 12. – P. 881–886.

submitted 14.10.2025;
accepted for publication 28.10.2025;
published 26.11.2025

Contact: sochilovs9777@gmail, com; dauran_1985@mail, ru

The Austrian Journal of Technical and Natural Sciences, No 9–10
ISSN 2310-5607

PREMIER Publishing
ppublishing.org

DOI:10.29013/AJT-25-9.10-114-118

AMPLITUDE-FREQUENCY CHARACTERISTICS OF A BEAM WITH HYSTERESIS-TYPE ELASTIC DISSIPATIVE PROPERTY AND A MOVING DYNAMIC ABSORBER

Zarnigor Yuldoshova [1]

[1] Department of Digital Economy and Information Technologies, Samarkand Branch of Tashkent State University of Economics

Cite: *Yuldoshova Z. (2025). Amplitude-Frequency Characteristics of a Beam With Hysteresis-Type Elastic Dissipative Property and a Moving Dynamic Absorber. Austrian Journal of Technical and Natural Sciences 2025, No 9–10.* https://doi.org/10.29013/AJT-25-9.10-114-118

Abstract

In this work, the amplitude-frequency characteristics of the transverse vibrations of a beam with a hysteresis-type elastic dissipative property, interacting with a moving dynamic absorber of the same type, has been analytically determined depending on the system parameters and variables, and analyzed on the basis of numerical calculations.

Keywords: *Beam, dynamic absorber, hysteresis, vibrations, the amplitude-frequency characteristics*

Introduction

Taking into account the nonlinearity of complex mechanical systems, a number of works have been devoted to the analysis of their vibrations and dynamics (Wu J. J., 2006; Mohamed G., Sinan M., 2005; Dusmatov O. M., 1997; Pavlovsky M. A., Ryzhkov L. M., Yakovenko V. B., Dusmatov O. M., 1997; Mirsaidov M. M., Dusmatov O. M., Khodjabekov M. U., 2023; Khodjabekov M. U., Buranov Kh. M., Qudratov A. E., 2022; Pisarenko G. S., Boginich O. E., 1981). To analyze the dynamics of the beam protected from the considered vibrations, we write down its differential equation of motion.

$$\ddot{q}_i + \{\left(1 + C_0\left(-\eta_1 + j\eta_2\right)\right)p_i^2 + \frac{3EI}{\rho A d_{2i}}\left(-\eta_1 + j\eta_2\right) \times \sum_{k=1}^{n} C_k q_{ia}^k \frac{h^k}{2^k\left(k+3\right)} \int_0^l u_i \frac{\partial^2}{\partial x^2}\left(\frac{\partial^2 u_i}{\partial x^2}\left|\frac{\partial^2 u_i}{\partial x^2}\right|^k\right) dx\} q_i -$$

$$-\mu\mu_0 n_0^2 u_{i0}\left(1 + \left(-\theta_1 + j\theta_2\right)\left(D_0 + f\left(\zeta_{ot}\right)\right)\right)\zeta H\left(\frac{1}{\nu} - t\right) = -d_i \frac{\partial^2 w_0}{\partial t^2}; \qquad (1)$$

$$u_{i0}\ddot{q}_i + \ddot{\zeta} + n_0^2\left(1 + \left(-\theta_1 + j\theta_2\right)\left(D_0 + f\left(\zeta_{ot}\right)\right)\right)\zeta = -\frac{\partial^2 w_0}{\partial t^2},$$

where

$$\mu = \frac{m}{\rho A l}; \mu_0 = \frac{l}{d_{2i}}; d_i = \frac{d_{1i}}{d_{2i}};$$

$$d_{1i} = \int_0^l u_i dx; d_{2i} = \int_0^l u_i^2 dx;$$

ρ, A are, respectively, the density of the beam material and the cross-sectional area; $w(x_0)$ is the displacement of the beam point where the dynamic absorber is located; $x_0 = vt$ is the point where the dynamic absorber is located; v is the velocity of the dynamic absorber; t is time; $\delta(x)$ is Dirac delta function; $H\left(\frac{l}{v}\right)$ is Heaviside function; l is the length of the beam; c, m are the stiffness and the mass of the dynamic absorber, respectively; ζ is the relative deformation of the dynamic absorber; w_a is the absolute displacement of the beam $w_a = w_0 + w$, w_0 is the displacement of the base; w is the deflection of the beam; $\theta_1, \theta_2 = \theta_{22} sign(\omega)$ are constant coefficients depending on the elastic dissipative properties of the dynamic absorber material, determined from the hysteresis loop; $j^2 = -1$; $f(\zeta_{ot})$ is the decrement of vibrations, ζ_{ot} is a function of the absolute value of the relative deformation,

$$f(\zeta_{ot}) = D_1\zeta_{ot} + D_2\zeta_{ot}^2 \ldots + D_n\zeta_{ot}^n,$$

$D_0, D_1, \ldots, D_n$ are the parameters of the hysteresis node determined experimentally, which depend on the damping properties of the dynamic absorber material (Pisarenko G. S., Boginich O. E., 1981) $\eta_1, \eta_2 = \eta_{22} sign(\omega)$ are constant coefficients depending on the elastic dissipative properties of the beam material, determined from the hysteresis loop; $f(\zeta_o)$ is the decrement of vibrations, which is a function of the absolute value of the relative deformation ζ_o.

$$f(\zeta_o) = C_1\zeta_o + C_2\zeta_o^2 \ldots + C_n\zeta_o^n,$$

$C_0, C_1, \ldots, C_n$ are the parameters of the hysteresis node determined experimentally, which depend on the damping properties of the beam material (Pisarenko G. S., Boginich O. E., 1981).

Materials and methods

Using the system of differential equations (1), we determine the transfer function in order to analyze the dynamics of the beam protected from the considered vibrations. First, for this purpose, we transform the system of differential equations (1) $S = \frac{d}{dt}$ we reduce it to a system of algebraic equations using the differential operator. $S^2 = -\omega^2$ taking into account that $H\left(\frac{1}{v} - t\right)$ of the Heaviside function $\frac{1}{v} - t > 0$ when $H\left(\frac{1}{v} - t\right) = 1$ taking into account the property, q_i and ζ we solve with respect to the variables.

$$q_i(t) = -\frac{A_1 + jA_2}{B_1 + jB_2} W_0; \qquad (2)$$

$$\zeta(t) = -\frac{A_3 + jA_4}{B_1 + jB_2} W_0,$$

where

$$A_1 = -\omega^2 + \left(1 + d_i\mu\mu_0 u_{i0}\right) n_0^2 (1 - \theta_1\left(D_0 + f\left(\zeta_{ot}\right)\right));$$

$$A_2 = \left(1 + d_i\mu\mu_0 u_{i0}\right) n_0^2 \theta_2 \left(D_0 + f\left(\zeta_{ot}\right)\right);$$

$$A_3 = (-\omega^2 + \left(1 - \eta_1 C_0\right) p_i^2 - \eta_1 \frac{3EI}{\rho A d_{2i}} \times \sum_{k=1}^{n} C_k q_{ia}^k \frac{h^k}{2^k (k+3)} \int_0^l u_i \frac{\partial^2}{\partial x^2} \left(\frac{\partial^2 u_i}{\partial x^2} \left| \frac{\partial^2 u_i}{\partial x^2} \right|^k \right) dx) d_i + u_{i0}\omega^2;$$

$$A_4 = d_i \eta_2 (C_0 p_i^2 + \frac{3EI}{\rho A d_{2i}} \sum_{k=1}^{n} C_k q_{ia}^k \frac{h^k}{2^k (k+3)} \int_0^l u_i \frac{\partial^2}{\partial x^2} \left(\frac{\partial^2 u_i}{\partial x^2} \left| \frac{\partial^2 u_i}{\partial x^2} \right|^k \right) dx);$$

$$B_1 = [-\omega^2 + \left(1 - \eta_1 C_0\right) p_i^2 - \eta_1 \frac{3EI}{\rho A d_{2i}} \times \sum_{k=1}^{n} C_k q_{ia}^k \frac{h^k}{2^k (k+3)} \int_0^l u_i \frac{\partial^2}{\partial x^2} \left(\frac{\partial^2 u_i}{\partial x^2} \left| \frac{\partial^2 u_i}{\partial x^2} \right|^k \right) dx] \times [-\omega^2 +$$

$$+n_0^2\left(1-\theta_1\left(D_0+f\left(\zeta_{ot}\right)\right)\right)]-\eta_2[C_0p_i^2+\frac{3EI}{\rho Ad_{2i}}\times\sum_{k=1}^{n}C_kq_{ia}^k\frac{h^k}{2^k\left(k+3\right)}\int_0^l u_i\frac{\partial^2}{\partial x^2}\left(\frac{\partial^2u_i}{\partial x^2}\left|\frac{\partial^2u_i}{\partial x^2}\right|^k\right)dx]\times$$

$$\times n_0^2\left(1+\theta_2\left(D_0+f\left(\zeta_{ot}\right)\right)\right)-\mu\mu_0n_0^2u_{i0}^2\omega^2\left(1-\theta_1\left(D_0+f\left(\zeta_{ot}\right)\right)\right);$$

$$B_2=[-\omega^2+\left(1-\eta_1C_0\right)p_i^2-\eta_1\frac{3EI}{\rho Ad_{2i}}\times\sum_{k=1}^{n}C_kq_{ia}^k\frac{h^k}{2^k\left(k+3\right)}\int_0^l u_i\frac{\partial^2}{\partial x^2}\left(\frac{\partial^2u_i}{\partial x^2}\left|\frac{\partial^2u_i}{\partial x^2}\right|^k\right)dx]\times$$

$$\times n_0^2\left(1+\theta_2\left(D_0+f\left(\zeta_{ot}\right)\right)\right)+\eta_2[C_0p_i^2+\frac{3EI}{\rho Ad_{2i}}\times\sum_{k=1}^{n}C_kq_{ia}^k\frac{h^k}{2^k\left(k+3\right)}\int_0^l u_i\frac{\partial^2}{\partial x^2}\left(\frac{\partial^2u_i}{\partial x^2}\left|\frac{\partial^2u_i}{\partial x^2}\right|^k\right)dx]\times$$

$$\times\left[-\omega^2+n_0^2\left(1-\theta_1\left(D_0+f\left(\zeta_{ot}\right)\right)\right)\right]-\mu\mu_0n_0^2u_{i0}^2\theta_2\left(D_0+f\left(\zeta_{ot}\right)\right))\omega^2.$$

Expression (2) represents the amplitude-frequency characteristic of the transverse vibrations of a beam with a hysteresis-type elastic dissipative property together with a moving dynamic absorber of the same type.

Results and discussion

Let us assume that the moving dynamic absorber is moving with a linear velocity of $v=0.125\frac{m}{s}$. In this case, when $t=1;2s$ we analyze the amplitude-frequency characteristics of the considered system.

The experimentally determined parameters of the hysteresis node of the beam material are taken as follows (Pisarenko G. S., Boginich O. E., 1981).

$C_1=6.760624;C_2=-8278.5937;C_3=5894761;$

$\eta_1=\frac{3}{4};\eta_2=\frac{1}{\pi}$. For the elastic damping element of the moving dynamic absorber, we assume the following:

$$\theta_1=\theta_2=0,D_0=0,D_1=0,D_2=0.$$

The remaining parameters are as follows:

$$d_1=0.3183098862;d_2=0.25;$$

$$d_i=1.273239545;\mu=0.1;\mu_0=2.0$$

$$u_{i0}=u_{10}=1;I=1.066666667\cdot10^{-10}m^4;$$

$$\varepsilon p_0=10^{-\frac{5}{2}}m.$$

When $t=1s$ the moving dynamic absorber is located at the point $x_0=0.125m$ of the beam. Based on the values of the parameters given above, we plot the amplitude–frequency characteristic of the system.

In Figure 1, the variation of the amplitude–frequency characteristic at the point where the dynamic absorber is installed is shown for the transverse vibrations of a beam with a hysteresis-type elastic dissipative property together with a moving dynamic absorber located at $x_0=0.125m$. From these graphs, it can be observed that as the stiffness of the dynamic absorber increases, its frequency approaches the natural frequency of the beam, and the resonance curve shifts along the frequency axis from left to right ($c=10\cdot10^2\frac{N}{m}$ (black), $c=12\cdot10^2\frac{N}{m}$ (red), $c=15\cdot10^2\frac{N}{m}$ (blue)). At these stiffness values, the maximum amplitudes around the resonance frequency are

$q_0=0.0036;0.0035;0.0024m,$ respectively .

From this, it can be concluded that for the point $x_0=0.125m$ with the above parameter values, $c=15\cdot10^2\frac{N}{m}$ represents the optimal value of the dynamic absorber stiffness.

Figure 1. *Amplitude–frequency characteristic (x_0=0.125 m)*

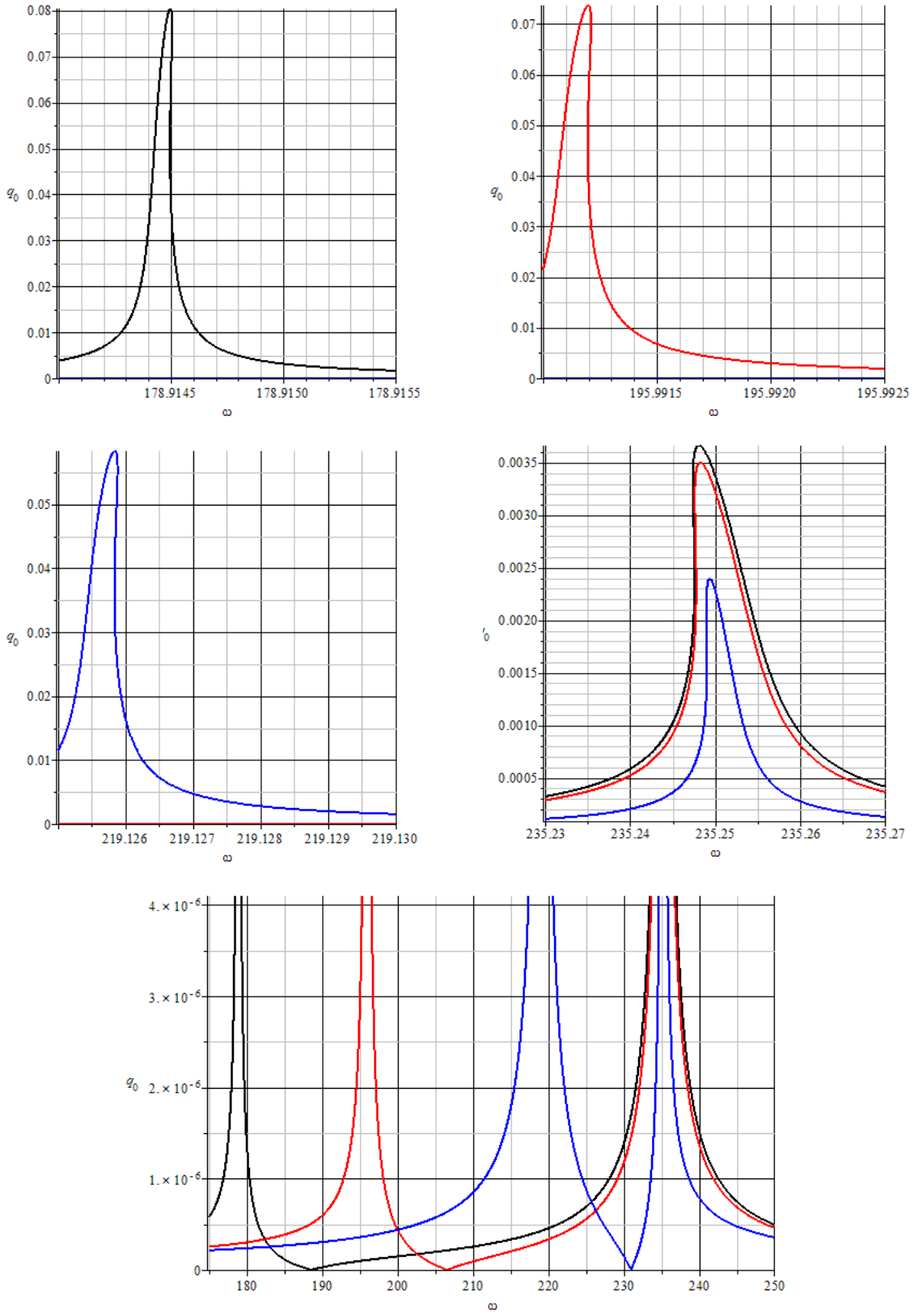

Conclusion

The obtained expression is an analytical representation of the amplitude–frequency characteristic of the transverse vibrations of a beam with a hysteresis-type elastic dissipative property together with a moving dynam-

ic absorber of the same type, which makes it possible to evaluate the efficiency of the moving hysteresis-type elastic dissipative dynamic absorber.

References

Wu J. J. (2006). Study on the inertia effect of helical spring of the absorber on suppressing the dynamic responses of a beam subjected to a moving load. Journal Sound and Vibration, – 297. – P. 981–999.

Mohamed G., Sinan M. (2005). Transverse vibration of two axially moving beams connected by an elastic foundation. Proceedings of 2005 ASME International Mechanical Engineering Congress and Exposition,, Florida. DOI:10.1115/IMECE2005-80377

Dusmatov O. M. (1997). Modeling the dynamics of vibration protection systems. –T.: Fan Publishing House. – 167 p.

Pavlovsky M. A., Ryzhkov L. M., Yakovenko V. B., Dusmatov O. M. (1997). Nonlinear problems of dynamics of vibration protection systems. – K.: Technology, – 204 p.

Mirsaidov M. M., Dusmatov O. M., Khodjabekov M. U. (2023). Stability of Nonlinear Vibrations of Elastic Plate and Dynamic Absorber in Random Excitations. E3S Web of Conferences – 410. – 03014. URL: https://doi.org/10.1051/e3sconf/202341003014

URL: https://www.scopus.com/authid/detail.uri?authorId=6507460407 Khodjabekov M. U., Buranov Kh. M., Qudratov A. E. (2022). Modal mass and stiffness of hysteresis type elastic dissipative characteristic plate. AIP Conf. Proc. 2637, 050004-1-050004-5; https://doi.org/10.1063/5.0118292

Pisarenko G. S., Boginich O. E. (1981). Oscillations of kinematically excited mechanical systems taking into account energy dissipation. – Kyiv: Nauk. Dumka, – 219 p.

submitted 14.10.2025;
accepted for publication 28.10.2025;
published 26.11.2025

Contact: z.yuldoshova30@gmail.com

The Austrian Journal of Technical and Natural Sciences, No 9–10
ISSN 2310-5607

PREMIER Publishing
ppublishing.org

Section 7. Information Technology

DOI:10.29013/AJT-25-9.10-119-124

ROUTE OPTIMIZATION AND TRANSPORTATION PLANNING USING ARTIFICIAL INTELLIGENCE

Samoilenko Sergii [1]

[1] Independent Research, Vinnytsia, Ukraine

Cite: *Samoilenko S. (2025). Route optimization and transportation planning using artificial intelligence. Austrian Journal of Technical and Natural Sciences 2025, No 9–10.* https://doi.org/10.29013/AJT-25-9.10-119-124

Abstract

The article discusses modern approaches to route optimization and transportation planning using artificial intelligence techniques. It analyzes machine-learning algorithms, neural networks, and heuristic methods to improve the efficiency of logistics operations, reduce fuel costs, and shorten delivery times. Special attention is given to the integration of intelligent systems with transport platforms, enabling real-time adaptive route management and improved demand forecasting accuracy. The results of a comparative study between traditional and intelligent planning models are presented. The article demonstrates the impact of these models on the productivity of transportation companies and the sustainability of the logistics industry.

Keywords: *artificial intelligence, route optimization, transportation planning, machine learning, logistics, transport systems, digitalization, data analysis*

The relevance of research

Modern transport and logistics systems face an increase in traffic volumes and the complexity of transport networks. They also need to respond quickly to changes in demand. Traditional route planning methods are not flexible enough to ensure optimal resource allocation. Using artificial intelligence (AI) technologies can automate the decision-making process, reduce costs, and improve forecasting accuracy. This makes the study of these technologies especially relevant in the context of digital transformation in logistics.

The purpose of the study

The aim of the research is to develop and validate approaches to route optimization and transportation planning using artificial intelligence techniques in order to improve the efficiency of transportation operations, reduce time and financial expenses, and enhance the quality of logistics services.

Materials and methods of research

The research materials include data on traffic flows, route structures, transportation schedules, and operational parameters

of logistics systems. To conduct the research, the following methods were used:

– Analysis of literature and existing routing models.

– Machine learning techniques, including both supervised and unsupervised learning;

– Neural networks for predicting demand and traffic conditions;

– Optimization algorithms such as genetic algorithms, ant colony optimization, and evolutionary algorithms;

– Modeling and comparative analysis of the effectiveness of proposed solutions based on both test data and real-world data.

The results of the study

The history of the use of artificial intelligence in route construction and transportation planning dates back to the mid XX century, when mathematical models and optimization problems were the focus.

In the 1960s and 1970s, scientists were actively investigating the traveling salesman problem and the vehicle routing problem (VRP). They created algorithms that could minimize distance and cost when servicing multiple delivery points. These early approaches were based on rigorous mathematical methods, such as linear and integer programming. They also used heuristics, which formed the basis for future intelligent systems.

In the 1980s and 1990s, the use of expert systems, the first form of artificial intelligence in logistics, began. These systems included knowledge and rules based on the experience of logistics experts, and they could recommend optimal routes considering constraints such as driver hours, transport capacity, and customer schedules. However, these decisions were static and depended on predefined rules, limiting their ability to adapt to changes in the external environment.

In the early 2000s, the development of digital technologies and the availability of large volumes of data enabled the use of machine learning to analyze and predict traffic patterns. Algorithms started to take into account dynamic factors such as traffic jams, weather conditions, and seasonal variations in demand. Routing systems started to learn from historical data and forecast optimal solutions, considering the behavior of transportation and infrastructure characteristics (Fig. 1).

Figure 1. *The scheme of distribution of orders and routing of delivery*

Since the 2010s, advances in neural networks and computing power have paved the way for the creation of intelligent platforms based on deep learning and Reinforcement Learning methods. These technologies have allowed routing systems to adapt in real-time, redistributing routes in case of changes in traffic conditions, accidents, or urgent orders. Companies such as Google, Uber, and Amazon, as well as logistics operators have begun to actively implement AI for transportation management. This has led to increased fleet utilization, reduced empty mileage, and improved delivery times.

At the present time (2020s), artificial intelligence (AI) has become an essential component of integrated transport management systems (TMS) and intelligent transport

systems (ITS). It integrates with the internet of things (IoT), demand forecasting systems, computer vision, and sensor networks to provide a continuous flow of data on vehicles, roads, and cargo.

Modern solutions use hybrid models that combine optimization algorithms and machine learning techniques to ensure the complete digitalization of logistics processes from planning to real-time monitoring of route execution. The development of AI applications in routing and transportation planning has evolved from mathematical models and simple expert systems to self-learning platforms that can predict, adapt, and make decisions independently. This transition is a key factor in enhancing the efficiency and sustainability of transportation networks in the age of smart logistics (Logistics and supply chain management: 2023).

It should be noted that modern technologies used in routing and transportation-planning systems are closely linked to the development of artificial intelligence (AI), big data analysis, and the Internet of Things (IoT).

AI can significantly improve the efficiency of transportation and logistics processes by providing adaptive information analysis, optimizing routes, and forecasting real-time situations. Machine learning is used to analyze vast amounts of data on traffic, weather conditions, driver behavior, and vehicle characteristics. This data is used to train algorithms that find optimal solutions, create flexible routes, and minimize time and resource costs.

Deep neural networks enable systems to analyze complex data sources, such as satellite images, video streams, and road sensor data. This allows for the detection of congestion, accidents, and real-time prediction of traffic changes.

Reinforcement learning algorithms are widely used in ride-hailing services such as Uber and Yandex to quickly reallocate vehicles when demand or traffic conditions change. These algorithms help optimize the performance of drivers, reduce customer-waiting times, and prevent empty runs (Arifdzhanova N. Z., 2023).

In corporate logistics, Amazon, DHL, and other major carriers are implementing intelligent planning systems that consider multiple factors – order priority, route specifics, warehouse conditions, weather forecasts, and traffic conditions. These systems generate optimal delivery plans, minimize transport downtime, and enhance the accuracy of order fulfillment. Predictive analytics allow them to anticipate transportation demand, plan vehicle loading, and prevent inefficient resource allocation.

The integration of AI and the Internet of Things is essential. Vehicles are equipped with sensors that collect data on their technical condition, fuel levels, travel times, and driving parameters. This information is used to analyze possible risks and prevent breakdowns, increasing the reliability of the transportation system. Additionally, the use of digital twins and cloud platforms allows for the simulation of various routing scenarios and automatic adjustment of logistics chains when conditions change (Tab. 1).

Table 1. *Artificial intelligence in corporate logistics* (Danilochkina N.G., Lysenko A. A., 2024)

No.	Indicator	Characteristic
1.	Route optimization	AI can analyze traffic data, weather conditions, and other factors to find the most efficient delivery routes. This helps reduce travel time and save fuel.
2.	Forecasting demand	With the help of machine learning, artificial intelligence can predict customer needs based on historical data and current trends. This helps to avoid overstocking or understocking of inventory.
3.	Inventory management	AI can help automate inventory management, helping companies maintain optimal levels of inventory and minimize storage costs.

No.	Indicator	Characteristic
4.	Process automation	AI can be used to automate repetitive tasks such as order processing and document management, freeing up employees to focus on more challenging tasks.
5.	Data analysis	AI systems can process and analyze vast amounts of data, revealing patterns and trends that would be difficult to identify manually.
6.	Risk management	AI can help assess supply-side risks by predicting possible disruptions in the supply chain and offering alternative solutions.
7.	Intelligent transportation systems	AI can be used to manage a fleet, including monitoring the condition of vehicles and ensuring proper maintenance.
8.	Customer service	Chatbots and AI-powered virtual assistants can enhance customer interaction by providing information on delivery status and resolving any issues that may arise.

Artificial intelligence is becoming an essential part of modern transportation and logistics management. It offers a shift from manual and static planning methods to dynamic, self-learning systems that not only create the most efficient routes, but can also predict future events, lower costs, and enhance the stability of the overall logistics infrastructure.

It should be noted that while artificial intelligence has achieved significant success in solving transportation planning and route construction problems, there are still several challenges associated with its use. One of the main difficulties is the quality and completeness of the input data. AI algorithms require a large amount of accurate and reliable information about road networks, traffic patterns, weather conditions, traffic restrictions, and the technical status of transportation vehicles. However, data can often be incomplete, outdated, or contain errors, which can reduce the accuracy of optimization models and lead to errors in predictions.

Another challenge is the difficulty in accurately modeling the complexities of the transportation system. A wide range of dynamic factors, such as traffic congestion, accidents, maintenance work, time constraints, and human behavior, influences routes. Even the most sophisticated machine learning algorithms are not always able to fully account for all of these variables in real-time. This necessitates the continuous updating and refinement of algorithms to ensure accurate predictions.

The computational complexity of optimization problems also creates a significant difficulty. Routing problems such as the traveling salesman problem or the Vehicle routing problem (VRP) are classified as NP-hard. For large transport networks, the number of possible solutions is growing exponentially, and even high-performance computing clusters do not always provide fast processing. As a result, you have to use heuristic or approximate methods, which reduces the accuracy of optimization.

Equally important is the issue of interpretability of AI solutions. Deep learning algorithms often operate like “black boxes,” making it difficult to understand why a system chooses one path over another. This lack of transparency reduces the trust of users and clients, especially in the field of transportation of valuable goods. Additionally, there is a risk of errors in the system that could lead to significant failures if the model is trained incorrectly or the data used is flawed.

Implementing AI technologies requires substantial investments in software, infrastructure, and training for specialists. Small and medium-sized businesses often lack the resources to support such solutions. Furthermore, there are concerns about the security of personal and business data, as optimiza-

tion algorithms utilize geolocation information and customer profiles for analysis.

The main challenges of route optimization and transportation planning using artificial intelligence include the difficulty in providing high-quality data, the high computational load, the need to adapt to changing conditions, the limited transparency of algorithms, and significant economic obstacles. Overcoming these challenges requires a comprehensive approach that includes infrastructure development, standardization of data, increased transparency of models, and a balanced approach between automation and human oversight.

In our opinion, to effectively address the challenges associated with the use of artificial intelligence in route optimization, a comprehensive approach combining technological, organizational, and methodological measures is necessary. One of the key aspects is improving data quality. To this end, modern data collection and cleansing systems, as well as the use of IoT sensors, satellite monitoring systems, and automatic map updates, are employed. Integrating various data sources such as transportation platforms, roadside services, weather stations, and transportation monitoring systems plays a crucial role in creating more accurate and up-to-date models.

Adaptive planning based on real-time streaming data processing is used to address the challenge of the dynamism of the external environment. Machine learning and predictive analytics techniques allow us to identify patterns in traffic changes and adjust routes ahead of time. The use of hybrid models that combine traditional optimization algorithms with neural networks helps increase the resilience of our solutions to changing conditions.

In the field of computational complexity, heuristic and metaheuristic methods have been actively developed, such as genetic algorithms, particle swarm algorithms, and simulated annealing. These approaches make it possible to find solutions that are close to optimal in a reasonable time, even with a large number of routes and restrictions. Additionally, distributed computing and cloud platforms are used to speed up processing, which scale to meet real business needs.

To increase confidence in AI solutions, it is important to develop interpretable artificial intelligence, also known as explicable AI. This allows users and managers to visualize the decision-making process and understand the impact of each factor on the outcome. By doing so, transparency in the results is ensured, which helps build trust in the system.

To reduce economic and ethical risks, open platforms, modular architectures, and hybrid solutions should be used. These can be implemented gradually, allowing for a smoother transition. Additionally, cybersecurity and data protection measures should be strengthened to prevent the leakage of sensitive information. Specialist training and staff development in areas such as data analysis, logistics, and AI are essential for ensuring the proper operation and development of these systems. These efforts will help create a more reliable and trustworthy AI system for the transportation industry.

Solving the challenges of route optimization and transportation planning through the use of artificial intelligence requires the coordinated interaction of various elements, including technology, infrastructure, and expert personnel. Only by adopting an integrated approach that incorporates high-quality data, adaptive algorithms, transparent models, and reliable information security measures can we achieve high levels of efficiency, sustainability, and safety in our transport solutions.

Conclusion

In conclusion, it is worth noting that the introduction of artificial intelligence into route optimization and transportation planning is a key area of digital transformation in the transport and logistics industry. Using intelligent systems allows for a more efficient allocation of resources, reduced costs, and faster decision-making. Advanced machine learning algorithms and big data analysis techniques enable us to consider various factors, such as traffic, weather conditions, infrastructure, and transportation demand.

At the same time, the use of AI presents a number of challenges. These include the need for high-quality data, the requirement for explainable solutions, and the importance of ensuring cybersecurity. To overcome these difficulties, an integrated approach is necessary. This includes the development of

information processing technologies, the use of hybrid models, training qualified specialists, and the creation of a regulatory framework for AI usage.

In the coming years, the development of intelligent transport systems will determine the competitiveness of companies and the efficiency of logistics processes. Successful AI implementation will lead to improved forecasting accuracy, minimized delays, reduced operating costs, and better environmental performance. Therefore, artificial intelligence is not just a tool for optimization, but also a strategic foundation for the creation of a sustainable, adaptable, and efficient transport system for the future.

References

Arifdzhanova N. Z. The use of artificial intelligence to optimize transport routes // Universum: technical sciences. – No. (5–4 (110)). 2023. – P. 10–12.

Danilochkina N.G., Lysenko A. A. Optimization of logistics routes with artificial intelligence technologies // Scientific Papers of the Free Economic Society of Russia. – No. 246 (2). – 2024. – P. 298–314.

Logistics and supply chain management: textbook and workshop for universities / V. S. Lukinsky, V. V. Lukinsky, N. G. Pletneva. – Moscow: Yurait Publishing House, 2023. – 359 p.

submitted 14.10.2025;
accepted for publication 28.10.2025;
published 26.11.2025

Contact: samalet19@ukr.net

Contents

Section 1. Chemistry

Section 6. Technical sciences in general

Section 7. Information Technology